

THEORETICALLY PREDICTED
IGNITION TRANSIENTS IN SOLID PROPELLANT
ROCKET MOTORS (U)

Aerospace and Mechanical Sciences
Report No. 802

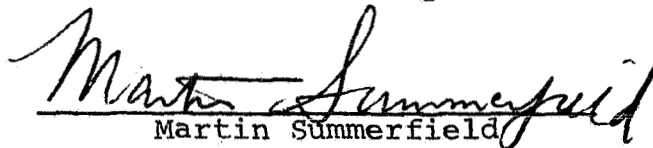
by

G. F. di Lauro, L. H. Linden, W. J. Most
and M. Summerfield

July 1967

This research was sponsored by the Office of Advanced Research & Technology, National Aeronautics & Space Administration, under Research Grant Nsg 200-60 for the period April 1, 1966 through September 30, 1966.

Transmitted by:


Martin Summerfield
Principal Investigator

Guggenheim Laboratories for the Aerospace Propulsion Sciences
Department of Aerospace & Mechanical Sciences
PRINCETON UNIVERSITY
Princeton, New Jersey

ACKNOWLEDGEMENT

This research was sponsored by the Office of Advanced Research and Technology, National Aeronautics & Space Administration under Research Grant Nsg 200-60 for the period April 1, 1966 through September 30, 1966. The Program Manager for this program was Mr. Robert W. Ziem, Chief, Solid Propellant Technology, Office of Advanced Research and Technology. The Technical Manager for this program was Mr. Warren L. Dowler, Solid Propellant Engineering Section, Jet Propulsion Laboratory. The Contracting Officer for the program was Mr. T. L. K. Smull, Office of Grants and Research Contracts.

Conditions of Reproduction

Reproduction, translation, publication, use and disposal in whole or in part by or for the United States Government is permitted.

TABLE OF CONTENTS

	<u>Page</u>
Title Page	i
Acknowledgement	ii
Table of Contents	iii
List of Tables	iv
List of Figures	v
Abstract	viii
CHAPTER I - INTRODUCTION	1
A. Ignition Systems	2
B. Preliminary Concepts	2
CHAPTER II - Preliminary Discussion	6
CHAPTER III - Theoretical Development	10
A. Chamber Filling	10
1. Momentum Equation	11
2. Continuity Equation	12
3. Energy Equation	13
4. The Chamber Filling Interval	18
5. Dynamic Burning Rate	19
B. Flame Spreading	21
CHAPTER IV - Discussion of Results	27
CHAPTER V - Conclusions	35
References	36
List of Symbols	39
Tables	43
Figures	49
Appendixes:	
A. Dynamic Burning Rate	A-1
B. Numerical Computations	B-1
C. Distribution List	C-1

LIST OF TABLES

TABLE 1	Design of Slab Geometry Solid Propellant Rocket Motor	44
TABLE 2	Compendium of Design Parameters	45
TABLE 3	Compendium of Computer Results	47

LIST OF FIGURES

	<u>Page</u>
1 Schematic Drawing of Experimental Rocket Motor	49
2 Burning Rate Curve of PBAA 80BM Propellant	50
3 $P_c - K_N$ Curve for PBAA 80BM Propellant	51
4 Experimental Heat Transfer Correlation	52
5 Comparison of Measured & Computed S & P	53
6 Schematic Layout of Modified Experimental Rocket System	54
7 Theoretical Pressure vs. Gas Temperature During Chamber Filling Interval	55
8 Comparison of Pressure vs. Time from Start of Igniter Curves -- Series A (Variable Igniter Flow Rate, Igniter Cut-off at S = .3)	56
9 Comparison of Instantaneous Burning Area vs. Time from Start of Flame Spreading -- Series A	57
10 Comparison of Pressure vs. Time from Start of Igniter Curves -- Series B (Variable Rocket Port Area)	58
11 Comparison of Instantaneous Burning Area vs. Time from Start of Flame Spreading -- Series B	59
12 Comparison of Pressure vs. Time from Start of Igniter Curves -- Series C (Variable Rocket Throat Area)	60
13 Comparison of Instantaneous Burning Area vs. Time from Start of Flame Spreading -- Series C	61
14 Comparison of Pressure vs. Time from Start of Igniter Curves -- Series D (Excess igniter duration, various flow rates)	62
15 Comparison of Instantaneous Burning Area vs. Time from Start of Flame Spreading -- Series D	63
16 Comparison of Pressure vs. Time from Start of Igniter Curves -- Series E (Variable Igniter Flow Rate, Constant Igniter Mass)	64
17 Comparison of Instantaneous Burning Area vs. Time from Start of Flame Spreading -- Series E	65

LIST OF FIGURES - Cont'd.

	<u>Page</u>
18 Comparison of Pressure vs. Time from Start of Igniter Curves -- Series F (Various Size Partial Nozzle Closures)	66
19 Comparison of Instantaneous Burning Area vs. Time from Start of Flame Spreading -- Series F	67
20 Chamber Conditions vs. Time from Start of Igniter -- Firing A-1	68
21 Chamber Conditions vs. Time from Start of Igniter -- Firing A-2	69
22 Chamber Conditions vs. Time from Start of Igniter -- Firing A-3	70
23 Chamber Conditions vs. Time from Start of Igniter -- Firing A-4	71
24 Chamber Conditions vs. Time from Start of Igniter -- Firing A-5	72
25 Chamber Conditions vs. Time from Start of Igniter -- Firing B-1	73
26 Chamber Conditions vs. Time from Start of Igniter -- Firing B-2	74
27 Chamber Conditions vs. Time from Start of Igniter -- Firing B-3	75
28 Chamber Conditions vs. Time from Start of Igniter -- Firing B-4	76
29 Chamber Conditions vs. Time from Start of Igniter -- Firing C-1	77
30 Chamber Conditions vs. Time from Start of Igniter -- Firing C-2	78
31 Chamber Conditions vs. Time from Start of Igniter -- Firing C-3	79
32 Chamber Conditions vs. Time from Start of Igniter -- Firing C-4	80
33 Chamber Conditions vs. Time from Start of Igniter -- Firing D-1	81
34 Chamber Conditions vs. Time from Start of Igniter -- Firing D-2	82
35 Chamber Conditions vs. Time from Start of Igniter -- Firing D-3	83

LIST OF FIGURES. - Cont'd.

	<u>Page</u>
36 Chamber Conditions vs. Time from Start of Igniter -- Firing E-1	84
37 Chamber Conditions vs. Time from Start of Igniter -- Firing E-2	85
38 Chamber Conditions vs. Time from Start of Igniter -- Firing E-3	86
39 Chamber Conditions vs. Time from Start of Igniter -- Firing E-4	87
40 Chamber Conditions vs. Time from Start of Igniter -- Firing E-5	88
41 Chamber Conditions vs. Time from Start of Igniter -- Firing F-1	89
42 Chamber Conditions vs. Time from Start of Igniter -- Firing F-2	90
43 Chamber Conditions vs. Time from Start of Igniter -- Firing F-3	91
44 Chamber Conditions vs. Time from Start of Igniter -- Firing F-4	92
B-1 Geometrical Representation of Second Order Predictor	B-6
B-2 Geometrical Representation of Second Order Corrector	B-6
B-3 Geometrical Representation of Heat Transfer Integration Scheme	B-7
B-4 Flow Chart of Computer Program	B-8

ABSTRACT

The overall ignition transient of a rocket motor is described by its three component processes: the ignition lag, the time between the start of the igniter action and the appearance of the first flame on the propellant surface; flame spreading, the time interval during which the propellant surface becomes fully ignited; and chamber filling, the time interval during which equilibrium conditions in the chamber are attained. The chamber filling process which dominates the entire transient is analyzed assuming essentially one-dimensional flow with uniform pressure and temperature at all times. Flame spreading is based on the hypothesis of successive ignitions of adjacent surface elements, and the ignition criterion is the attainment of a critical temperature at the surface. The implications of the transient effects of changing pressure and of propellant pre-heating on the instantaneous burning rate are discussed but are not included in the analyses. The analysis in this paper is limited to the case of an internal burning grain with a pyrogen-type igniter located at the forward end of the rocket motor. Convection is assumed to be the dominant mode of heat transfer to the propellant and is correlated by a turbulent boundary layer law that was determined experimentally with a similar rocket motor and igniter gas in a previous research program:

A system of equations is derived and then used to determine numerically the gas pressure, the gas temperature, and the burning area during the ignition transient of a series of hypothetical pyrogen-ignited rocket motors for various series of firings. Computations with systematic variation of the igniter mass flow rate indicate several results of practical interest. One is that the ignition lag is inversely related to the igniter mass flow rate. Pressure overshoots due to over-duration igniters are demonstrated by calculation. Reduction of the chamber port area decreases the time to ignition and steepens the rate of pressure rise. Also studied are the cases of an igniter of constant mass, but with different rates of flow, and the use of a partial nozzle closure to speed up the ignition transient. The former showed that even though an igniter may have sufficient total mass for an adequate ignition when burned at rated flow, a malfunction that causes some reduction in the rate of flow (but with no reduction in combustion efficiency) may result in a hangfire. A partial nozzle closure was found to affect the ignition transient by speeding up the pressure rise especially in the chamber filling interval;

it had no effect on the induction time. This means that nozzle closures are not of great benefit in this class of rocket motor. The maximum value of $(\delta p/\delta t)$ is found to occur at the beginning of the pure chamber filling interval in all the cases studied, that is, before 35% of the equilibrium pressure is reached.

This research indicated that, given the igniter characteristics, a measured heat flux distribution, and a suitable ignition criterion, the ignition transient for a given rocket motor can be predicted.

CHAPTER I

INTRODUCTION

In the past several years, as part of the design procedure of a solid propellant rocket motor, internal ballistics engineers have been able to predict with precision the steady state thrust vs. time curve and the thrust tail-off curve of a given solid propellant rocket motor. However, when dealing with the thrust transient during ignition, that is, during the interval between the initiation of the igniter action and the onset of full thrust, the design engineer must resort simply to empirical knowledge of previous firings. This empirical and statistical approach to the design problem sheds very little light on the basic physical processes that are involved and cannot be relied upon for the performance analysis of new designs. The development of large, high performance solid propellant rockets costing large sums for each charge and each test firing emphasizes the need for a better understanding of the ignition transient.

The designer must concern himself with various aspects of the ignition transient. The overall time of the transient and the shape of the pressure rise are of primary importance. As for the overall time, that is, the delay in onset of full thrust, it usually must be kept within some limit and must be reproducible. As for the shape of the pressure rise, the possibility of a pressure overshoot is always present, and the stress limits of the motor shell must not be exceeded. Since the grain and the casing of the rocket have a viscoelastic nature, the rate of rise of the chamber pressure as well as the pressure level itself are critical parameters in the structural design. An excessive rate of pressurization can cause a failure even though the pressure is below the critical level, especially at low ambient temperature. The rate of rise of thrust is also important when the vehicle possesses a delicate guidance system or a delicate payload which must be isolated from strong shocks; this is the "ignition shock" problem. A detailed knowledge of pressure variations during the ignition transient may be required when solid propellant rockets are used for critical trajectory and attitude control.

It is the purpose of this report to contribute quantitative answers to these problems of ignition transient prediction and igniter design.

A. IGNITER SYSTEMS

The igniter system subjects the surface of the solid propellant to a complicated combination of conductive, convective, and radiative heat transfer. The strength and duration of this igniter should be such that once the igniter is shut off the solid propellant grain will be able to burn on its own. There are several classes of igniters that are usually employed. The purely pyrotechnic type igniters are composed of material which produces mainly incandescent particles, solid or molten, that are scattered all over the exposed surface of the main propellant charge, starting ignition at many spots simultaneously. These igniters are usually placed at several points in the core of the motor so that the evolved hot condensed products which heat the propellant surface by conduction will be distributed over the entire grain. The purely pyrogenic igniter produces mainly hot gas and is basically a small rocket motor within the main rocket system. After ignition of this small motor the resultant exhaust gases heat the main propellant charge primarily by convection. Other methods such as an electric heater on the surface of the grain or the injection of a liquid which is hypergolic with the propellant have been used to a limited extent.

In addition to the choice of igniter type, the designer has control of several other factors which alter the character of the ignition transient. Many of the techniques used can be found in the literature and only a few are mentioned here. Various transient characteristics are found with similar igniters when the placement of the igniter is changed, or the geometry of the grain is altered. The impingement angle and velocity of the igniter gas on the main rocket grain will increase or decrease the ignition time; fast ignitions are obtained at high impingement angles and high gas velocities. The composition of the igniter gas also can affect the ignition transient, particularly if the grain surface has been painted with inhibitors or chemically active materials.

B. PRELIMINARY CONCEPTS

The goal of this report is an attempt to describe analytically the ignition transient in solid propellant rocket motors. This subject, however, is still in its infancy, and only recently has a vocabulary been developed. The vocabulary is repeated here for clarity and completeness.

The ignition transient is defined as the interval between the first ignition signal and the beginning of steady state thrust. The latter situation occurs when steady state

conditions are reached in the rocket chamber. It is very convenient to separate the ignition transient into three time intervals:

(1) The ignition lag is defined as the interval between the initiation of the igniter action and the appearance of the first flame on the surface of the propellant. A detailed and accurate description of this time delay must include the ballistics of the igniter system and the delays associated with the actual ignition of an element of solid propellant. Critical reviews of the current theories of the ignition process are given in References 1 and 2. The ignition criterion is assumed in this report to be the attainment of a threshold temperature at the surface of the propellant, even though the ignition process is known to be complex, and may be expected to lead to a far more complex criterion. However, this simple temperature criterion can serve here as a first rough approximation to the actual criterion. Hence, the ignition delay reported in this report is merely the time it takes to heat the surface to the specified critical temperature.

(2) The flame spreading interval is the time from the first ignition to the time when the entire surface of the propellant is ignited. The mechanism by which the state of ignition is propagated over the surface of the propellant is based on the hypothesis of successive ignitions. Each element of the propellant surface is ignited individually, and the induction time for each surface element depends on the heat flux to that element and not the thermodynamic state of the neighboring elements. The model of flame spreading is as follows: The igniter mass flow transfers energy to the propellant by convection until some portion of the surface of the grain ignites. This, by definition, is the beginning of flame spreading. The products of solid propellant combustion then augment the energy transfer to the remaining unignited portions of the surface. This process continues until every element of surface is ignited, and then by definition, flame spreading is finished.

(3) The chamber filling interval is the interval between complete ignition of the propellant surface and the attainment of steady state conditions in the combustion chamber. The chamber filling process is the problem of internal ballistics throughout the entire ignition transient. However, once the complex ignition process is completed, the internal gas dynamic problem of the chamber filling interval is considered. This, however, should not imply that the question of the dynamic filling of a vented chamber by the products of solid propellant combustion is simple.

Before completing these introductory remarks, a brief survey of previous analytical studies of ignition transients is given. The previous and current investigations of this subject are described either as the study of the ignition transient in general or the study of the flame spreading mechanism in particular.

The study of flame spreading and the ignition transient was started in Princeton about June 1962, with the doctoral thesis project of K. H. Parker. The initial results of this work were reported in January 1964 in Reference 15. A related project was launched earlier at Rocketdyne on the initiative of Professor M. Summerfield, acting as a consultant to Rocketdyne, and this was published ultimately in Reference 11. Both projects were conducted on the basis of the concepts described herein, and were focused entirely on flame spreading in a convective environment.

An extensive research program based on similar concepts was carried out by Fullman et. al. This was reported in Reference 6.

The flame spreading over propellants in stagnant atmospheres was studied at about the same time by McAlevy, et. al.^{3,4,5} The spreading velocity was found to be a function of the pressure and the composition of the surrounding atmosphere, and steady state velocities measured were found to be of the order of about 0.5 cm/sec. Mitchell and Ryan⁷ conducted flame spreading experiments in which a relatively cool gas stream flowed parallel to the surface, which was ignited at one end. Spreading velocities were measured, and a diffuse flame front similar to that reported by Parker was observed. Brown, Wirrick, and Anderson⁸ presented a theory for flame spreading in a flowing environment. Energy transfer to the propellant by forced convection, radiation, and hypergolic reaction was considered in conjunction with a constant temperature ignition criterion. The gas dynamic conditions in the chamber were assumed prescribed.

The chamber filling interval has been analyzed, assuming isothermal conditions in the chamber in a standard text on rocket propulsion.⁹ Von Karman and Malina¹⁰, relaxed the isothermal assumption, but their energy equation contained an error which invalidates the results. DeSoto and Friedman¹¹ obtained a computer solution for an isothermal analysis of the chamber, using the hypotheses suggested to them by Professor Summerfield of successive ignitions in conjunction with a constant temperature ignition criterion for a flame spreading mechanism. However, the results reported are in numerical form and are for a particular rocket motor design. Bradley¹² considered

a non-isothermal rocket chamber, but a linear relation between flame spreading rate and mass burning rate was assumed. Paul and Lovine¹³ considered a non-isothermal analysis of the chamber but no flame spreading mechanism. In a later paper this group did insert an arbitrary flame spreading equation in an isothermal chamber, and the results were compared to experimental firings.

A more detailed discussion of most of these papers is given by Parker, Most, and Summerfield^{16,17}. The theoretical and experimental work at the Guggenheim Laboratory at Princeton University is discussed in detail in the next chapter.

CHAPTER II

PRELIMINARY DISCUSSION

This report presents an analytical extension of the theory of the ignition transient proposed by Parker, Most, and Summerfield^{16,17}. It will be very beneficial to the ensuing analysis to discuss both the theoretical and experimental work of Parker, and outline the experimental program now underway at the Guggenheim Laboratories of Princeton University.

The Parker analysis considers both the chamber filling process and a flame spreading mechanism. The conservation equations for a low Mach number flow in the chamber are written for the case of a gasless igniter. All the assumptions used in this analysis are discussed in the next chapter. Two separate cases for the chamber filling process are discussed.

First the temperature of the combustion gases is assumed strictly constant. This implies that there is no compressional work done on the chamber gases. Although this is not a realistic assumption, it does provide in most cases a lower boundary for the temperature and pressure conditions in an actual rocket motor. The advantage is that the resulting differential equation can be solved exactly in analytical form for the chamber filling interval. The solution for the constant temperature case shows that the pressure approaches its equilibrium value monotonically and hence, the maximum rate of rise of pressure for the given conditions is found at the beginning of the chamber filling interval. The maximum rate of rise possible under all conditions is also determined.

The other analysis allows the temperature of the combustion gases to vary with time -- Dynamic Temperature case. A system of two simultaneous differential equations are derived. If the temperature is assumed close to unity, the resulting differential equation for the chamber pressure can also be solved. This solution also shows that pressure approaches its equilibrium value monotonically and that the maximum rate of rise of pressure is at the beginning of the chamber filling interval. The solutions to these two cases differ mainly by a factor of γ , the specific heat ratio, which represents the adiabatic compression effect on the chamber gases.

The flame spreading mechanism is based on the hypothesis of successive ignitions, and the ignition criterion is

assumed for simplicity to be the attainment of a critical temperature at the surface of the grain, as was discussed in the previous chapter. A thermal analysis of the propellant, along with the ignition criterion and the chamber filling equations for the dynamic temperature case, was used for a numerical solution of the entire ignition transient.

The parameters used for the numerical solution in Parker's thesis were chosen from a small laboratory rocket motor and are listed in Table I. A schematic drawing of this rocket motor is shown in Figure (1). The slab geometry, which may be thought to represent a very thin wedge from a rocket motor with a cylindrical grain whose web thickness is small compared to the radius of curvature of the inner surface, was chosen for its convenience in diagnostic experimentation. The propellant used has the steady combustion burning rate curve shown in Figure (2), and the corresponding $P_c - K_N$ curve is shown in Figure (3). In keeping with the gasless igniter assumption of the analysis, ignition was accomplished using a hot wire igniter; nichrome wires are imbedded in a prescribed percentage of the total burning area at the head end of the rocket.

In addition to pressure measurements, the heat transfer to the propellant was measured using thin film platinum resistance gauges, and the flame spreading over the surface was observed using high speed motion pictures. The photographic observation indicated that the flame did have a front as a flame spreading model implies, but it was rather diffuse. Quite often, ahead of the front there were occasional isolated points of ignition, but these points did not appear to act as centers of flame propagation. This observation was very significant because it demonstrated that flame spreading did not start from an adjacent point of flames, that flame spreading is indeed a phenomenon of successive ignitions, each point springing to flame when its surface reached the critical value. The presence of an adjacent flamelet had no effect on this timing.

The heat transfer data suggested convection as the method of energy transfer. From the measured pressure and the assumption of no axial variation in the chamber properties, the local Reynolds number was calculated. From the output of the two heat transfer gages, one located at the mid point of the propellant slab and the other at the aft end, and the approximation that the difference in temperature between the chamber gases and the propellant surface is constant, equal to 1600°C, the Nusselt number was calculated. This result is shown in Figure (4). The line drawn through the data points has the equation

$$Nu_x = 0.09 Re_x^{0.8}$$

This equation corresponds to the heat transfer law for a rough flat plate in a turbulent free stream. A smooth flat plate would show a coefficient of 0.029; a rough plate would show a coefficient as large as 0.09 or larger. This empirical correlation appears therefore to be a logical one and may be accepted with some degree of confidence. The computer results presented by Parker are based on this heat transfer correlation.

The experimentally determined pressure was used with the theoretical chamber filling equations in order to calculate an instantaneous burning area at each instant of time. The result at first showed a physically impossible "area overshoot" at the end of flame spreading. A burning rate modification was then introduced to take account of propellant pre-heating and the re-calculated area-time curves showed a proper termination, or nearly so. These experimental area-time curves were then compared to the predicted burning area vs. time results; a typical case is shown in Figure (5). Although the predicted absolute times are not exact they are of the same order of magnitude as the spreading times obtained from the pressure data and the general shapes of the two curves are very similar. The experimental pressure curve in the chamber filling interval is higher than the computed pressure curve. This means that the actual burning rate is higher than that predicted by the power law $\dot{r}_{ss} = K p_c^n$. Possible causes of this are discussed by Parker and will be discussed in the next chapter.

This report, as mentioned before, is a theoretical extension of the above investigation. At present, the concomitant experimental program is still in progress. The basic rocket motor is the same as that used by Parker. Ignition is now accomplished by a gaseous oxygen-methane torch. The characteristic of this pyrogen igniter is discussed in References 18, 19, and 20 and a schematic of the composite system is shown in Figure (6). This experimental program is still in its early stage, and the results are of a preliminary nature and are not reported here.

However, one aspect of this system is discussed. In order to adapt the gas torch to the slab rocket motor a connecting channel $3/4$ " in length is used. The forward end of this channel serves as the leading edge of the boundary layer. Hence, the leading edge of the propellant is completely submerged in the boundary layer. If the boundary layer and propellant leading edges coincide, the empirical heat transfer law given above states that this point will experience an infinite heat transfer initially.

It should be noted here that until heat transfer measurements are made with the new system the previously determined law will be used. Because the igniter product gases of the system used in this report are considerably hotter than the propellant gas, the temperature in the chamber changes with time as the propellant gases mix with the igniter product gases. This, combined with the changing temperature of the slab due to the heat transfer, meant that a constant temperature difference between the propellant slab and the chamber gases could not be assumed. This is discussed further in a later section.

CHAPTER III

THEORETICAL DEVELOPMENT

In the previous chapter a general discussion of the ignition transient was presented. In particular, the theoretical work of Parker and the experimental work of Parker and Most were discussed in some detail. In the present chapter the basic theory presented recently by Parker, Most, and Summerfield¹⁷ is extended to the cases where an external mass source serves as an ignition stimulus. The mass source employed is characteristic of pyrogen type igniters.

A. CHAMBER FILLING

The gas dynamic equations governing the chamber filling process are discussed first. These equations not only describe the chamber filling interval fully, but they also set the environment for the induction and flame spreading intervals. Hence, it is extremely important to understand the chamber filling process before attempting to describe the other processes which occur during the general ignition transient.

The chamber filling process is, in general, a complex problem which does not lend itself to a detailed analysis. By considering certain special cases, a good deal of knowledge about the general problem can be gained. The assumptions leading to these simplified cases must be checked by diagnostic experiments, and the ultimate results of the theory must agree with the experimental results.

It is extremely helpful in the analysis of the chamber filling process to define the control volume as the free volume of the rocket chamber. The assumption that the thickness of the flame above the propellant is small compared to the dimensions of the combustion chamber insures a reaction free control volume. There are cases when this assumption is not valid. In particular, when the propellant contains metal additives the combustion process is carried throughout the combustion chamber. By assuming that the convergent section of the nozzle is short compared to the length of the rocket chamber, the control volume will contain only negligible nozzle effects. Extreme care must be exercised when the following analysis is applied to cases where these assumptions are violated.

As the propellant burns the chamber free volume is altered, and hence, the defined control volume varies with time. Depending on the grain design, the instantaneous burning area may also vary with time even after flame spreading is complete. Since the total time for the ignition transient is rather short, and since the burning rates of many propellants are relatively low, the increase in chamber volume and the change in burning area after completion of flame spreading are negligible during the chamber filling interval. During the induction and the flame spreading intervals the chamber volume may be considered constant, but the burning area is a definite function of time.

1. MOMENTUM EQUATIONS

The momentum equations for the defined control volume is

$$-\frac{1}{\rho} \nabla p = \frac{\partial \bar{V}}{\partial t} + \bar{V} \cdot \nabla \bar{V}$$

In some solid propellant rocket motors there is a low Mach number flow in the combustion chamber at the start, and hence gradients in chamber pressure are negligibly small. For high performance rocket motors with small port-to-throat area ratios, the assumption of low Mach number is taken here as an approximation. An order of magnitude analysis of the momentum equation clearly shows the range of validity of this approximation.

Selecting a characteristic chamber dimension χ_{ref} and a characteristic time t_{ref} so the dimensionless quantities are:

$$\hat{\chi} \equiv \frac{\chi}{\chi_{ref}}, \quad \hat{t} \equiv \frac{t}{t_{ref}}$$

The momentum equation (one dimensional for convenience in notation) in dimensionless form is

$$-\frac{\partial}{\partial \hat{\chi}} (\ln p) = \frac{u}{(p/\rho)} \frac{\chi_{ref}}{t_{ref}} \frac{\partial}{\partial \hat{t}} (\ln u) + \frac{u^2}{(p/\rho)} \frac{\partial}{\partial \hat{\chi}} (\ln u)$$

Assuming a perfect gas;

$$\frac{p}{\rho} = \frac{1}{\gamma} \left(\frac{\partial p}{\partial \rho} \right)_s = \frac{a^2}{\gamma}$$

Hence each term on the right hand side of the equation can be written in terms of the Mach number, M .

$$\begin{aligned} -\frac{\partial}{\partial \hat{x}} (\ln p) &= \frac{\gamma}{u} \frac{x_{ref}}{t_{ref}} M^2 \frac{\partial}{\partial \hat{t}} (\ln u) + \gamma M^2 \frac{\partial}{\partial \hat{x}} (\ln u) \\ &= 0 + O(M^2, \frac{M^2}{u} \frac{x_{ref}}{t_{ref}}) \end{aligned}$$

For low Mach number flows it can be concluded that

$$p = p(t).$$

2. CONTINUITY EQUATION

The law of mass continuity for the combustion chamber control volume, in general, is

$$\frac{dm_c}{dt} + \dot{m}_N - \dot{m}_s = 0$$

where

$$m_c = \text{instantaneous chamber mass} = \rho_c V_c$$

$$\dot{m}_N = \text{total rate of mass flow through the nozzle}$$

$$\dot{m}_s = \text{sources of mass flow}$$

There are two sources supplying mass to the control volume. The burning propellant can be represented by an overall mass burning rate, \dot{m}_b , and the ignition system injects mass into the system at a rate \dot{m}_{ign} . Hence continuity becomes;

$$\frac{dm_c}{dt} + \dot{m}_N - \dot{m}_b - \dot{m}_{ign} = 0.$$

III-I

The mass generated by the igniter depends entirely upon the properties of the given ignition system, thus making a general analysis impossible. However, given the igniter specifications, it should be possible to predict the ignition transient for a specific rocket motor.

3. ENERGY EQUATION

Since the nature of the flow in the combustion chamber is turbulent, the analysis is based on the assumption that the temperature gradients in the control volume are negligibly small. This has been called in the literature the "well-stirred combustor" assumption, but clearly there is no such stirring here, where one dimensional flow is assumed to prevail. However, the uniform temperature assumption is expected to be a fairly good approximation applicable to most rocket motors. For the very large motor a detailed analysis including the effects of the gradients of pressure and temperature must be made.

Conservation of energy in the combustion chamber control volume is

$$\begin{aligned} \frac{\partial}{\partial t} \int_V \left(e + \frac{u^2}{2} \right) \rho dV + \int_S \left(e + \frac{u^2}{2} \right) \rho \bar{u} \cdot d\bar{\sigma} \\ = - \int_S \rho \bar{u} \cdot d\bar{\sigma} + \left(\text{Heat Addition} \right) + \left(\text{Body Work} \right). \quad \text{III-2} \end{aligned}$$

Since the flame zone is assumed thin and the control volume is defined to exclude this flame zone, there is no heat release due to chemical reaction in the control volume. The heat addition term in the energy equation represents the heat loss to the chamber walls and the nozzle. Both the heat addition and the body work within the control volume are assumed negligible when compared to other terms in energy equation.

The energy equation is rearranged so that the internal energy is expressed in terms of the enthalpy.

$$\frac{\partial}{\partial t} \int_V \left(h + \frac{u^2}{2} \right) \rho dV + \int_S \left(h + \frac{u^2}{2} \right) \rho \bar{u} \cdot d\bar{\sigma} - \frac{\partial}{\partial t} \int_V p dV = 0$$

If the product gases of solid propellant combustion are assumed calorically perfect, then the enthalpy of the control volume is a function of the temperature alone. This assumption could only be valid if a thin flame zone is also assumed. With propellants that contain metal additives such as aluminum, the reaction zone would be distributed throughout the combustion chamber. Under these circumstances the gases would not be calorically perfect nor would the heat addition term in the energy equation be negligible.

Recalling the discussion concerning the momentum equation, the low Mach number flow in the chamber leads to the conclusion that the velocity term is negligible compared to the enthalpy. The reasoning is simply,

$$M^2 = \frac{U^2}{a^2} = \frac{U^2}{\gamma R T} \ll 1$$

hence

$$U^2 \ll c_p T = h \quad (\text{See footnote below})$$

From these assumptions the energy equation simplifies to

$$\frac{d}{dt} \int_V c_p T \rho dV + \int_S c_p T \rho \bar{u} \cdot d\bar{\sigma} - \frac{d}{dt} \int_V p dV = 0$$

Using the condition $\nabla p = 0$ and $\nabla T = 0$, this equation can be integrated directly. When integrating about the surface of the control volume, it is necessary to assume that the flame zone is collapsed, i.e., the products of solid propellant combustion entering the control volume, \dot{m}_b , are at the adiabatic flame temperature, T_f . It is assumed further that the composition of the igniter gas is the same as the solid propellant product gas; this assumption is used to simplify the analysis, otherwise a third equation must be introduced to account for the mixing of two gases of different compositions. The resultant energy equation is

$$\frac{d}{dt} (m_c T_c) + \dot{m}_N T_c - \dot{m}_b T_f - \dot{m}_{ign} T_{c_{ign}} - \frac{1}{c_p} \frac{d}{dt} (p_c V_c) = 0 \quad \text{III-3}$$

Using the perfect gas law and the relation $m_c = \rho_c V_c$ Equation III-3 can be rearranged to yield

$$\frac{1}{\gamma} \frac{d}{dt} (m_c T_c) + \dot{m}_N T_c - \dot{m}_b T_f - \dot{m}_{ign} T_{c_{ign}} = 0 \quad \text{III-4}$$

Actually, $h = h_o + \int_{T_o}^T c_p dT$. If we take c_p as constant in the range of interest, then $h = c_p T + (h_o - c_p T_o)$. The term in parentheses vanishes in the next step when the continuity equation is applied.

Now if the continuity equation for the control volume, Equation III-1, is multiplied by T_c and subtracted from Equation III-4, multiplied by γ , the energy equation finally can be written in the form

$$\frac{dT_c}{dt} + \frac{\dot{m}_N}{m_c} T_c (\gamma - 1) - \frac{\dot{m}_b}{m_c} (\gamma T_f - T_c) - \frac{\dot{m}_{ign}}{m_c} (\gamma T_{c_{ign}} - T_c) = 0 \quad \text{III-5}$$

If \dot{m}_b and \dot{m}_N are expressed as functions of chamber pressure and chamber temperature, all igniter properties and characteristics are known, and proper initial conditions are specified, then Equations III-1 and III-5 form a system of equations which can be used to solve the chamber conditions.

The nozzle is assumed choked throughout the entire ignition transient. This is not precisely true. The nozzle will be choked after the chamber reached a pressure level which is approximately twice the back pressure. Since this occurs very early in the chamber filling process, the assumption of a choked nozzle is made for all times. If it is assumed further that there is isentropic flow in the convergent section of the nozzle, then the mass flow through the nozzle is

$$\dot{m}_N = \frac{\Gamma P_c A_t}{\sqrt{RT_c}}$$

The mass burning rate of the propellant depends mainly upon which law for burning is used. The burning rate is a complex function of pressure, rate of change of pressure, gas velocity over the propellant surface, temperature distribution in the propellant, etc. There exists no general burning rate law. From studies on steady combustion of solid propellants, steady state burning laws do exist, but nothing substantial exists for combustion under transient conditions. A burning rate equation under certain conditions of transient pressure is discussed below and derived in Appendix I. For the present, however, the simple power law is assumed adequate.

$$r_{ss} = k p_c^\eta$$

The constants k and η are empirically determined from the steady combustion of the propellant. The mass burning rate is therefore

$$\dot{m}_b = \rho_p S_b r_{ss}$$

The mass flow from the igniter can be simply a general function of time, which goes to zero at some specified time. In an effort to describe a practical igniter system, the igniter mass source term will characterize the pyrogen igniter developed by Grant¹⁸ and used by Most at the Guggenheim Laboratories of Princeton University. A schematic drawing of the system used by Most is shown in Figure (6). The operational characteristic of this gas torch is, for the times considered in the ignition transient of the solid propellant rocket motor, approximately a square wave output in terms of mass flow, i.e., it is assumed that the gas torch reaches its steady state instantaneously*. Hence, the nozzle of the igniter is assumed to be choked throughout its operation. The mass flow which enters the solid propellant combustion chamber is therefore given by

$$\dot{m}_{ign} = \frac{\Gamma}{\sqrt{R'}} \frac{P_{c,ign}}{\sqrt{T_{c,ign}}} A_{t,ign} f(t).$$

Again it must be stated that the composition of the igniter gas is the same as the products of solid propellant combustion. The function $f(t)$ contains the cut-off criterion for the igniter. It is assumed that the capacitance of the igniter chamber does not induce any back flow from the main rocket chamber after igniter cut-off. Also the chamber conditions in the rocket chamber are assumed to have no effect on the igniter mass flow. Hence, the mass source characterized a very ideal pyrogen type igniter.

Substituting these expressions for the individual mass flow into the continuity equation, Equation III-1 becomes

$$\frac{d}{dt} (\rho_c V_c) + \frac{\Gamma P_c A_t}{\sqrt{R' T_c}} - \rho_p S_b r_{ss} - \frac{\Gamma}{\sqrt{R'}} \frac{P_{c,ign}}{\sqrt{T_{c,ign}}} A_{t,ign} f(t) = 0$$

Using the perfect gas law and the assumption that changes in the control volume are negligible during the ignition transient, continuity becomes

$$\frac{V_c}{R} \frac{d}{dt} \left(\frac{P_c}{T_c} \right) + \frac{\Gamma P_c A_t}{\sqrt{R' T_c}} - \rho_p S_b r_{ss} - \frac{\Gamma}{\sqrt{R'}} \frac{P_{c,ign}}{\sqrt{T_{c,ign}}} A_{t,ign} f(t) = 0$$

The igniter will generally cut off before equilibrium conditions are attained. (Series D is an exception.) When equilibrium is reached, $P_c = P_{eq}$, $T_c = T_f$, $\frac{d}{dt} \left(\frac{P_c}{T_c} \right) = 0$ and $S_b = A_b$, and continuity reduces to

$$P_{eq} = \left(\frac{\rho_p A_b K C^*}{A_t} \right)^{\frac{1}{1-n}} \quad \text{III-6}$$

*This function can be of any mathematical form--a step or ramp function for example--or it can be a detailed curve fitted to the igniter mass flow of an experimental igniter firing. Arbitrarily we have chosen a square wave for this particular study.

where

$$C^* = \frac{\sqrt{RT_c}}{\Gamma}$$

At this stage of the analysis it is convenient to write the governing equations in dimensionless form. From the form of the conservation equations the most convenient form of the dimensionless variables are:

$$p = \frac{P}{P_{eq}}, \quad T = \frac{T_c}{T_f}$$

$$p_{cign} = \frac{P_{cign}}{P_{eq}}, \quad T_{cign} = \frac{T_{cign}}{T_f}$$

$$S = \frac{S_b}{A_b}, \quad \tau = \frac{t}{t^*}$$

The characteristic time t^* is chosen proportional to the residence time of a gas particle in the chamber L^*/C^*

$$t^* = \frac{L^*}{\Gamma^2 C^*}$$

Continuity and energy assume the dimensionless form

$$\frac{d}{d\tau} \left(\frac{p}{T} \right) + \frac{p}{T^{1/2}} - S p'' - \frac{p_{cign} A_{cign}}{T_{cign}^{1/2} A_z} f(\tau) = 0$$

$$\frac{dT}{d\tau} + (\gamma-1) T^{3/2} + S T p'' - (\gamma-1) p T^{1/2} + \frac{p_{cign} A_{cign} T (T - \gamma T_{cign})}{T_{cign}^{1/2} A_z p} f(\tau) = 0$$

Substituting the second equation into the first in order to eliminate $dT/d\tau$ in the first equation, yields two dimensionless equations -- one for the pressure derivative and the other for the temperature derivative;

$$\frac{dp}{d\tau} = \gamma \left[S p'' - p T^{1/2} + \frac{p_{cign} T^{1/2}}{T_{cign}^{1/2} A_z} \frac{A_{cign}}{A_z} f(\tau) \right] \quad \text{III-7}$$

$$\frac{dT}{d\tau} = \frac{T}{p} \left[(\gamma-1) S p'' - (\gamma-1) p T^{1/2} + \frac{p_{cign} A_{cign} (\gamma T_{cign} - T) f(\tau)}{T_{cign}^{1/2} A_z} \right] \quad \text{III-8}$$

The presence of $S(\tau)$ in these equations makes a general solution impossible. A more detailed analysis of the interaction and an ignition criterion will combine to yield the function $S(\tau)$. This analysis is performed below.

As a note of interest, here the effect of an over-duration igniter can be seen. For the simple case of $T_{cign} = 1$, then the final equilibrium condition is found by setting $dp/d\tau$ and $dT/d\tau$ equal to zero in Equations III-7 and III-8. The equations become

$$T = 1$$

$$p - p'' = p_{cign} \frac{A_{tign}}{A_x}$$

This effect is discussed in the subsequent chapter on the results of the calculations.

4. THE CHAMBER FILLING INTERVAL

During the chamber filling interval $S(\tau)$ is, by definition, unity. The conservation equations become

$$\frac{dp}{d\tau} = \gamma \left[p'' - pT^{1/2} + p_{cign} T_{cign}^{1/2} \frac{A_{tign}}{A_x} f(\tau) \right]$$

$$\frac{dT}{d\tau} = \frac{T}{p} \left[(\gamma - T)p'' - (\gamma - 1)pT^{1/2} + \frac{p_{cign}}{T_{cign}^{1/2}} \frac{A_{tign}}{A_x} (\gamma T_{cign} - T) f(\tau) \right]$$

In most cases the igniter mass flow is cut off long before flame spreading is completed. These equations are applicable when the igniter duration, for some reason, is prolonged. The more common cases are described by

$$\frac{dp}{d\tau} = \gamma (p'' - pT^{1/2})$$

$$\frac{dT}{d\tau} = \frac{T}{p} [(\gamma - T)p'' - (\gamma - 1)pT^{1/2}]$$

III-9

This system was investigated extensively by Parker. Since the right hand side of these equations does not contain τ explicitly, a single differential equation can be considered.

$$\frac{dp}{dT} = \frac{\gamma p}{T} \left[\frac{p'' - pT^{1/2}}{(\gamma - T)p'' - (\gamma - 1)pT^{1/2}} \right]$$

A phase plane analysis of this differential equation is shown in Figure (7). For most physically realizable conditions at the beginning of chamber filling the temperature is near and slightly above unity and the pressure is relatively low, the pressure and temperature will both approach unity, the equilibrium conditions, and there will be no pressure overshoots.

A solution can be obtained to Equations III-8 to order of the deviation of the dimensionless temperature from unity. Assuming temperature can be expressed as

$$T = 1 + \Theta$$

where Θ is a small number, then to order Θ Equations III-9 reduce to

$$\frac{dp}{d\tau} = \gamma(p^n - p)$$

This is the Bernoulli differential equation for which an analytical solution is known. Hence to order Θ ,

$$p = \left[1 - (1 - p_i^{1-\pi}) e^{-\gamma(1-\pi)\tau} \right]^{\frac{1}{1-\pi}}$$

This is a monotonically increasing function of time. After examining the differential equation, the maximum $(dp/d\tau)$ is seen to occur at the beginning of the chamber filling interval. The maximum rate of rise of pressure possible is found by a straightforward differentiation process;

$$\left(\frac{dp}{d\tau} \right)_{\text{MAX}} = \gamma(1-\pi) \pi^{\frac{\pi}{1-\pi}}$$

This result is only valid to order Θ . It is expected that Θ remains small in many applications.

5. DYNAMIC BURNING RATE

The previous analysis is based on the assumption that burning rate obeys the steady state power law $r_{ss} = k p^n$. This is probably a good first approximation, but the comparison of experimental and theoretical results of Parker indicates that the burning rate law needs modification.

Recent efforts to characterize the response of solid propellant burning to rapid depressurization²¹ and rapid pressurization²² have shown that the quasi-steady burning law is not sufficiently accurate to describe the burning

rate during a pressure transient. Von Elbe's integral analysis (based on an incorrect derivation) indicates a significant change in burning rate for relatively high rates of pressure change. Parker¹⁶, using small perturbation techniques, corrected the von Elbe results by a factor of 1/2 and obtained a range of validity for the formula. The physical models used in neither of these analyses made any allowance for the energy utilized or liberated by the vaporization of the propellant. The exact problem of non-steady burning with no limits on the pressure variation has not yet been showed. However, Parker's small perturbation analysis, despite its limitations and simplifications, is adequate for the purpose of indicating how large a rate of pressure change can be permitted without modifying the burning rate laws.

The non-steady burning rate analysis of the propellant is performed in Appendix I. This analysis assumes that the pressure transient does not affect the combustion chemistry of the solid propellant; the flame temperature and surface temperature of the propellant are assumed constant. Under these circumstances the new burning rate equation, to the order of the square of the dimensionless pressure derivative, is

$$r_b = r_{ss} \left[1 + \frac{C_p(T_s - T_o)}{Q + C_p(T_s - T_o)} \frac{\eta}{2} \frac{\alpha_p}{P_c r_{ss}^2} \frac{dP_c}{dt} \right]$$

where Q , the heat of pyrolysis, is positive for an endothermic process, and $r_{ss} = k P_c^\eta$ is the steady burning law. If this equation is substituted into the continuity and energy equation, the resultant equations represent the next order of sophistication in the chamber filling analysis. This correction parameter becomes significant for values of (dP/dt) which are much higher than those encountered in this investigation. Thus, the added complexity in order to gain accuracy is not necessary. However, for cases of extremely high rates of pressure rise the burning rate correction should be used.

If the depth of the thermal wave penetrating the propellant during the pre-heating period is significant compared to the depth of propellant burned during the time from ignition to equilibrium, then during the ignition transient, burning occurs in layers of propellant which were preheated. Hence, the initial temperature distribution does affect the burning rate during the ignition transient. This was clearly illustrated by the results of Parker's investigation. In order to determine this effect on the propellant

burning rate, a detailed knowledge of the heat transfer prior to ignition must be known. Since a general analysis of the effect of the initial temperature distribution upon the burning rate does not exist, Parker resorted to a relationship of the form;

$$r_b = r_{ss} (1 + \beta \Delta T)$$

where β is a constant with units of reciprocal degrees, and ΔT is the initial temperature superiority of the layer of propellant over that for which r_{ss} was determined.

In extreme cases the pre-heating mechanism can cause a very high burning rate during pressure equilibration. The overall result might be a type of pressure overshoot sometimes observed in practical rocket motors. This type of overshoot is distinct from overshoots caused by oversized igniters. The latter type of overshoot can be predicted even with the steady state burning law.

B. FLAME SPREADING

In the previous discussion only the chamber filling process is considered. Analytical and numerical solutions of Equations III-9 are possible only during the chamber filling interval. Prior to this interval all the effects of the flame spreading process enter the problem through the parameter S , the instantaneous burning area. This section is devoted to a discussion and analysis of this process.

As explained in Chapter I, the process of flame spreading is as follows: When the igniter is fired, energy is transferred to the surface. Eventually, some portion of the surface is ignited. The newly ignited propellant burns and combines with the igniter gas to establish new conditions of energy transfer to the remaining unignited portion of the surface. This new energy transfer serves to ignite more elements of the surface. This process continues until the entire surface is ignited. The hypothesis of successive ignition states that the spreading process is simply the successive ignition of adjacent elements of the surface. The ignition of each element of surface results from the energy transfer from the gas flowing igniter from the igniter and from the previously ignited propellant upstream, not from the adjacent flame front.

Based on this hypothesis, flame spreading can be determined from a knowledge of the energy transfer to the propellant and an ignition criterion. Since the ignition

of a single element of propellant is a very complex process, a very naive approach is taken to the ignition criterion; it is assumed that this criterion is simply the attainment of a critical temperature at the surface of the propellant. This is, as Parker points out, at best, a first approximation to the actual ignition criterion.

Using the simple criterion, a temperature-time history will determine the time-to-ignition for each element of the propellant surface. Hence, a thermal analysis of the propellant will generate the function $S(\tau)$ and the chamber filling equation can be solved.

The heat conduction equation in the solid is, in general,

$$\frac{\partial T_p}{\partial t} = \alpha_p \nabla^2 T_p$$

Since the thermal conductivity of a solid propellant is very small, the depth of thermal penetration is also very small. Hence, curvature effects of the propellant can be neglected and the propellant can be assumed semi-infinite in thickness. The thermal gradient in the axial direction is relatively small, hence, conduction in this direction can be neglected. It is assumed further that there are no reactions in the solid, and the propellant is initially at a uniform temperature T_0 . Under these circumstances, the heat conduction equation and the boundary and initial conditions are

$$\frac{\partial T_p}{\partial t} = \alpha_p \frac{\partial^2 T_p}{\partial y^2}$$

$$t = 0, \quad T_p = T_0$$

$$y \rightarrow \infty, \quad T_p \rightarrow T_0$$

III-10

$$y = 0, \quad \lambda_p \frac{\partial T}{\partial y} = -q_s(x, t) = -h(T_s - T_0)$$

where x is the coordinate in the axial direction, and y is the coordinate normal to the propellant surface.

Expressing these equations in dimensionless form using the characteristic dimensions of the chamber fill process;

$$\frac{\partial T_p}{\partial \tau} = A \frac{\partial^2 T_p}{\partial^2 \eta}$$

$$\tau = 0, \quad T_p = T_o$$

$$\eta \rightarrow \infty, \quad T_p \rightarrow T_o$$

where l = length of the propellant grain, and

$$A = \left(\frac{\alpha_p}{l^2} \frac{L^*}{\Gamma^2 C^*} \right)$$

$$\eta = y/l$$

$$\xi = x/l$$

$$T_p = T_p/T_o$$

In order to write the boundary condition for the flux at the surface of the propellant, the empirical heat transfer correlation determined by Parker is used;

$$Nu_x = 0.09 Re_x^{0.8} \quad \text{III-11}$$

The heat transfer law is based on a chamber gas stream that is uniform in the axial direction. From considerations of continuity of mass, the mass flow past a given axial station x can be written;

$$\dot{m} = \dot{m}_N + \frac{l-x}{l} \frac{dm_c}{dt}$$

This equation applies only to a station x that lies downstream of the instantaneous flame front, that is, to an unignited station.* Using the perfect gas law, and the assumption of a choked nozzle (where the flow in the convergent section of the nozzle is isentropic), this mass flow equation becomes

$$\dot{m} = \frac{p_{eq} A_t}{C^*} \left[\frac{p}{T^{1/2}} + (1 - \xi) \frac{d}{d\tau} \left(\frac{p}{T} \right) \right] \quad \text{III-11a}$$

*The second term in this equation represents the mass which flows over the station x but which is stored in the chamber volume between station x and the nozzle. Thus it must be added to the \dot{m}_N term.

Hence, the mass flow per unit area is known, and using Equation III-11 the heat transfer is also known. The discussion in Chapter II explained that the leading edge of the boundary layer is a distance "a" ahead of the leading edge of the propellant, the $x=0$ point. In applying the empirical heat transfer correlation, there must be a transformation of axial distance;

$$Nu_{(a+x)} = 0.09 Re_{(a+x)}^{0.8}$$

Hence, the final boundary condition becomes;

$$\frac{\partial T}{\partial \eta} = -B \frac{(T - T_p)}{\left(\frac{a}{l} + \xi\right)^{0.2}} \left[\frac{p}{T^{1/2}} + (1 - \xi) \frac{d(p/T)}{d\tau} \right]^{0.8} \quad \text{III-12}$$

where

$$B \equiv 0.09 \left(\frac{\lambda_g}{\lambda_p} \right) \left(\frac{p_{eq} A_t l}{c^* A_p \mu_g} \right)^{0.8}$$

Assuming that there is no significant pre-heating of the propellant so that the assumption of a uniform initial temperature in the solid is valid, Equation III-10 together with its boundary conditions can be transformed into an integral equation. A standard technique, known as the Fourier Cosine Integral is used;

$$T_p(\xi, 0, \tau) - T_o = \left(\frac{A}{\pi} \right)^{1/2} \frac{B}{\left(\frac{a}{l} + \xi\right)^{0.2}} \int_0^\tau \left\{ [T(\tau') - T_p(\xi, 0, \tau')] \right. \\ \left. \cdot \left[\frac{p(\tau')}{T^{1/2}(\tau')} + (1 - \xi) \frac{d(p/T)(\tau')}{d\tau} \right]^{0.8} \frac{d\tau'}{(\tau - \tau')^{1/2}} \right\} \quad \text{III-13}$$

When a given element of surface at station ξ has reached the condition at time $\tau_{I\epsilon}$ such that

$$T_p(\xi, 0, \tau_{I\epsilon}) = T_{I\epsilon},$$

then this element of surface is said to ignite. The particular time $\tau_{I\epsilon}$ at which the ξ element of surface (the leading edge) ignites is known as the induction time τ_{IND} . Prior to this time, the flow in the chamber is from the igniter alone, and it is a constant, assuming a square wave igniter input.

$$T_{I\epsilon} - T_o = \left(\frac{A}{\pi}\right)^{1/2} \frac{B}{(\alpha/l)^{0.2}} \dot{m}_{ign}^{0.8} \int_0^{\tau} \frac{[T(\tau') - T_p(0, 0, \tau')]}{(\tau - \tau')^{1/2}} d\tau'$$

Assuming that $T - T_p(0, 0, \tau)$ is a constant and equal to the average temperature difference in this time interval, the induction time can be estimated as

$$\tau_{IND}^{1/2} \approx \frac{1}{2} \frac{(T_{I\epsilon} - T_o)(\alpha/l)^{0.2}}{\left(\frac{A}{\pi}\right)^{1/2} B \dot{m}_{ign}^{0.8}}$$

or

$$\tau_{IND} \sim \frac{1}{\dot{m}_{ign}^{1.6}}$$

Equation III-13 together with the ignition criterion and Equation III-9 form a system of equations sufficient to describe the ignition transient in solid propellant rockets. These equations, however, do not lend themselves to an exact analytical solution. Numerical solutions are obtained from a digital computer. The details of the numerical scheme are presented in Appendix II.

By physical reasoning and inspection of the dimensionless groups and equations, general trends of the solution of the chamber filling process can be anticipated:

τ (flame spreading) increases with:

$$\begin{aligned} &\text{decreasing } A^{1/2} B = \left[\left(\frac{\alpha_p}{l^2} \frac{L^*}{\Gamma^2 c^*} \right)^{1/2} \frac{0.09 \lambda_g}{\lambda_p} \left(\frac{P_{c2} A_{K2} l}{c^* A_p A_g} \right)^{0.8} \right] \\ &\text{increasing } \eta \\ &\text{increasing } \gamma \end{aligned}$$

decreases with:

$t_{\text{(induction)}}$

increasing \dot{m}_{ign}

increasing $A^{1/2} B$

increases with:

$t_{\text{(chamber filling)}}$

increasing t^*

increasing η

decreasing γ

and $P_{c.f.I}$ itself decreases with:

increasing $A^{1/2} B$

These trends will be shown in the results of the numerical solutions to the chamber filling equations.

CHAPTER IV

DISCUSSION OF RESULTS

In the previous chapter a series of equations were developed, which are sufficient to determine the flame spreading rate and the chamber properties throughout the entire ignition transient, provided suitable initial conditions are specified. These equations, even under the simplest conditions of igniter mass flow, do not lend themselves to analytical solution. However, this simple case does demonstrate the method of approach to the general ignition transient problem. These equations are repeated here for ease of discussion.

The Equations III-7 and III-8 governing the chamber filling process are:

$$\frac{dp}{d\tau} = \gamma \left[Sp^n - pT^{1/2} + p_{cign} T_{cign}^{1/2} \frac{A_{tign}}{A_t} f(\tau) \right] \quad \text{IV-1}$$

$$\frac{dT}{d\tau} = \frac{T}{p} \left[(\gamma - T) Sp^n - (\gamma - 1) pT^{1/2} + \frac{p_{cign} A_{tign}}{T_{cign}^{1/2} A_t} (\gamma T_{cign} - T) f(\tau) \right] \quad \text{IV-2}$$

where $f(\tau)$ contains the igniter cut-off criterion. The integral form of the heat conduction Equation III-13 for the surface temperature of the propellant is:

$$T_p(\xi, 0, \tau) - T_0 = \left(\frac{A}{\pi} \right)^{1/2} \frac{B}{\left(\frac{a}{\lambda} + \xi \right)^{0.2}} \int_0^\tau \left\{ \left[T(\tau') - T_p(\xi, 0, \tau') \right] \cdot \left[\frac{p(\tau')}{T^{1/2}(\tau')} + (1 - \xi) \frac{d(p/T)(\tau')}{d\tau} \right]^{0.8} \frac{d\tau'}{(\tau - \tau')^{1/2}} \right\} \quad \text{IV-3}$$

and the ignition criterion is: $T_p(\xi, 0, \tau_{IG}) = T_{IG}$

The initial conditions which must be specified are $p(0)$, $T(0)$, and $S(0)$. The physical situation dictates a zero initial burning area, and the initial pressure is at the ambient into which the rocket exhausts. Zero time is defined as that time when the igniter begins firing. In

all cases, the igniter was chosen to fire as a square wave, i.e., instantaneous onset of a constant mass rate of flow, and instantaneous ending when the igniter cut-off criterion is reached. The initial temperature of the chamber gas was taken to be the temperature of the igniter gas.

The calculation of $S(\tau)$, $p(\tau)$ and $T(\tau)$ from these equations is presented in Appendix II along with the actual Fortran program that was used. The results of the calculations are shown in Figures (8) through (44). The rocket motor design and ignition system design parameters are summarized in Table II, and main results of six series of calculations are summarized in Table III.

Before considering these series of calculations, however, it will be beneficial to explain certain results which are characteristic of all the individual calculations. Firing 2 of Series A, Figure (22), is a typical case. Initially at $t=0$, the chamber pressure is 15 psia, and the gas temperature is 2600°K , the temperature of the igniter gas. The pressure then begins to rise due to the filling process, and the gas temperature rises due to compression, but as the pressure reaches its pre-ignition equilibrium value, the temperature returns to its initial value of 2600°K . The chamber properties remain at these values (steady flow situation) until the grain begins to burn. The pressure then rises as the mass flow from the propellant becomes significant, and the temperature decreases as the cooler combustion gas of the main propellant mixes with the igniter gas.

When 30% of the grain has been ignited, mass flow from the igniter is cut off, as planned for the series, causing a discontinuous change in mass flow rate. Consequently, the pressure decreases momentarily; similarly, the heat transfer to the propellant surface decreases. This causes a sharp drop in flame spreading rate (almost to zero). As the flame spreading continues, the pressure, obeying the chamber filling equations, continues to rise. The temperature, responding to the compressive effect of the steep part of the pressure rise, climbs again, but its rise is neutralized to some extent by the fact that the propellant combustion gas happens to be cooler than the igniter gas. Depending on the relative magnitudes of these two processes, the temperature may rise, fall or remain fairly constant. As more and more of the propellant burns, the pressure rises to its equilibrium value, and the temperature begins to fall toward the equilibrium value for the main propellant.

When the flame spreading is complete, a process of feedback ensues whereby the pressure increases, thus increasing

the burning rate, and thereby sending more mass into the chamber to increase the pressure further. In this manner, equilibrium conditions are reached in the chamber.

Several interesting results can be pointed out. One is that when flame spreading is complete, the chamber pressure is usually well below 50% of the design equilibrium pressure. Also, it was noticed empirically that the maximum value for (dp/dt) occurred at the very beginning of the chamber filling interval. As was shown in the previous chapter, if the maximum (dp/dt) occurs within the chamber filling interval and if the temperature is reasonably close to its equilibrium value, then it can be proved that the maximum value of the pressure rise must occur exactly at the beginning of the interval. However, it must remain an empirical fact so far that $(dp/dt)_{max}$ does indeed occur during the chamber filling interval, and its value depends on the pressure level at the beginning of the interval.

With these ideas in mind, the results of each series can be discussed. Series A is a set of 5 individual calculations for fixed motor geometry and variable igniter flow rate. The results of the individual firings are shown in Figures (20) - (24). Figures (8) and (9) represent composites of the individual firings. As seen from these graphs, the induction times all show the proper relative order of magnitude. This is the primary effect of increasing the igniter flow, as can be seen in Table III. Since the igniter cuts off in the middle of flame spreading, the times for flame spreading are all similar. Because the pressure at the end of flame spreading is nearly the same for all five cases, and the igniter has been shut off, the length of the chamber filling interval is nearly the same for all five.

The very low mass flow rate igniter (Firing A-1) is similar to the cases considered by Parker. If his choice of initial burning area at the low initial pressure is converted to an exterior mass flow source, this would be a very low mass flow igniter. This firing yielded an induction time of fifty-five t^* units; hence there is a good deal of pre-heating of the propellant. This analysis does not account for any burning rate modification due to propellant pre-heating.

The time at which the igniter cuts off in the different runs of the series decreases for increasing mass flow. This is not surprising, since the heat transfer is proportional to the mass flow, and hence the time at which 30% area is ignited, which is the cut-off criterion, occurs sooner. There is a surprising result for the flame spreading rate.

This is seen clearly in Figure (9). Before the igniter is cut off, the initial flame spreading rate is roughly proportional to the mass flow rate of the igniter. After the cut-off, however, the mass flow rate is reduced discontinuously. This change is, of course, most drastic for the very high mass flow rate, and hence, the heat transfer drops with greatest sharpness for such cases. Consequently, the total time for flame spreading is longer than for a lower igniter mass flow rate. Another observation is that the maximum rate of rise of pressure decreases with increasing igniter flow rate, mainly because the value of the pressure at the beginning of the chamber filling interval increases, and the maximum (dp/dt) was shown to occur at the start of chamber filling.

Reference to Figure (8) shows that, after a certain point, increasing the igniter strength does not shorten the total length of the transient. In fact, doubling the mass rate of flow of the igniter from Firing A-4 to A-5 increased the time to reach ninety-eight percent of equilibrium pressure. It must be remembered, though, that, due to the igniter cut-off criterion in this series, we are comparing igniters of different total mass. This is true for all the series except E.

Decreasing the port area will decrease the overall time to attain equilibrium. This set of calculations is represented by Series B, where the port area is systematically decreased while the motor length is held constant. The chamber volume is therefore lowered, and thus the L^* and characteristic times are also decreased. The individual firings are shown in Figures (25) - (28), and the composite results are shown in Figures (10) and (11). Several expected trends are exhibited. Even though the mass flow is the same for each firing, the mass flow per unit area in the chamber does increase, hence, the heat transfer to the propellant increases. Consequently, the induction time and the total time for flame spreading decrease with decreasing port area. An interesting point is that, for the very low port area, the bootstrap rise of burning rate is sufficiently rapid to overcome the pressure decrease seen in other runs due to the igniter mass flow cut-off. The ignition shock, or $(dp/dt)_{max}$, increases with decreasing port area. This is due to two effects: first, the pressure at the end of flame spreading is lower, and second, the characteristic time of the motor is smaller. The latter tends to accelerate all chamber events, but does not affect the rate of flame spreading. The shorter characteristic time also accounts for the faster chamber filling intervals of the smaller port area firings.

Opening the nozzle throat area results in decreased equilibrium pressure. Figures (29) - (32) represent the individual calculations for this series of firings, Series C. The composite results of Series C are shown in Figures (12) and (13). The induction times are identical because the heat transfer depends on the mass rate of flow per unit area and the temperature of the chamber gases, and these are the same for the whole series. The flame spreading times, though, go up with decreasing throat area. During most of flame spreading the igniter is off, and the principal source of mass flow is the part of the propellant that has been ignited. This mass flow is larger with higher chamber pressure, and thus with smaller throat areas. Thus the heat transfer is greater for the smaller throat, and the flame spreading time is faster. On the other hand, the chamber filling times decreased with increasing throat area, due to the decreasing characteristic time of the chamber. These two effects nearly canceled out, in this series, and the overall ignition transient length was nearly constant.

Series D [Figures (33) - (35), (14) and (15)] demonstrates the possibility of a pressure overshoot due to an igniter which keeps firing after the normal equilibrium pressure of the motor has been reached. In these cases the igniter was cut off six \pm units after the completion of flame spreading. As shown in a previous section, the magnitude of the overshoot depends on the amount of mass the igniter injects into the system. This was demonstrated by the three firings of this series. In each case, after the igniter was cut off, the pressure in the motor subsided to the normal equilibrium condition.

In Series E the effect of changing the mass rate of flow in an igniter of constant total mass has been demonstrated. This series is shown in Figures (36) - (40), (16) and (17). Firing E-1 is the design operation of the igniter -- it fired until ninety-eight per cent of the equilibrium pressure of the motor was reached. After igniter cut-off, the chamber pressure stayed near equilibrium.

From Equation IV-3 it can be seen that

$$T_s \sim \dot{m}^{0.8} t^{0.5}$$

for constant \dot{m} and $(T - T_p)$, so that the Equation IV-3 can be directly integrated. For a constant mass flow igniter, it is apparent that

$$t_{ign} = \frac{m_{ign}}{\dot{m}_{ign}}$$

Where t_{ign} is the total firing time of the ignitor. Thus:

$$T_s \sim \dot{m}_{ign}^{0.3}$$

for an igniter of constant total mass, and T_s is the temperature at the end of the igniter firing. From this bit of reasoning, it can be seen that, although a given igniter may contain enough total mass for a successful ignition transient, if it is fired at too low a mass rate of flow, a hangfire may occur. This was exactly the result of Series E. As the igniter mass rate of flow was lowered from the design operation at E-1 to E-3, which fired at two-thirds the design mass rate of flow, the length of each of the three intervals as well as the sum increased. The lengths of the first two intervals increased due to the lower heat transfer, and that of the last due to the double effect of a shorter firing of a weaker igniter during the chamber filling interval. Firing E-5 was a definite hangfire, where the surface temperature of the first bit of grain had not attained the ignition temperature by the time the igniter was cut off. Firing E-4 was an intermediate case -- when the igniter cut off, four per cent of the grain had been ignited. The cut-off drastically reduced the mass rate of flow in the motor, greatly diminishing the heat transfer to successive elements of the grain. The calculations indicated that flame spreading would eventually restart, successfully igniting the motor, but not within a reasonable length of computer time.

The results of Series C indicated that reducing the throat area of a given solid propellant rocket motor has the following effects: (1) no change in the induction time; (2) a slight reduction in the flame spreading time; (3) a substantial increase in the rate of pressure rise right after the completion of flame spreading. It can therefore be seen that if the throat area of a motor could be kept small during the first two intervals and during part of the third, and then released to the design area condition just before the pressure exceeds the design pressure the overall transient would be shortened. The reduction in the overall time achieved with this temporary closure comes about, first, by the attainment of a higher pressure at the end of flame spreading and the start of chamber filling, and second, a more rapid rate of pressure rise in the early part of the chamber filling interval. Some of the advantage is retained even if the temporary closure is released right at the end of the flame spreading interval, but the greatest reduction is achieved by releasing it right at the design pressure (a tricky business, in practice).

This conclusion was tested on the computer in the final series, Series F [Figures (18), (19), and (41) - (44)]. Firing F-1 is the rocket motor with no nozzle closure. In Firings F-2, 3, and 4 the throat area was kept smaller than the design condition, until the end of flame spreading, when the partial nozzle closure was removed and the throat area became the design size. The cases run were for partial nozzle closures designed to give three, five, and seven times the design equilibrium pressure. As can be seen from Table II, the use of the partial nozzle closure was not overly effective. In Firing F-3 the closure was removed at ninety-five per cent of the final equilibrium pressure; the ignition transient was shortened by twenty per cent. With smaller nozzle closures, the chamber filling time was successively reduced due to the higher pressure at the end of flame spreading. Of importance also is the fact that the ignition shock was greatly intensified by the partial nozzle closures.

An interesting effect of the throat size in flame spreading was demonstrated in Series F. In Figure (19) it can be seen that while the smaller throat accelerates the early stages of flame spreading, for very small throats the rate of flame spreading actually declined near the end. Equation III-11a shows that there are two terms in the mass rate of flow over a station on the grain: the first term is the flow through the nozzle, the second is the part of the mass accumulation that must pass over the station. Table III shows that, relative to the equilibrium pressures with the nozzle closures in, flame spreading ended at successively lower pressures for lower throat sizes. These lower pressures cause high ρ/τ derivatives, and thus the mass accumulation term in Equation III-11a is the more important of the two. But - as $\xi \rightarrow 1$, i.e. flame spreading nears completion, this term disappears, as $(1-\xi) \rightarrow 0$. Thus, near the nozzle, and toward the end of the flame spreading interval, the grain sees less mass flow - most of the mass is being accumulated in the chamber behind it, and thus the rate of flame spreading drops off as shown. This was accentuated by the smaller throat size. The smaller throat accelerated flame spreading, causing it to occur while ρ was lower and $d(\rho/\tau)/d\tau$ was higher.

On the whole, then, the computer predictions generally confirmed conclusions that were drawn from analysis of the dimensionless groups of the equations, as well as agreeing with most long-held ideas of rocket engineers. However, examination of the details of the computer-predicted firing curves brought to the fore one point that is not generally known by rocket test engineers whose job it is to interpret pressure traces in terms of events taking place in the rocket motor, that is, that flame spreading in a rocket motor

is often complete long before the 50% point is reached on the pressure rise curve. Therefore, efforts to soften a pressure rise or to contain the rise curve within specified limits should be focused on the factors that affect the chamber filling process.

CHAPTER V

CONCLUSIONS

The theory of the ignition transient in solid propellant rocket motors proposed by Summerfield and Parker was extended in this report to cases where the burning in the main rocket motor is initiated by a pyrogen type igniter. The goal of the present work was the application of this theory to practical rocket systems. The theory is developed mainly from first principles, except where empirical laws for burning rate and convective heat transfer had to be used. An experimental program is underway at Princeton which will serve to compare theoretical and experimental results, but it is still in its early stages, and systematic results are yet to be obtained.

In the theoretical model, the ignition interval is divided into three consecutive intervals, the ignition lag or induction interval, the flame spreading interval, and the chamber filling. The ignition lag is simply the time it takes to heat the first element of surface to ignition. This ignition lag is basically a function of the mass flow rate of the igniter and the chamber geometry. Since the ignition criterion is taken to be merely the attainment of a critical temperature, the ignition delay reported here can be regarded only as a first approximation to the actual delay. A more accurate ignition criterion would take into account pressure, gas velocity, and other factors.

A few of the more interesting results of the computer study can be summarized as follows. Increasing the igniter mass flow rate decreases the induction time to first ignition and increases the rate of flame spreading. This is due to the increased heat flux to the propellant surface. The induction interval is relatively independent of the magnitude of the exhaust nozzle area, if other things are held fixed. Decreasing the port cross-sectional area decreases the time to reach equilibrium operating conditions, i.e., steepens the rate of rise. The maximum pressure overshoot above the final equilibrium value increases with increasing igniter mass flow rate.

The maximum rate of rise of pressure in the chamber is found to occur at the beginning of the chamber filling interval, but it depends also on the chamber pressure at the end of flame spreading and hence on the rate of flame spreading. In particular, the maximum rate of rise of pressure (which occurs after flame spreading is complete) can be reduced by

(Continued on page 35-A)

arranging conditions to slow down the rate of flame spreading. Increasing the igniter flow rate, decreasing the port cross-sectional area and decreasing the nozzle area all increase the maximum rate of rise of pressure.

It was found, as expected, that a closure of the exhaust nozzle that ruptures at some mid-pressure hastens the rise to full pressure. However, it was observed that the effect was much smaller than is popularly supposed in the rocket design field.

Although direct experimental comparisons have yet to be produced, it appears from examination of the four series of theoretical firings that the present theory is on the right track. Useful predictions of ignition pressure transients, hence initial thrust transients are now possible, at least for rocket motors with head-end igniter of the pyrogen type.

REFERENCES

1. M. Summerfield, R. Shinnar, C. E. Hermance, and J. Wenograd, "A Critical Review of Recent Research on the Mechanism of Ignition of Solid Propellant Rocket Propellants, Aero. Engng. Report 661, Princeton University, Princeton, New Jersey, 26 August 1963.
2. E. W. Price, H. H. Bradley, Jr., G. L. Dehority, M. M. Ibirice, "Theory of Ignition of Solid Propellants", AIAAJ, 4, 1153-1181 (1966).
3. R. F. McAlevy, R. S. Magee and J. A. Wrubel, "Flame Spreading Over the Surface of Double Base Propellants", AIAA Preprint No. 64-109, January 1964.
4. R. F. McAlevy, R. S. Magee, J. A. Wrubel and F. Horowitz, "Flame Spreading Over the Surface of Igniting Solid Rocket Propellants and Propellant Ingredients", AIAA Paper No. 66-68, January 1966.
5. R. F. McAlevy, R. S. Magee, J. A. Wrubel and F. Horowitz, "Flame Spreading Over the Surface of Igniting Solid Rocket Propellants and Propellant Ingredients", AIAA J., Vol 5 No. 2, (1967).
6. C. H. Fullman, F. B. Nielsen, J. J. Priapi and C. M. Frey, "Theoretical and Experimental Investigations of Ignition Systems for Very Large Solid-Propellant Motors", United Technology Center, Sunnyvale, California, Final Report, Contract No. AF 04(611)-7559, May, 1963. (Classified)
7. R. C. Mitchell and N. W. Ryan, "Flame Spreading on Solid Propellant", AIAA Preprint No. 64-128, January 1964.
8. R. S. Brown, T. K. Wirrick and R. Anderson, "Theory of Ignition and Ignition Propagation of Solid Propellants in a Flow Environment," AIAA Preprint No. 64-157, January 1964.
9. M. Barrere, A. Jaumotte, B. Fraeijs de Veubeke and J. Vandenkerckhove, Rocket Propulsion (Elsevier, Amsterdam, 1960), pp. 237-239.
10. T. von Karman and F. J. Malina, "Characteristics of the Ideal Solid Propellant Rocket Motor", Jet Propulsion Laboratory, Calif. Inst. of Tech. Report No. 1-4, 1940. Reprinted in Collected Works of Theodore von Karman, Vol. IV, 1940 - 1951 (Butterworth, London, 1956).
11. S. de Soto and H. A. Friedman, "Flame Spreading and Ignition Transients in Solid Grain Propellants", AIAA J. 3, 405-412 (1965).

REFERENCES - Cont'd.

12. H. H. Bradley, "Theory of a Homogeneous Model of Rocket Motor Ignition Transients", AIAA Preprint No. 64-127, January 1964.
13. B. E. Paul and R. L. Lovine, "Ignition Problems in Solid Propellant Rockets", Aerojet General Corp., Sacramento, Calif., 1 February 1965.
14. D. S. Allan, E. K. Bastress, and K. A. Smith, "Heat Transfer During Ignition of Solid Propellant Rockets", AIAA Paper No. 66-66, January 1966.
15. K. H. Parker, J. Wenograd, and M. Summerfield, "The Ignition Transient in Solid Propellant Rocket Motors", AIAA Preprint No. 64-126, January 1964.
16. M. Summerfield, K. H. Parker, W. J. Most, "The Ignition Transient in Solid Propellant Rocket Motors", Aerospace and Mechanical Science Report 769, Princeton University, Princeton, New Jersey, 10 February 1966.
17. K. H. Parker, W. J. Most, and M. Summerfield, "The Ignition Transient in Solid Propellant Rocket Motors", Astronautica Acta Vol. 12, No. 4 (1966).
18. R. W. Lancaster and M. Summerfield, "Experimental Investigation of the Ignition Process of Solid Propellants in a Practical Motor Configuration", Aero. Engng. Report 548, Princeton University, Princeton, New Jersey, 3 May 1961.
19. E. H. Grant, J. Wenograd, M. Summerfield, "Research on Solid Propellant Ignitability and Igniter Characteristics", Aero. Engng. Report 662, Princeton University, Princeton, New Jersey, 31 October 1963.
20. E. H. Grant, Jr., R. W. Lancaster, J. Wenograd, and M. Summerfield, "A Study of the Ignition of Solid Propellants in a Small Rocket Motor", AIAA Preprint No. 64-153, January 1964.
21. G. von Elbe, "Theory of Solid Propellant Ignition and Response to Pressure Transients", (Unclassified), Bulletin of the Interagency Solid Propulsion Meeting, July 1963, Vol. III (Classified), p. 95.
22. H. Krier, G. di Lauro, L. Kurylko, M. Summerifeld, "Non-Steady Combustion of Solid Propellants with Special Reference to Rocket Instability" Aero. & Mech. Science Report 773, Princeton University, Princeton, New Jersey, March 1966.

REFERENCES - Cont'd.

23. M. Summerfield, et al., "Burning Mechanism of Ammonium Perchlorate Propellants", Progress in Astronautics and Rocketry: Solid Propellant Rocket Research (Academic Press, Inc., New York, 1960), pp. 141-182.
24. D. D. McCracken and W. S. Dorn, Numerical Methods and Fortran Programming (John Wiley and Sons, Inc., New York, 1965), Chapter 10.

LIST OF SYMBOLSLatin

a distance of boundary layer leading edge ahead of propellant leading edge

A_b total grain surface

A_p port area

A_t main rocket nozzle throat area

$A_{t_{ign}}$ igniter nozzle throat area

C_p specific heat of propellant gas products

c^* characteristic velocity $\equiv \frac{\sqrt{RT_f}}{\Gamma}$

d_t diameter of main rocket nozzle throat

$d_{t_{ign}}$ diameter of igniter nozzle throat

e internal energy

h heat transfer coefficient

k constant and burning rate law, $r_{ss} = k P_e^n$

K_N ratio of burning area to nozzle throat area $\equiv \frac{A_b}{A_t}$

l length of propellant grain

LIST OF SYMBOLS - Cont'd.

L^*	characteristic length $\equiv V_c/A_t$
\dot{m}_b	mass burning rate
m_c	mass of gas in combustion chamber
m_{eq}	mass of gas in combustion chamber at equilibrium
\dot{m}_{ign}	mass flow rate from igniter
m_{ign}	total mass of igniter gas
\dot{m}_N	mass flow rate through main rocket nozzle
n	power in burning rate law,
Nu_x	Nusselt number $\equiv \frac{h x}{\lambda_g}$
p	dimensionless chamber pressure $= p_c/p_{eq}$
p_c	chamber pressure
$p_{c_{ign}}$	pressure of igniter gas
p_{eq}	chamber pressure at equilibrium
p_I	initial chamber pressure
Q	heat of pyrolysis of propellant
r_b	dynamic burning rate
r_{ss}	quasi-steady burning rate

LIST OF SYMBOLS - Cont'd.

R	specific gas constant
Re_x	Reynolds number based on x , $\equiv \frac{\rho_g u x}{\mu_g}$
S	dimensionless burning area $\equiv \frac{S_b}{A_b}$
S_b	instantaneous burning area
t	time
t^*	characteristic time $\equiv \frac{L^*}{\Gamma^2 c^*}$
T	dimensionless chamber temperature $\equiv T_c/T_f$
T_c	chamber temperature
$T_{c_{ign}}$	temperature of igniter gas
T_f	flame temperature
T_{ig}	ignition temperature of propellant
T_o	initial temperature of propellant
T_s	surface temperature of propellant
u	gas velocity
V_c	chamber volume
x	axial distance

LIST OF SYMBOLS - Cont'd.

y distance normal to propellant surface

Greek

d_p thermal diffusivity of propellant

β coefficient of thermal sensitivity of propellant

γ ratio of specific heats

Γ a function of γ , $\equiv \sqrt{\gamma \left(\frac{2}{\gamma-1} \right)^{\frac{\gamma+1}{\gamma-1}}}$

η dimensionless distance normal to propellant surface $= y/l$

λ_g thermal conductivity of chamber gases

λ_p thermal conductivity of propellant

μ_g viscosity of chamber gases

ξ dimensionless axial distance $\equiv x/l$

ρ_c density of chamber gases

ρ_p density of propellant

τ dimensionless time $\equiv \frac{t}{t^*}$

τ_{IND} time for first element of surface to ignite
(induction time of rocket motor)

$\bar{\sigma}$ area normal to flux

TABLE I

DESIGN OF SLAB GEOMETRY SOLID PROPELLANT ROCKET MOTOR

Rocket Motor

$$d_t = 44 \text{ cm.}$$

$$V_c = 140 \text{ cm}^3$$

$$A_b = 46 \text{ cm}^2$$

$$l = 24 \text{ cm.}$$

$$A_p = 4.0 \text{ cm}^2$$

Propellant

$$\eta = 0.4$$

$$k = 2.0 \times 10^{-2} \text{ in/sec } \left(\frac{1}{\text{psia}}\right)^{0.4}$$

$$= 5.9 \times 10^{-4} \frac{\text{cm}}{\text{sec}} \left(\frac{\text{cm}^2}{\text{dyne}}\right)^{0.4}$$

$$\rho_p = 1.6 \text{ g/cm}^3$$

$$C_p = 0.3 \text{ cal/g } ^\circ\text{C}$$

$$\lambda_p = 9 \times 10^{-4} \text{ cal/cm sec } ^\circ\text{C}$$

$$T_{ig} = 420^\circ\text{C}$$

Combustion Gases

Theoretical @ 90 psia

$$T_f = 2076 \text{ } ^\circ\text{K}$$

$$c^* (\text{frozen}) = 4384 \text{ ft/sec}$$

$$c^* (\text{equilibrium}) = 4397 \text{ ft/sec}$$

$$C_f = .441 \text{ cal/g } ^\circ\text{C}$$

$$\gamma = 22.22$$

TABLE I
(continued)

Theoretical @ 300 psia

$$T_f = 2078^\circ\text{K}$$

$$c^* (\text{frozen}) = 4386 \text{ ft/sec}$$

$$c^* (\text{equilibrium}) = 4397 \text{ ft/sec}$$

$$C_g = .441 \text{ cal/c } ^\circ\text{C}$$

$$\gamma_g = 22.23$$

Composition

<u>Species</u>	<u>Mole Fraction</u>
CO	.256
H ₂ O	.242
H ₂	.215
HCl	.152
N ₂	.176
CO ₂	.060

$$\gamma = 1.26$$

$$\mu_g (2000^\circ\text{K}) = 6.6 \times 10^{-4} \text{ g/cm sec}$$

$$\mu_g (1200^\circ\text{K}) = 4.9 \times 10^{-4} \text{ g/cm sec}$$

$$\lambda_g (2000^\circ\text{K}) = 3.6 \times 10^{-4} \text{ cal/cm sec } ^\circ\text{C}$$

$$\lambda_g (1200^\circ\text{K}) = 2.4 \times 10^{-4} \text{ cal/cm sec } ^\circ\text{C}$$

TABLE II
COMPENDIUM OF DESIGN PARAMETERS
SERIES A,B,C,D

Serial No.	p_{eq} psia	A_t cm ²	K_N	A_p cm ²	A_p/A_t	L^* in	t^* msec	\dot{m}_{ign} lb/sec	$P_{pre-ign}$ % Peq	% burning area	Igniter cut off criterion	Igniter duration	
A-1	600	.150	307	4.0	26.7	368	17.6	2.65	2.62	30		1082	
A-2	600	.150	307	4.0	26.7	368	17.6	7.95	7.85	30		204	
A-3	600	.150	307	4.0	26.7	368	17.6	10.6	10.5	30		130	
A-4	600	.150	307	4.0	26.7	368	17.6	26.5	26.2	30		31.2	
A-5	600	.150	307	4.0	26.7	368	17.6	53.0	52.5	30		11.5	
												2.87	
												1.62	
												1.37	
												.828	
												.610	
B-1	600	.150	307	4.0	26.7	368	17.6	7.95	7.85	30		204	
B-2	600	.150	307	2.0	13.3	241	11.6	7.95	7.85	30		66.4	
B-3	600	.150	307	1.0	6.67	178	8.54	7.95	7.85	30		21.1	
B-4	600	.150	307	0.5	3.33	131	6.28	7.95	7.85	30		6.92	
												.0548	
C-1	600	.150	307	4.0	26.7	368	17.6	7.95	7.85	30		204	
C-2	500	.168	274	4.0	23.8	328	15.7	7.95	8.52	30		205	
C-3	400	.191	241	4.0	20.9	289	13.8	7.95	9.34	30		206	
C-4	300	.228	202	4.0	17.5	242	11.6	7.95	10.4	30		204	
												1.62	
												1.62	
												1.63	
												1.62	
D-1	600	.150	307	4.0	26.7	368	17.6	26.5	26.2	$6 L^*$ units after $P=1.0$			150
D-2	600	.150	307	4.0	26.7	368	17.6	15.9	15.7			190	
D-3	600	.150	307	4.0	26.7	368	17.6	7.95	7.85			327	
												2.60	

TABLE II - Cont'd.
COMPENDIUM OF DESIGN PARAMETERS
SERIES E, F

Serial No.	P_{01} psia	A_E cm ²	K_N	A_p cm ²	A_p/A_L	L^* in	t^* msec	\dot{m}_{ign} lb/sec	$P_{pre-ign}$ % Peq	% burning area	Igniter cut off criterion	Igniter duration
E-1	600	.150	307	4.0	26.7	368	17.6	7.95	7.85			269
E-2	600	.150	307	4.0	26.7	368	17.6	6.62	6.54			321
E-3	600	.150	307	4.0	26.7	368	17.6	5.30	57.5			401
E-4	600	.150	307	4.0	26.7	368	17.6	3.97	3.93			536
E-5	600	.150	307	4.0	26.7	368	17.6	2.05	2.62			802
F-1	600	.150	307	4.0	26.7	368	17.6	7.95	8.85			203
F-2	1800	.078	590	4.0	51.2	706	33.9	7.95	15.2			190
F-3	3000	.057	808	4.0	70.2	967	46.1	7.95	20.3			182
F-4	4200	.047	479	4.0	85.0	1179	55.3	7.95	25.2			171
	600	.150	307	4.0	26.7	368	17.6	7.95				1.36

When
 $\dot{m}_{ign} t = m_{ign}$

COMPENDIUM OF COMPUTER RESULTS
TABLE III
SERIES A, B, C

Serial No.	$\left(\frac{dp}{dt}\right)_{max}$	Induction Time	Time for Flame Spreading	Time for Chamber Filling (To 98% p_g)	Total time to 98% p_g	Pressure Overshoot	Pressure at end of Flame Spreading
	psia/sec	msec	msec	msec	msec	% Peq	% Peq
A-1	12,270	963	146	100	1210	0	.285
A-2	12,410	163	77.7	104	345	0	.330
A-3	12,560	102	79.9	102	284	0	.334
A-4	12,760	19.0	119	105	243	0	.326
A-5	12,790	5.9	137	105	247	0	.323
B-1	12,410	163	77.7	104	345	0	.330
B-2	19,700	52.1	30.0	69.9	152	0	.284
B-3	27,300	16.0	13.1	52.7	81.8	0	.239
B-4	38,100	5.05	6.10	39.8	50.9	0	.195
C-1	12,410	163	77.7	104	345	0	.330
C-2	11,420	163	83.0	92	338	0	.349
C-3	10,370	163	96.7	82	342	0	.363
C-4	8,480	163	119.6	67	350	0	.384
D-1	19,600	18.7	10.4	32	61.0	39.9	.584
D-2	17,200	48.6	35.7	38	112	23.7	.473
D-3	15,000	163	58.9	43	267	11.1	.381

COMPENDIUM OF COMPUTER RESULTS
TABLE III - Cont'd.
SERIES A, B, C

Serial No.	$\left(\frac{dp}{dt}\right)_{MAX}$	Induction Time	Time for Flame Spreading	Time for Chamber Filling (To 98% p_y)	Total time to 98% p_y	Pressure Overshoot	Pressure at end of Flame Spreading
	psia/sec	msec	msec	msec	msec	% p_{eq}	% p_{eq}
E-1	14,900	163	58.4	67	288	0	.381
E-2	14,500	221	71.4	96	388	0	.356
E-3	14,200	318	81.8	102	502	0	.353
E-4	1,000	495	1000		1500	0	
E-5	648					0	
F-1 S 1		163	77.7				.330
S 1	12,500			104	345	0	.330
F-2 S 1		156	65.5				.229
S 1	20,300			86	307	0	.687
F-3 S 1		149	65.4				.190
S 1	25,000			60	275	0	.950
F-4 S 1		143	65.5				.165
S 1	28,900			0	197	15.7	1.16

SCHEMATIC OF EXPERIMENTAL ROCKET MOTOR

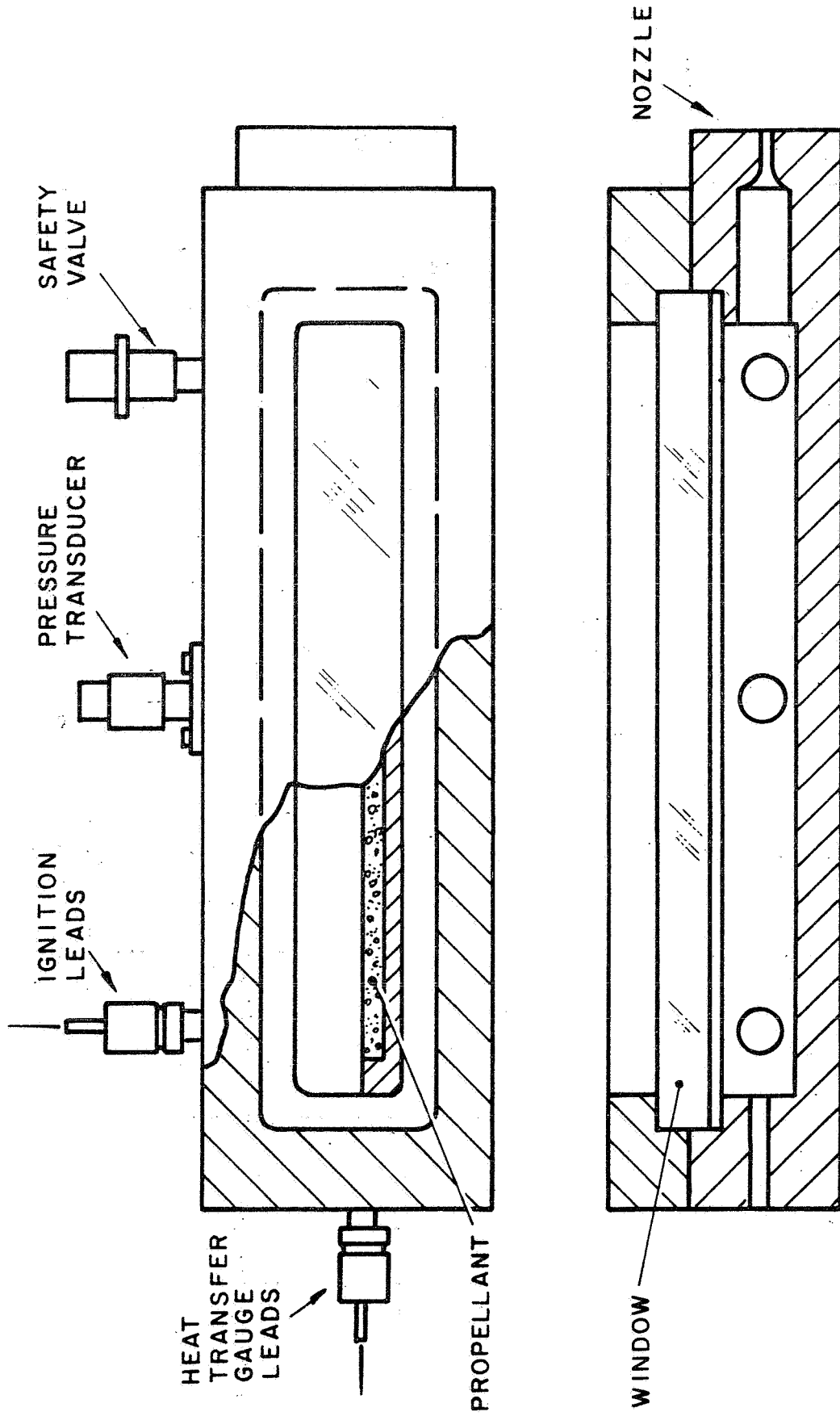
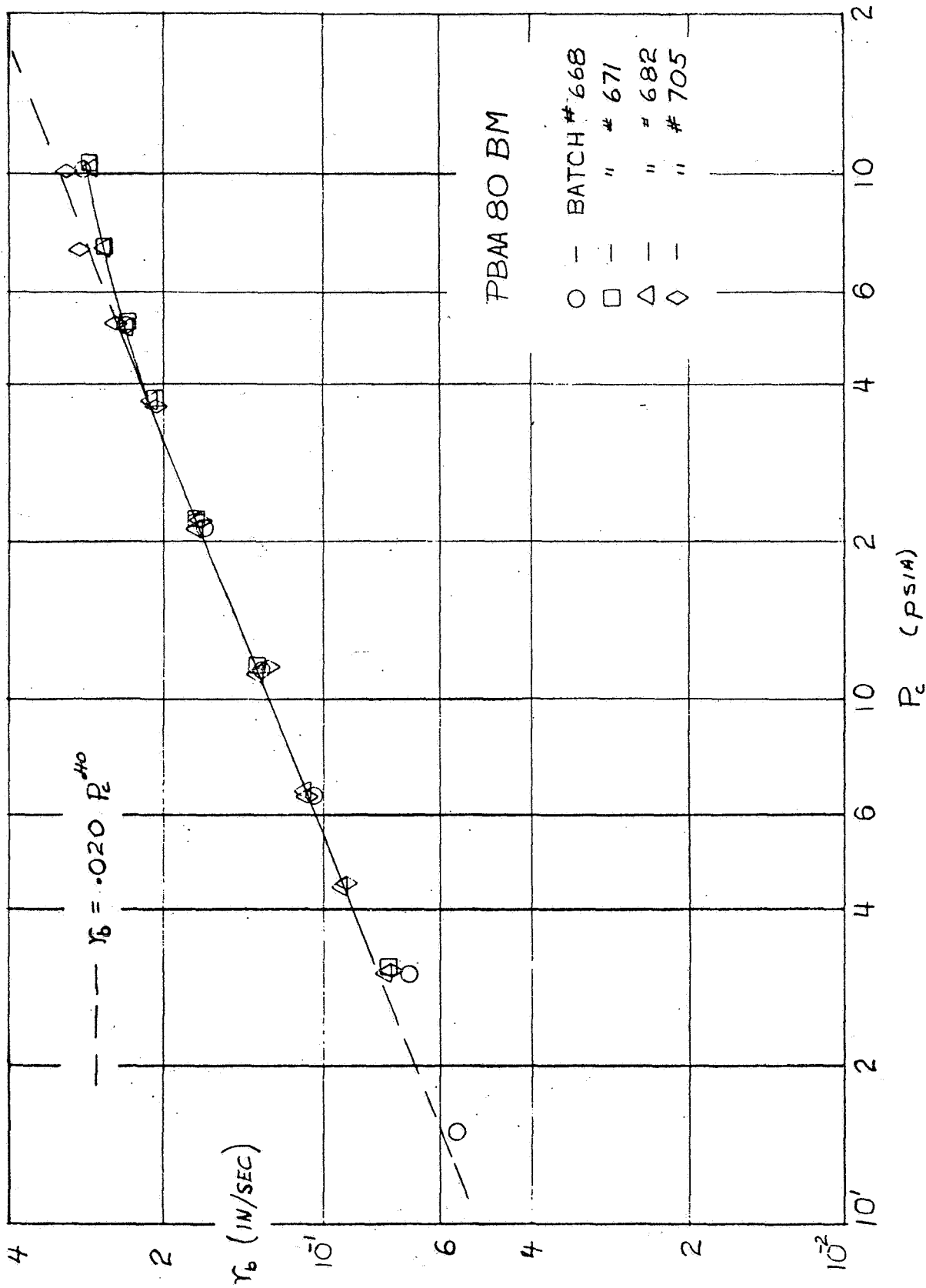


FIGURE 1

AP26-R4033-66



BURNING RATE CURVE OF PBAA 80 BM

FIGURE 2

AP-26-18 4034-a-66

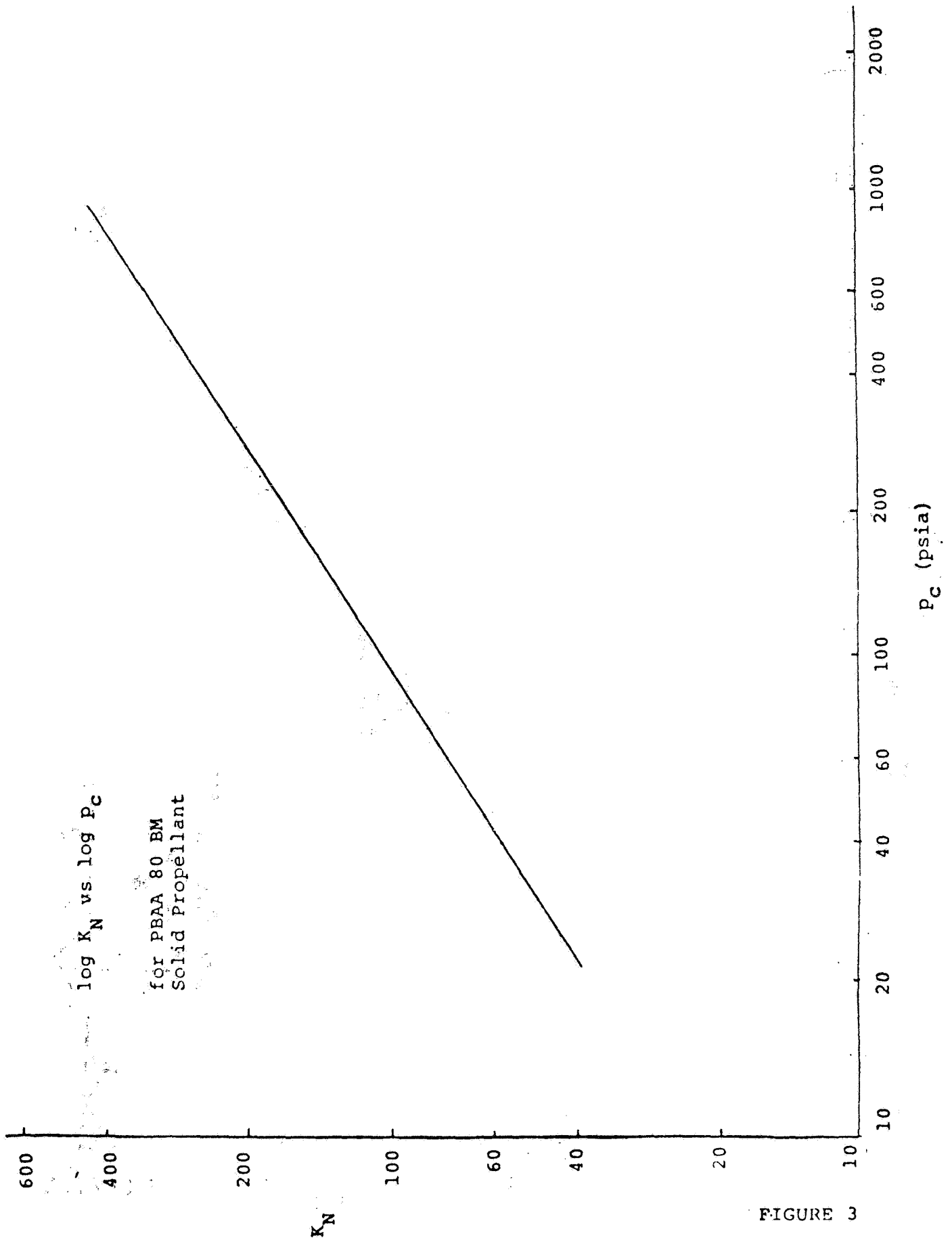


FIGURE 3

EXPERIMENTAL HEAT TRANSFER CORRELATION LOG Nu_x vs LOG Re_x

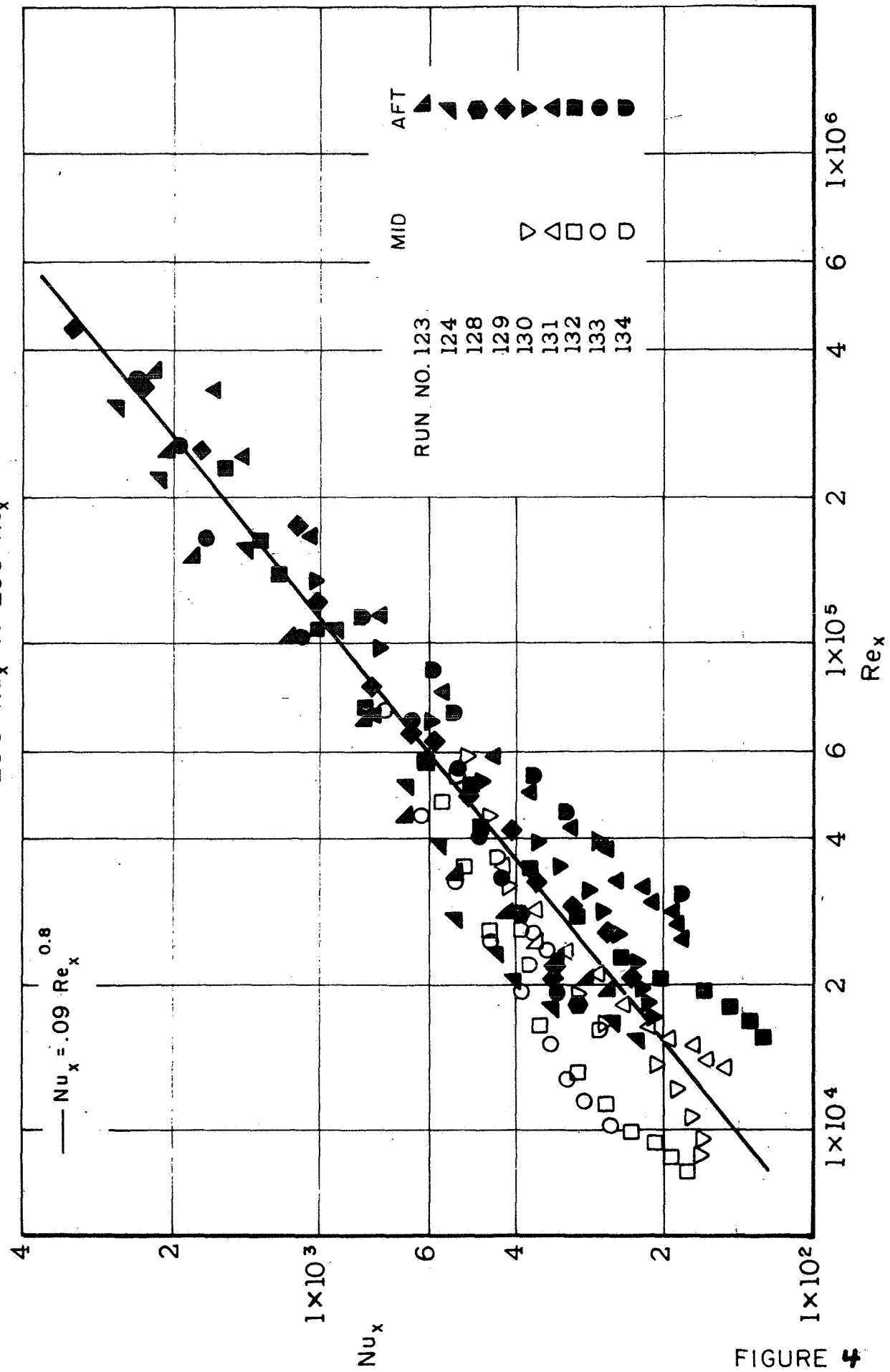


FIGURE 4

AP26-R4054-66

COMPARISON OF MEASURED & COMPUTED S & P

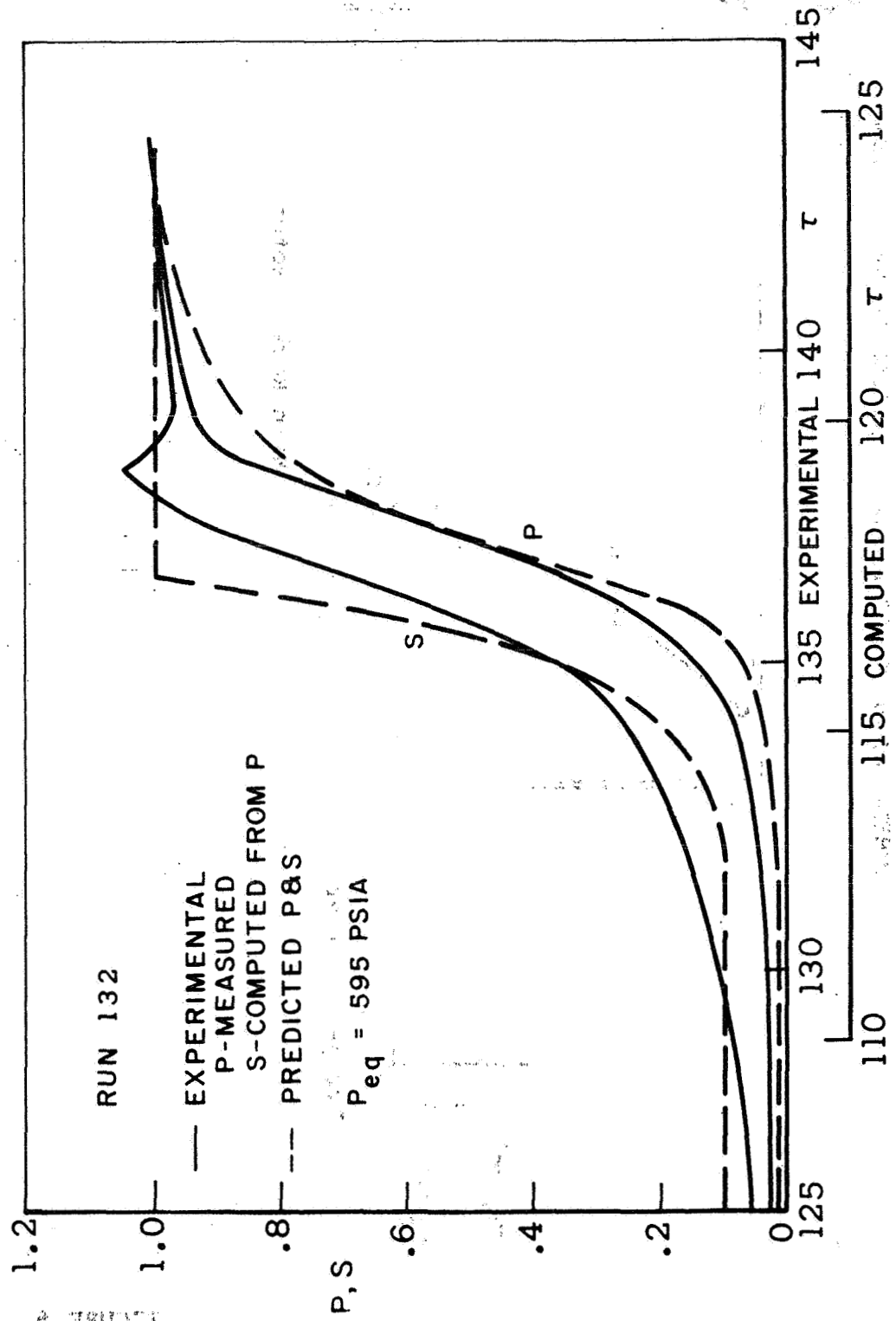


FIGURE 5

SCHEMATIC OF MODIFIED EXPERIMENTAL ROCKET SYSTEM

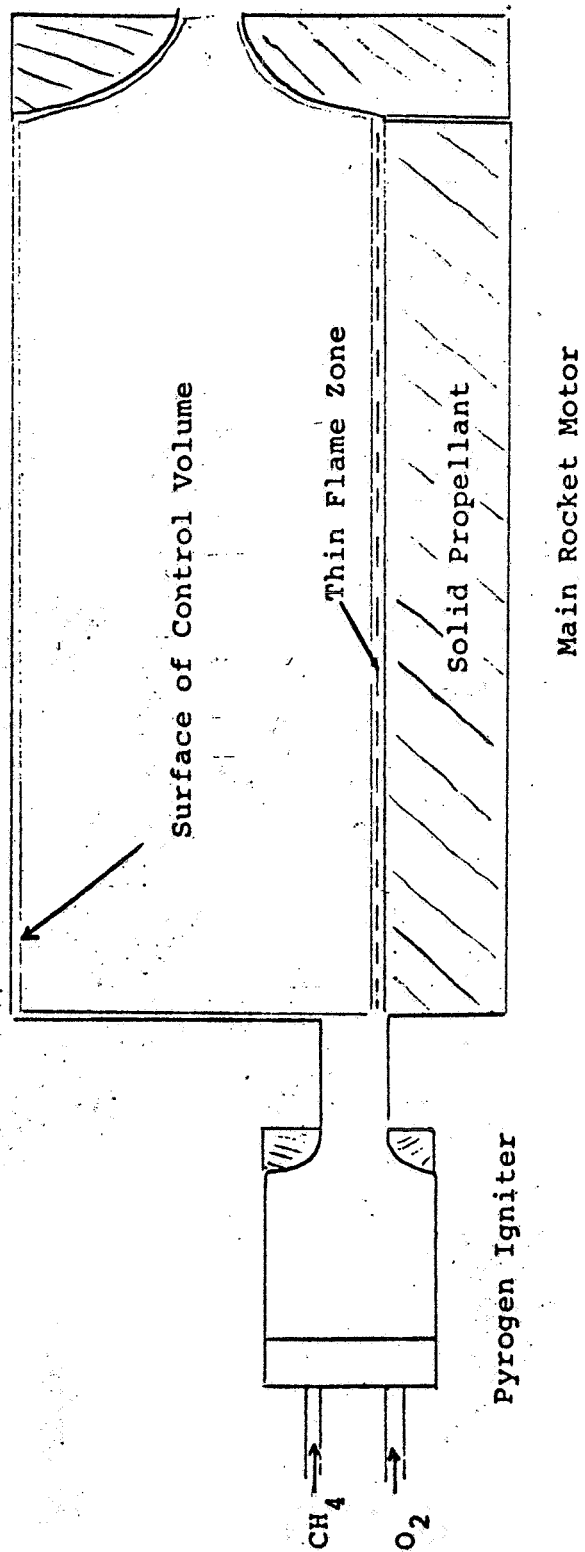


FIGURE 6

JPRS 4181 61

THEORETICAL PRESSURE VS GAS TEMPERATURE DURING CHAMBER FILLING INTERVAL

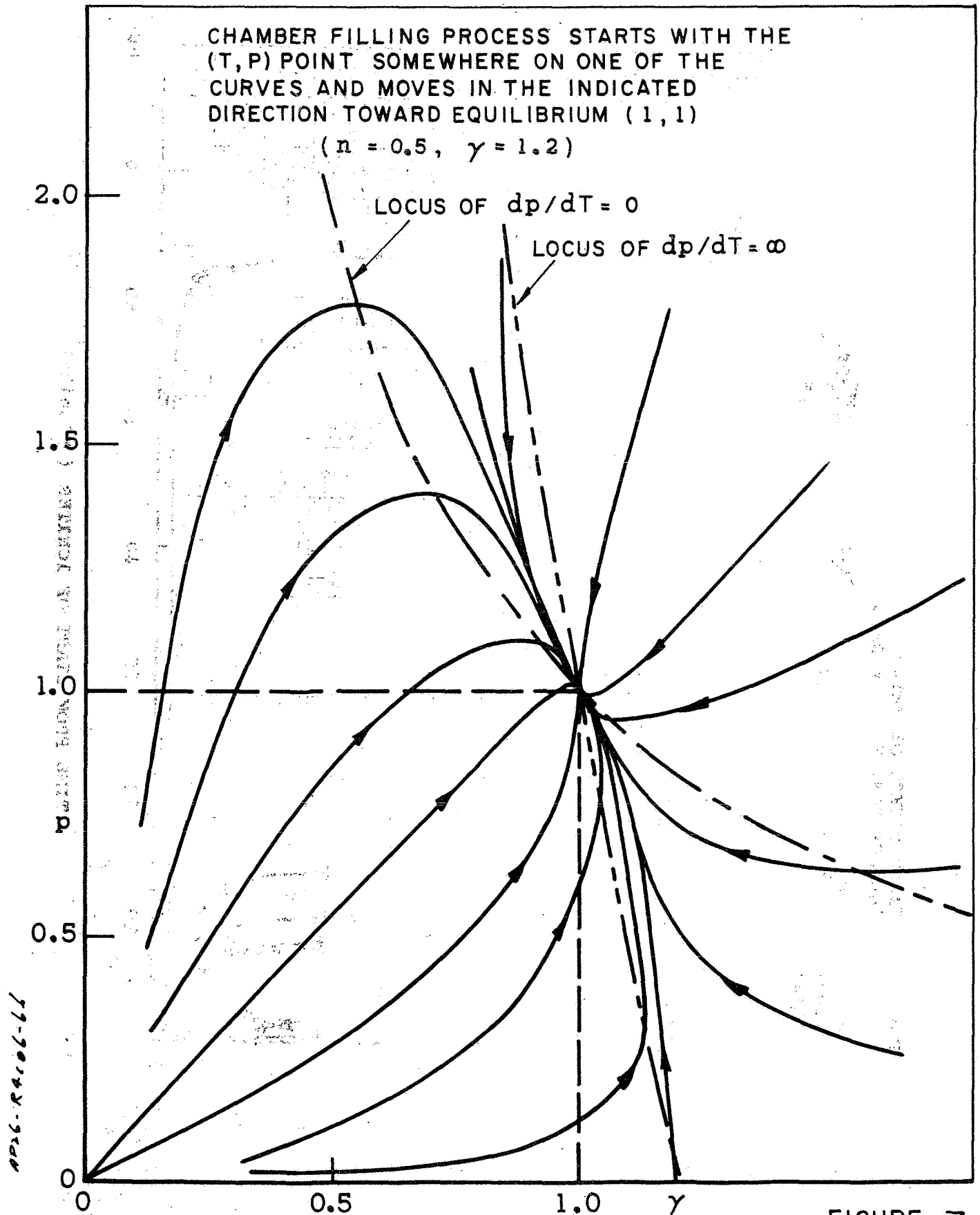


FIGURE 7

SERIES A - FIXED ROCKET GEOMETRY
VARIOUS IGNITER FLOW RATES

	Firing	\dot{m}_{ign}
○ First Flame on Grain	1	2.65×10^{-3} lbm/sec
▽ Igniter Flow cut-off (at $S=3$)	2	7.95 "
■ Grain Fully Ignited	3	10.6 "
	4	26.5 "
	5	53.0 "

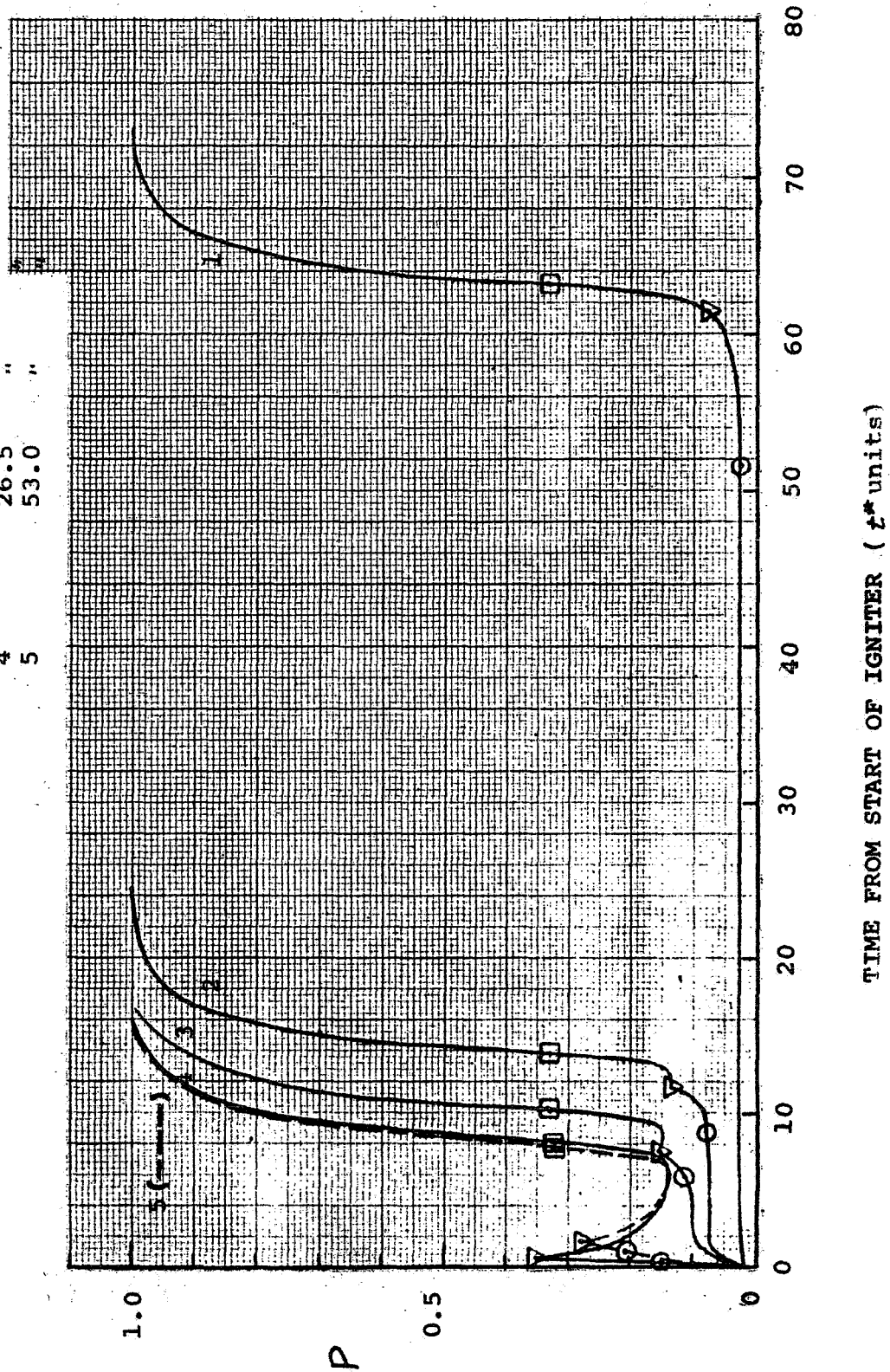


FIGURE 8

**SERIES A - FIXED ROCKET GEOMETRY
VARIOUS IGNITER FLOW RATES**

IGNITER FLOW CUT-OFF	FIRING	\dot{m}_{ign} 2.65×10^{-3} lbm/sec	lbm/sec
1	1	2.65	"
2	2	7.95	"
3	3	10.6	"
4	4	26.5	"
5	5	53.0	"

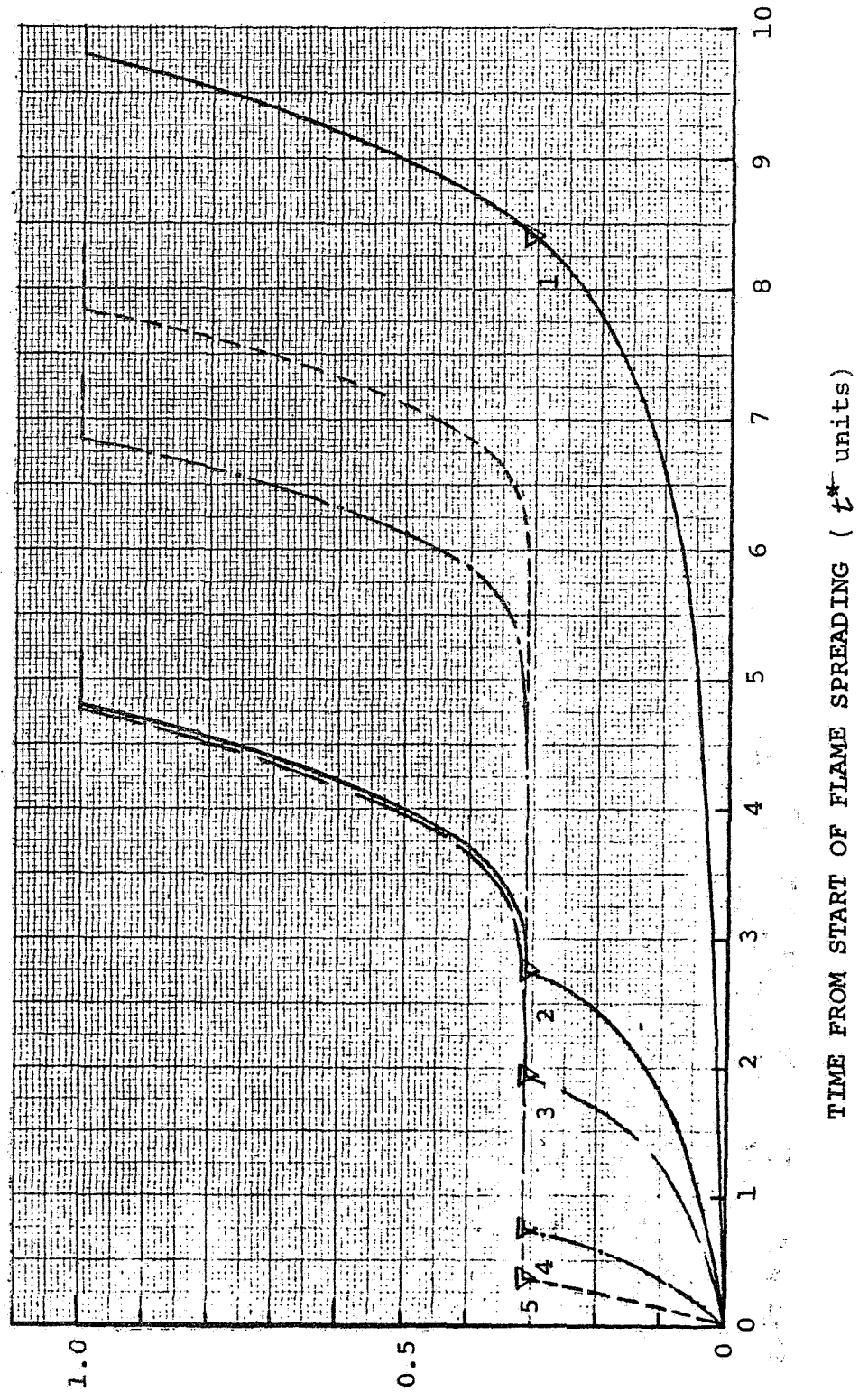
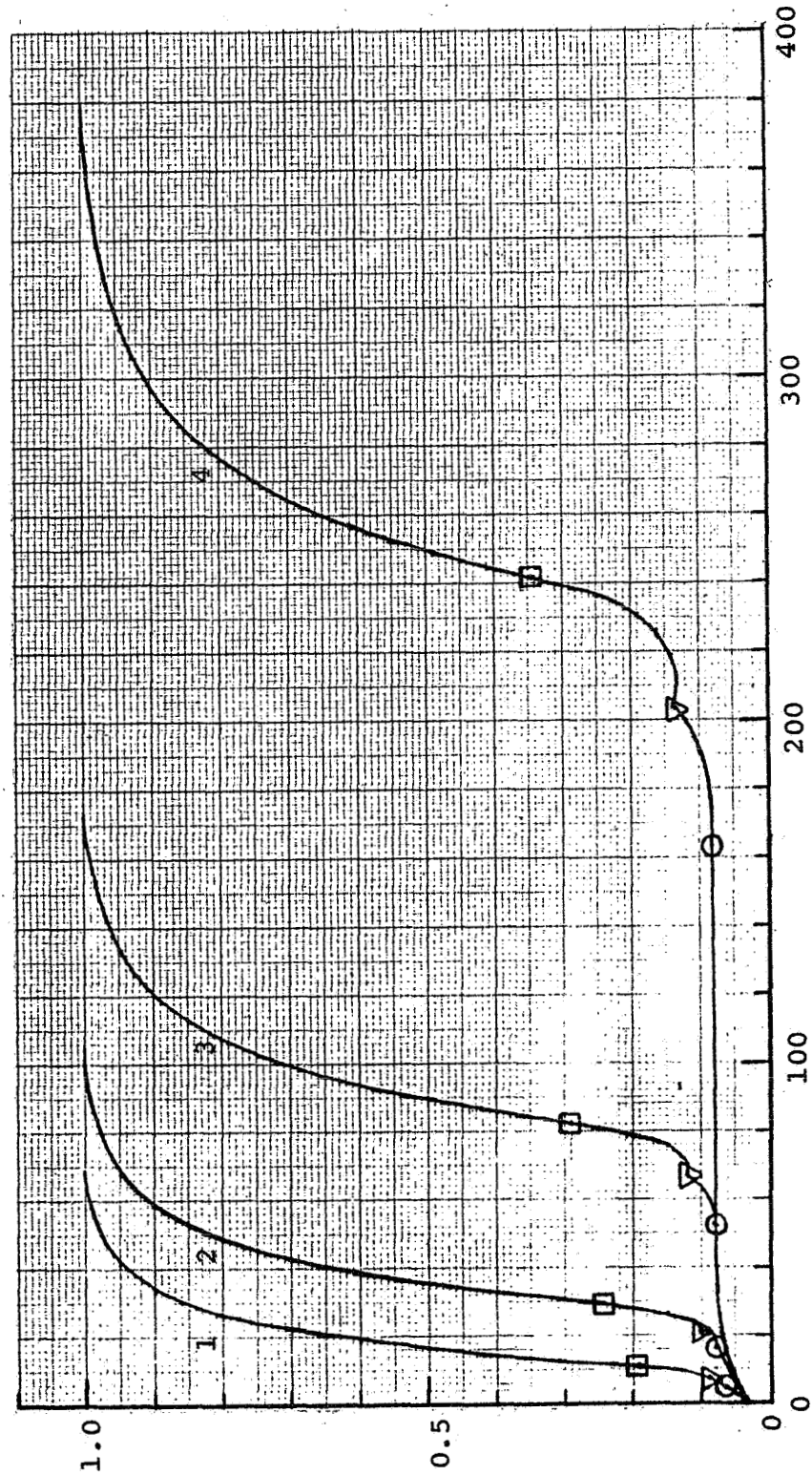


FIGURE 9

SERIES B - FIXED ROCKET THROAT AREA
FIXED IGNITER MASS FLOW RATE
VARIOUS ROCKET PORT AREAS

	FIRING	PORT AREA
○ FIRST FLAME ON GRAIN	1	4.0 cm ²
▽ IGNITER FLOW CUT-OFF (at S=3)	2	2.0 "
□ GRAIN FULLY IGNITED	3	1.0 "
	4	0.5 "



TIME FROM START OF IGNITER (msec.)

FIGURE 10

SERIES B - FIXED ROCKET THROAT AREA
FIXED IGNITER MASS FLOW RATE
VARIOUS ROCKET PORT AREAS

IGNITER FLOW CUT-OFF	FIRING	PORT AREA
1	1	4.0 cm ²
2	2	2.0 "
3	3	1.0 "
4	4	0.5 "

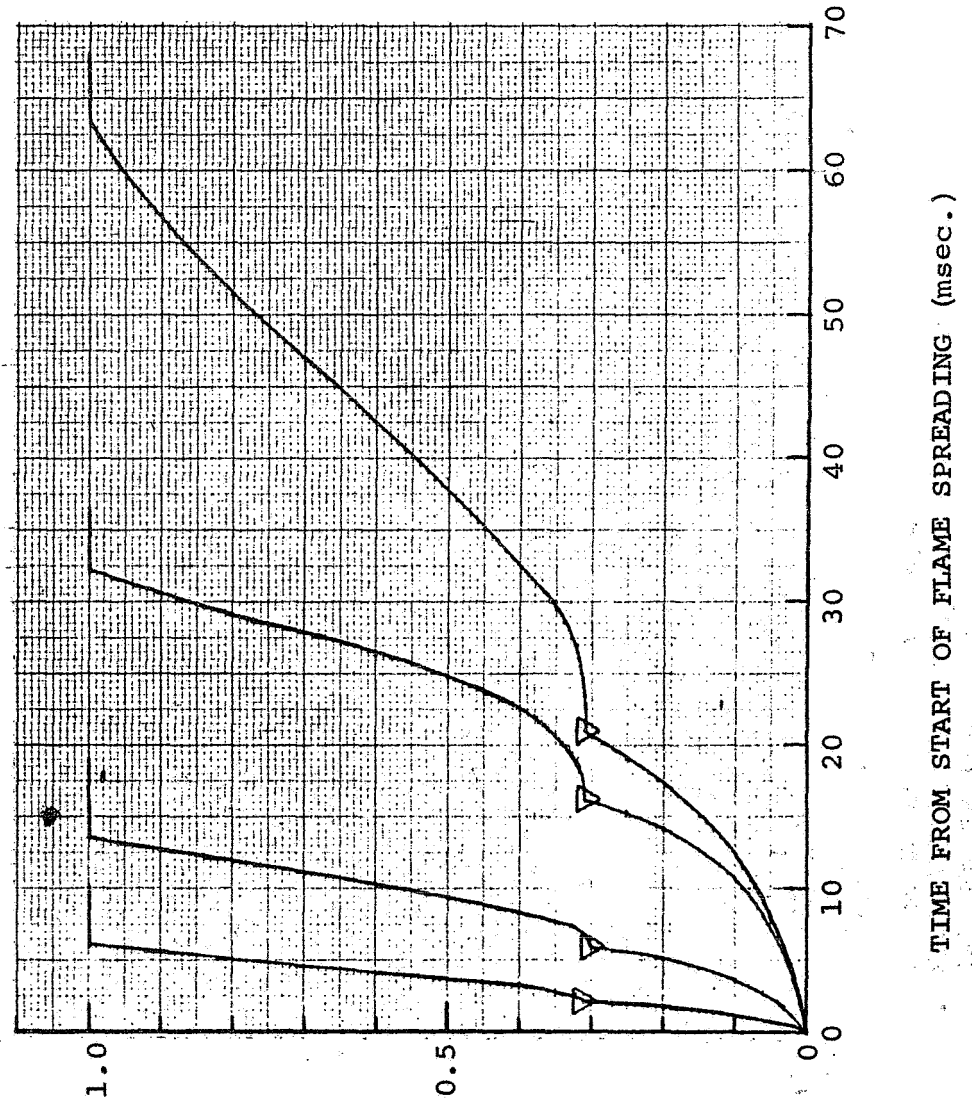


FIGURE 11

SERIES C - FIXED ROCKET PORT AREA
 FIXED IGNITER MASS FLOW RATE
 VARIOUS ROCKET THROAT AREAS

○ FIRST FLAME APPEARS ON GRAIN
 ▽ IGNITER FLOW CUT-OFF ($S = .3$)
 □ GRAIN FULLY IGNITED

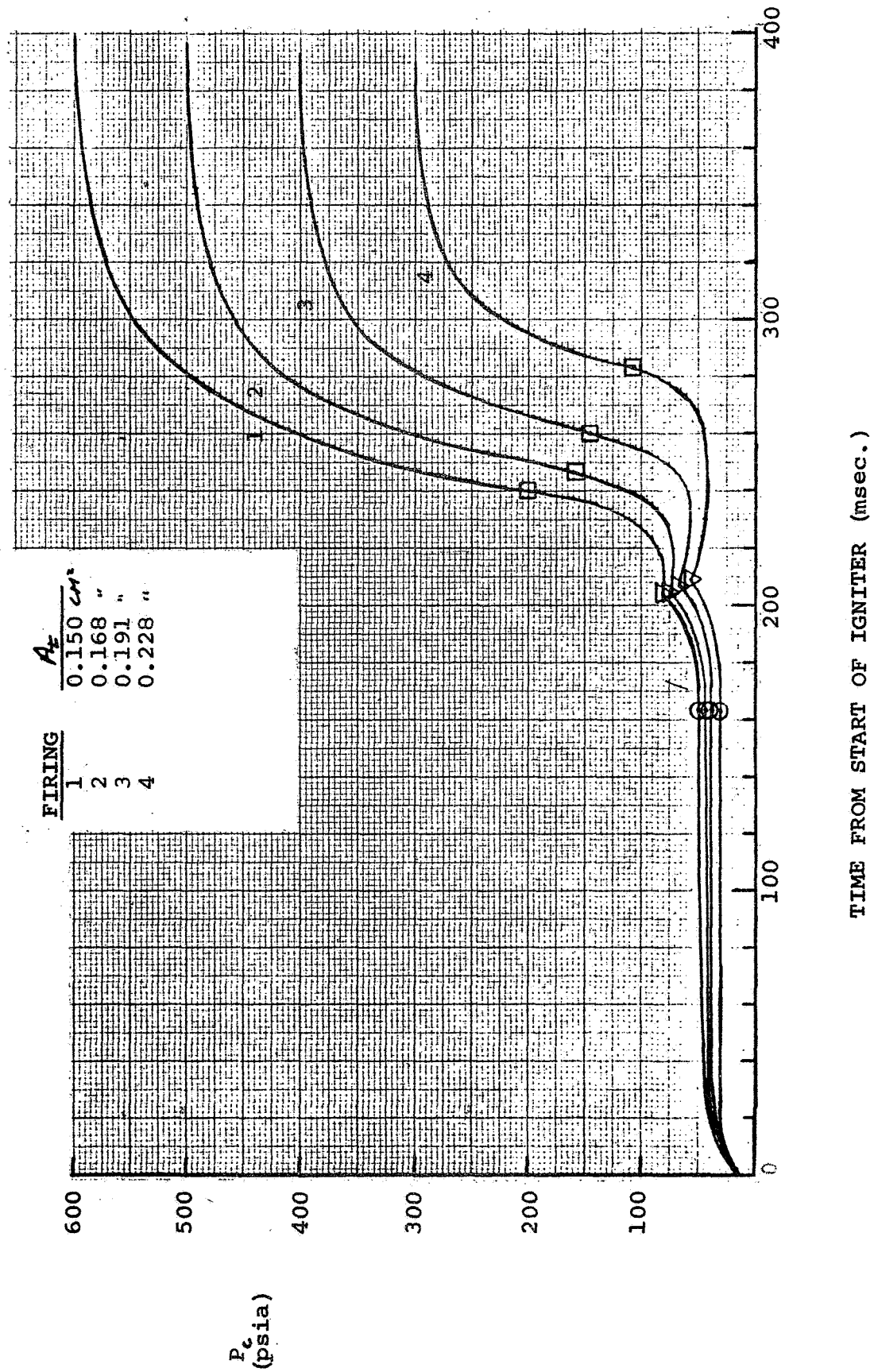
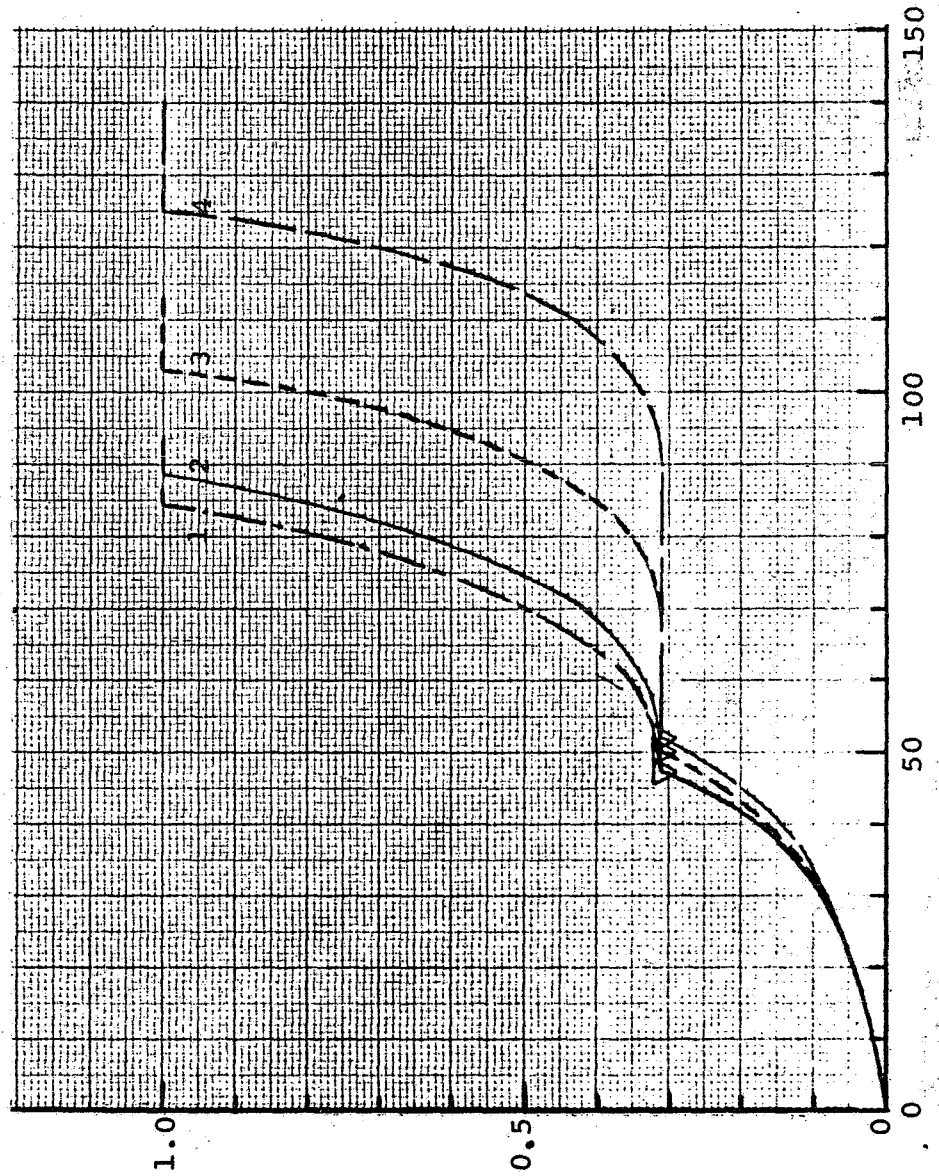


FIGURE 12

SERIES C - FIXED ROCKET PORT AREA
 FIXED IGNITER MASS FLOW RATE
 VARIOUS ROCKET THROAT AREAS

∇ IGNITER FLOW CUT-OFF ($S=.3$)	FIRING	A_t	CM^2
1	1	0.150	0.150
2	2	0.108	0.108
3	3	0.191	0.191
4	4	0.228	0.228



TIME FROM START OF FLAME SPREADING (msec.)

FIGURE 13

SERIES D - FIXED ROCKET GEOMETRY
 VARIOUS IGNITER FLOW RATES
 EXTENDED IGNITER DURATION

FIRING	\dot{m}_{ign}	26.5×10^{-3}	lbm/sec
1	15.9	"	"
2	7.95	"	"
3		"	"

62

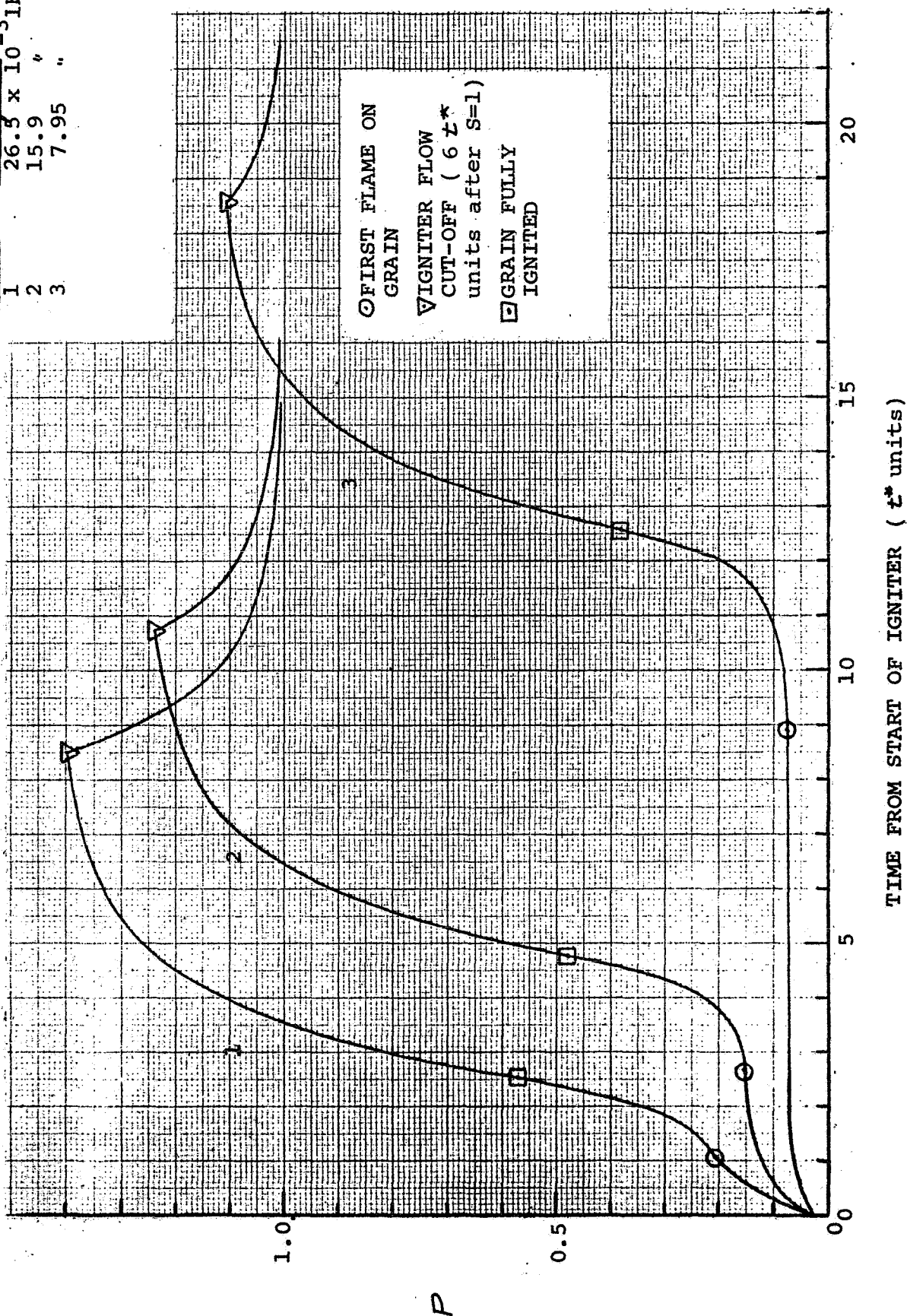


FIGURE 14

SERIES D - FIXED ROCKET GEOMETRY
VARIOUS IGNITER FLOW RATES
EXTENDED IGNITER DURATION

FIRING	$\dot{m}_{ign} \times 10^{-3}$ lbm/sec
1	26.5
2	15.9
3	7.95

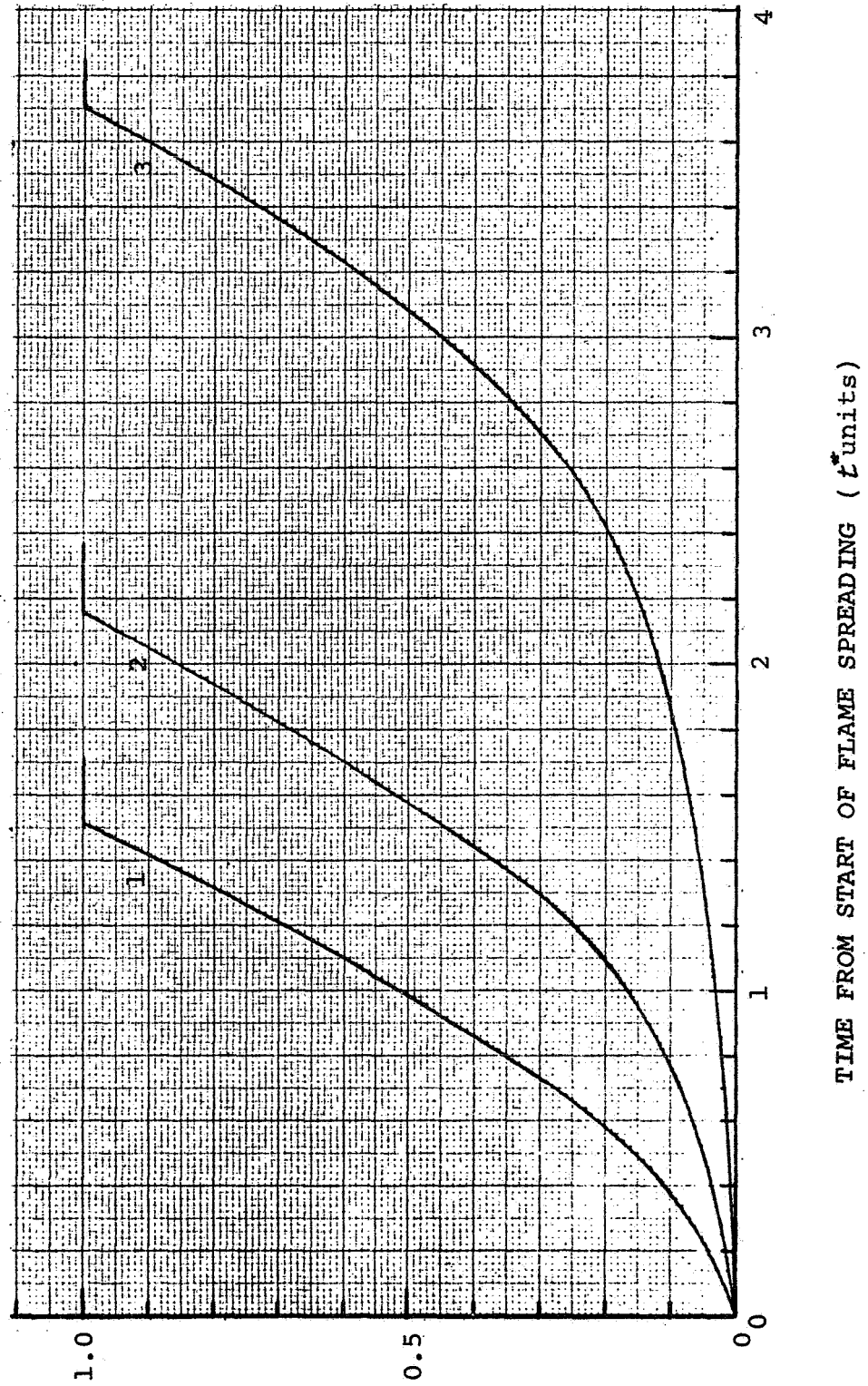


FIGURE 15

SERIES E - FIXED ROCKET GEOMETRY
 FIXED TOTAL IGNITER MASS
 VARIOUS IGNITER FLOW RATES

○ FIRST FLAME ON GRAIN
 ▽ IGNITER FLOW CUT-OFF
 □ GRAIN FULLY IGNITED

FIRING	$\frac{\dot{m}_{ign}}{7.95 \times 10^{-3}}$	lbm/sec
1	6.62	"
2	5.30	"
3	3.97	"
4	2.65	"
5		"

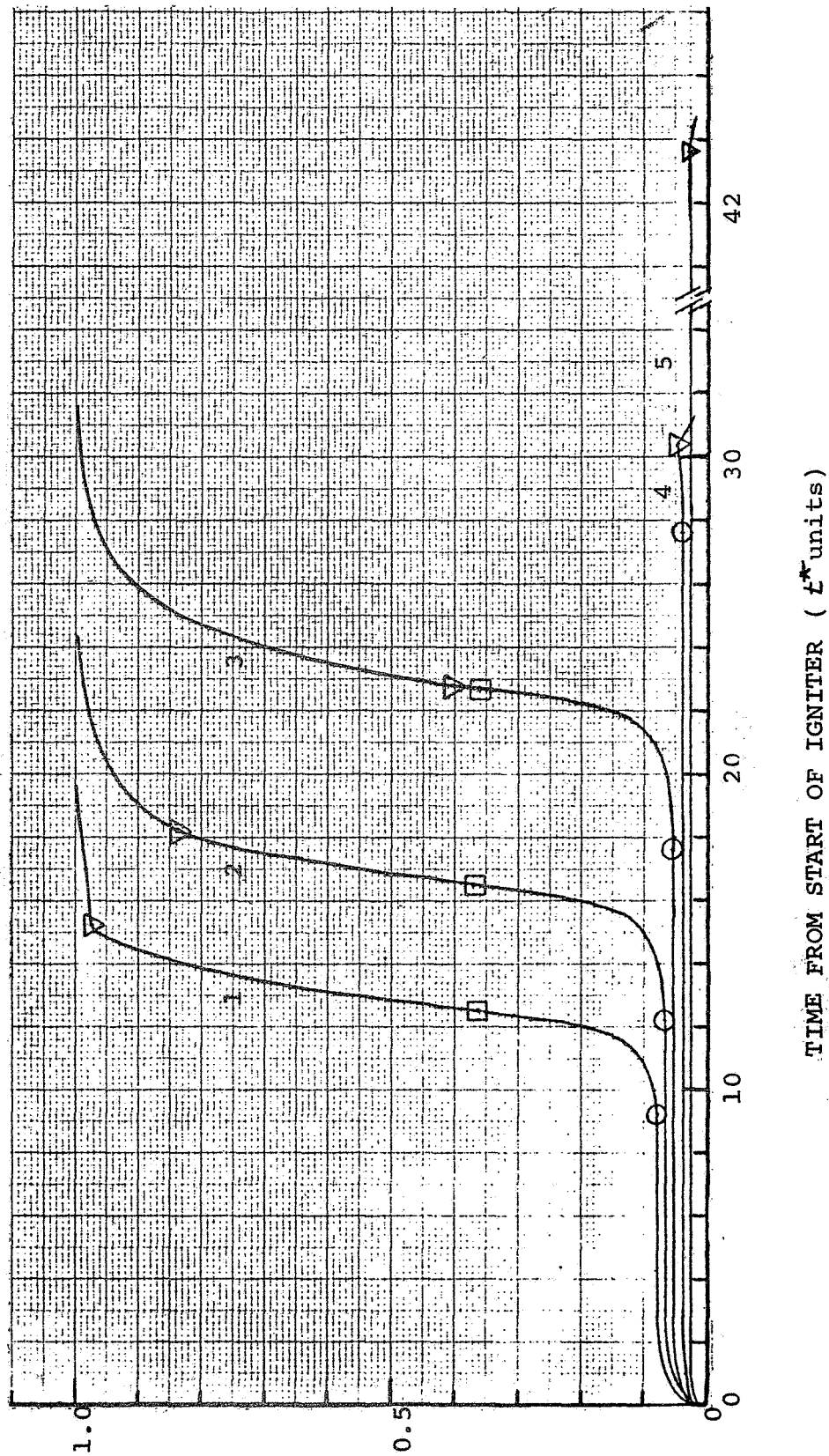


FIGURE 16

SERIES E - FIXED ROCKET GEOMETRY
 FIXED TOTAL IGNITER MASS
 VARIOUS IGNITER FLOW RATES

IGNITER FLOW CUT-OFF

FIRING	$\frac{m_{ign}}{7.95 \times 10^{-3}}$	lbm/sec
1	6.62	"
2	5.30	"
3	3.97	"
4	2.65	"
5	"	"

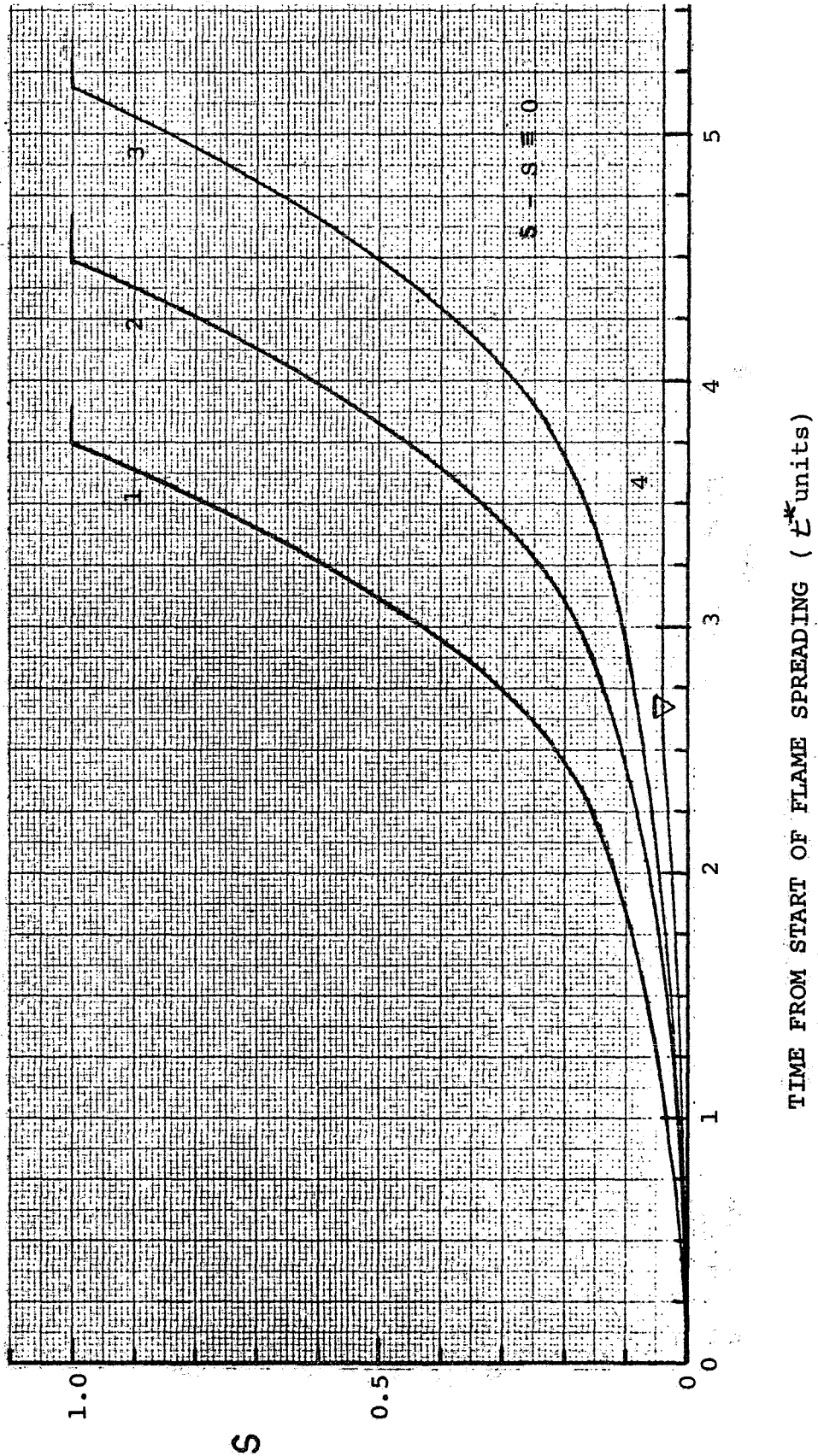


FIGURE 17

SERIES F- PARTIAL NOZZLE CLOSURES
 FIXED IGNITER MASS FLOW RATE
 $S < 1$ - VARIOUS ROCKET THROAT AREAS
 $S > 1$ - FIXED ROCKET GEOMETRY

VARIABLES NON-DIMENSIONALIZED
 BY FINAL PARAMETERS

○ FIRST FLAME ON GRAIN
 ◊ IGNITER FLOW CUT-OFF
 ■ GRAIN FULLY IGNITED

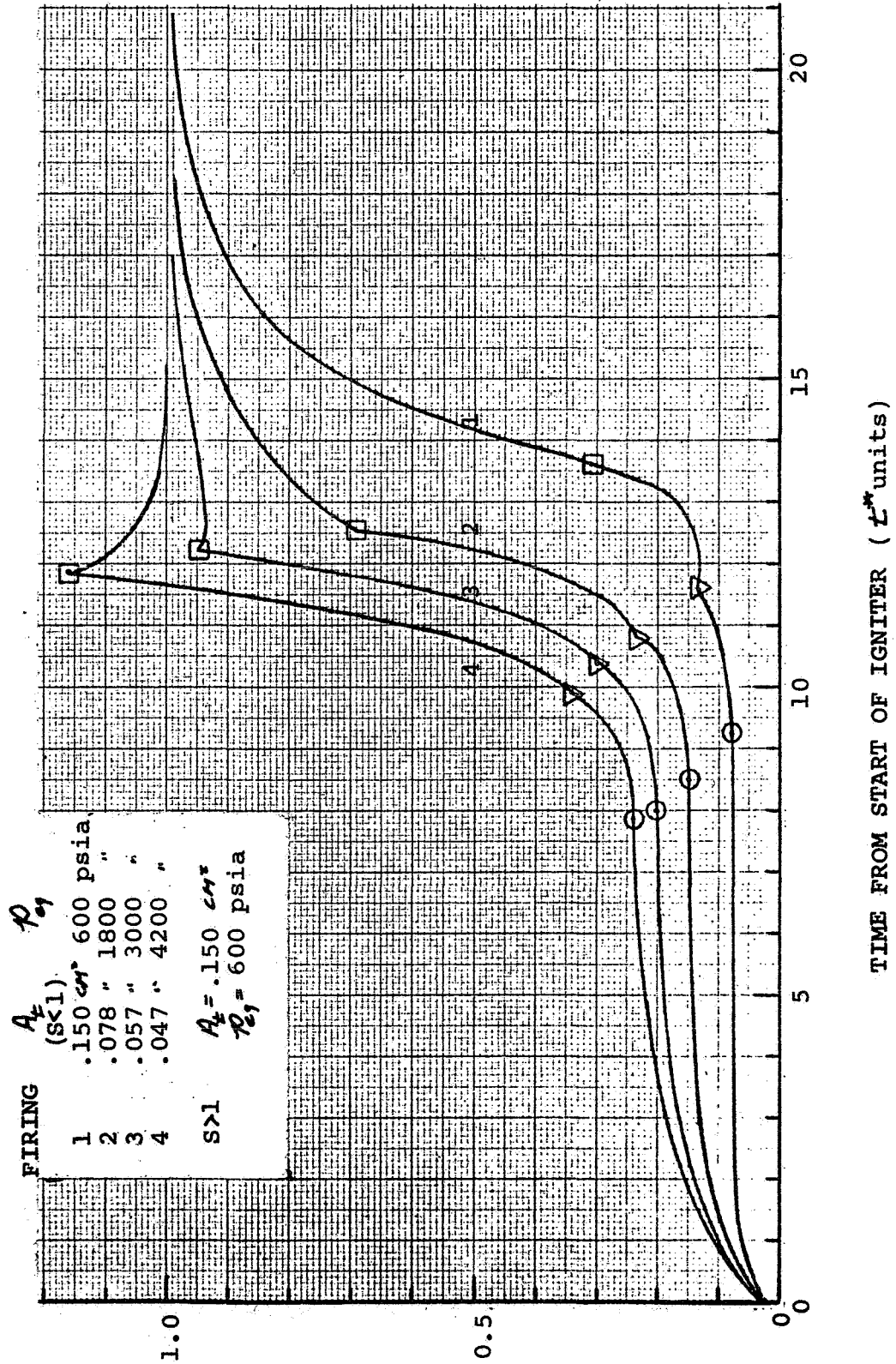


FIGURE 18

SERIES F - PARTIAL NOZZLE CLOSURES
 FIXED IGNITER MASS FLOW RATE
 S<1 - VARIOUS ROCKET THROAT AREAS
 S>1 - FIXED ROCKET GEOMETRY

VARIABLES NON-DIMENSIONALIZED
 BY FINAL PARAMETERS

○ FIRST FLAME ON GRAIN
 ▽ IGNITER FLOW CUT-OFF
 ◻ GRAIN FULLY IGNITED

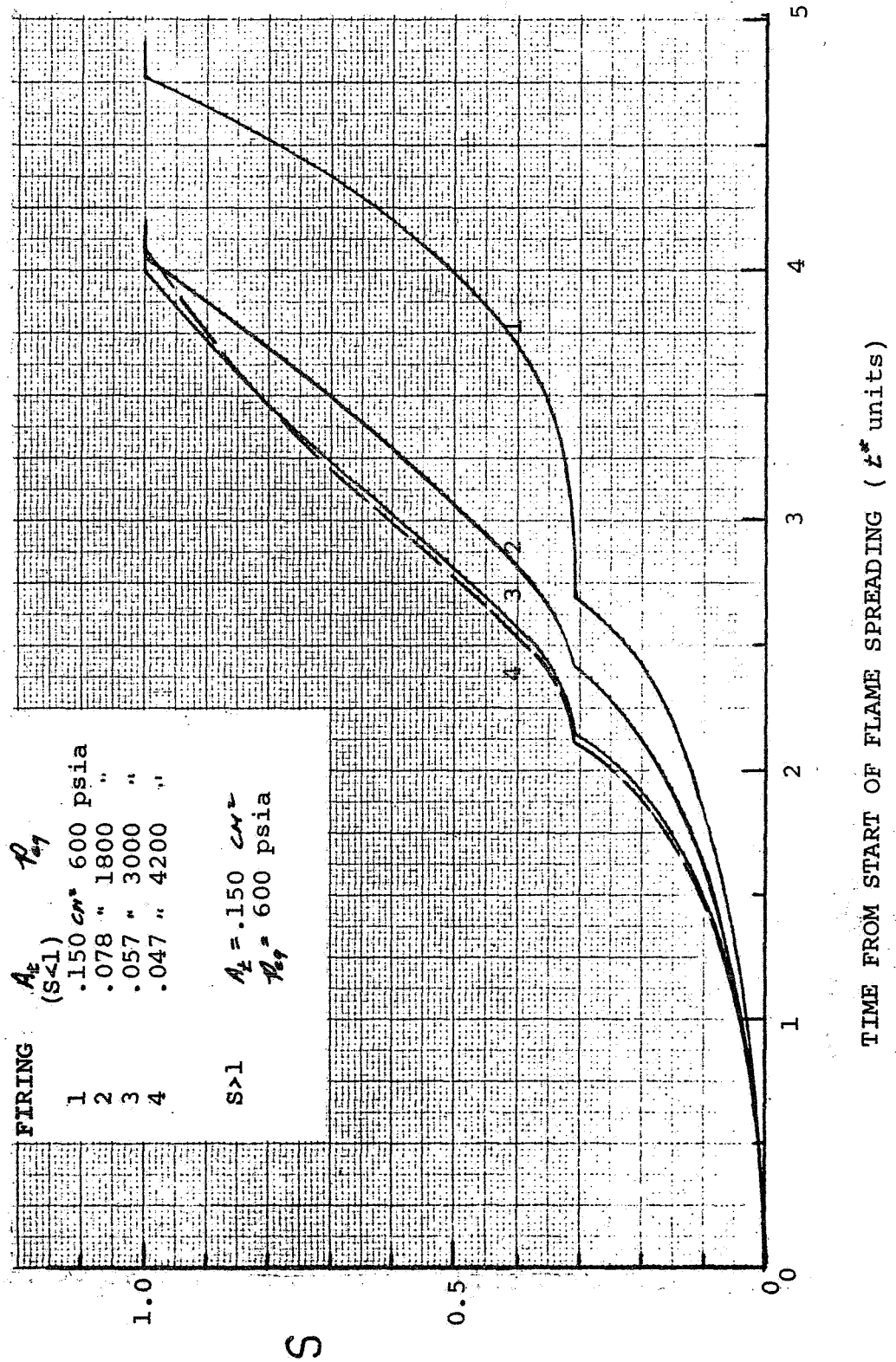


FIGURE 19

SERIES A - FIXED ROCKET GEOMETRY
VARIOUS IGNITER FLOW RATES

FIRING A-1 $\dot{m}_{ig} = 2.65 \times 10^{-3}$ lbm/sec

▽ IGNITER FLOW CUT-OFF

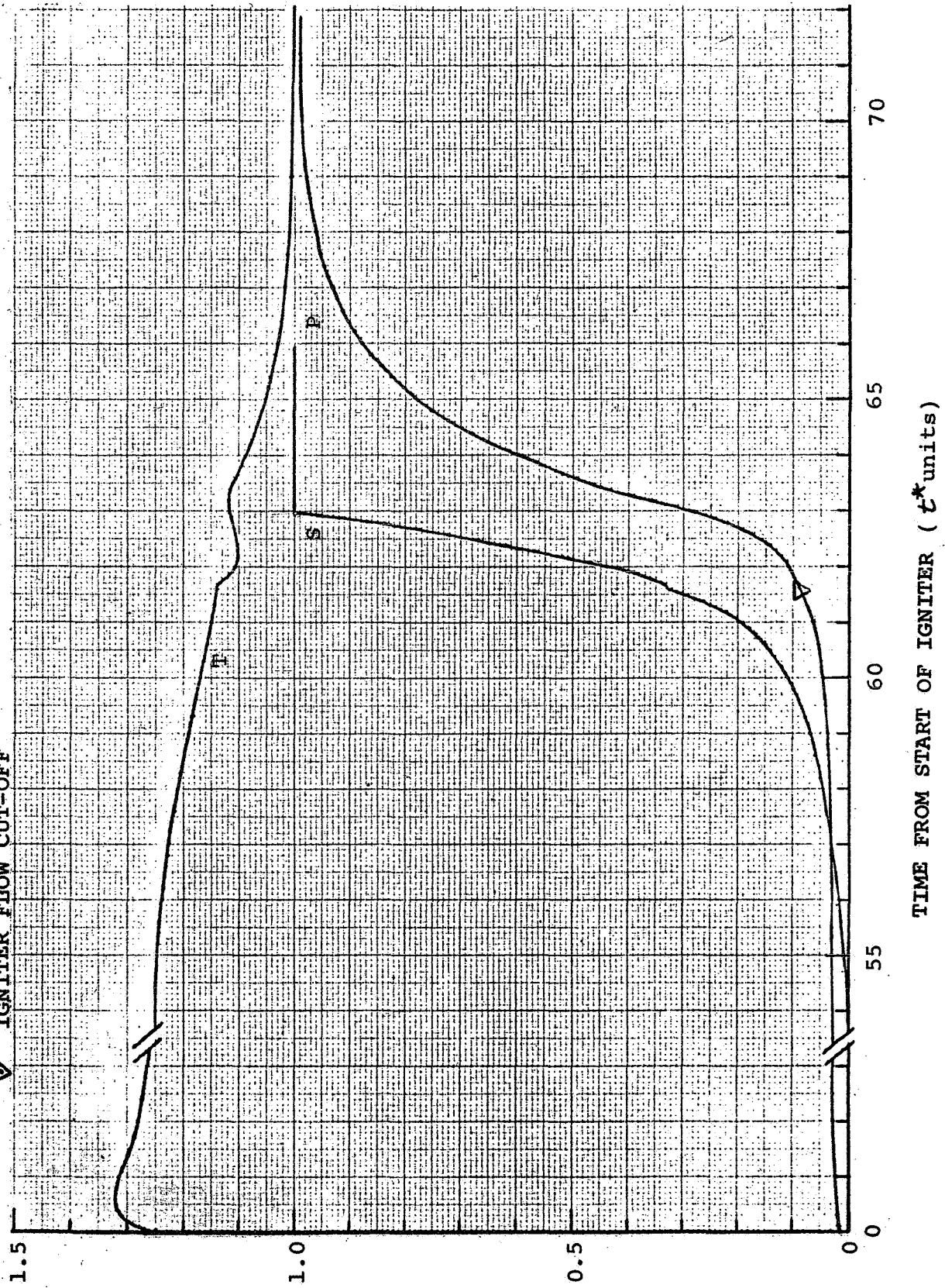


FIGURE 20

SERIES A - FIXED ROCKET GEOMETRY
VARIOUS IGNITER FLOW RATES

FIRING A-2 $\dot{m}_{ig} = 7.95 \times 10^{-3}$ lbm/sec

▽ IGNITER FLOW CUT-OFF

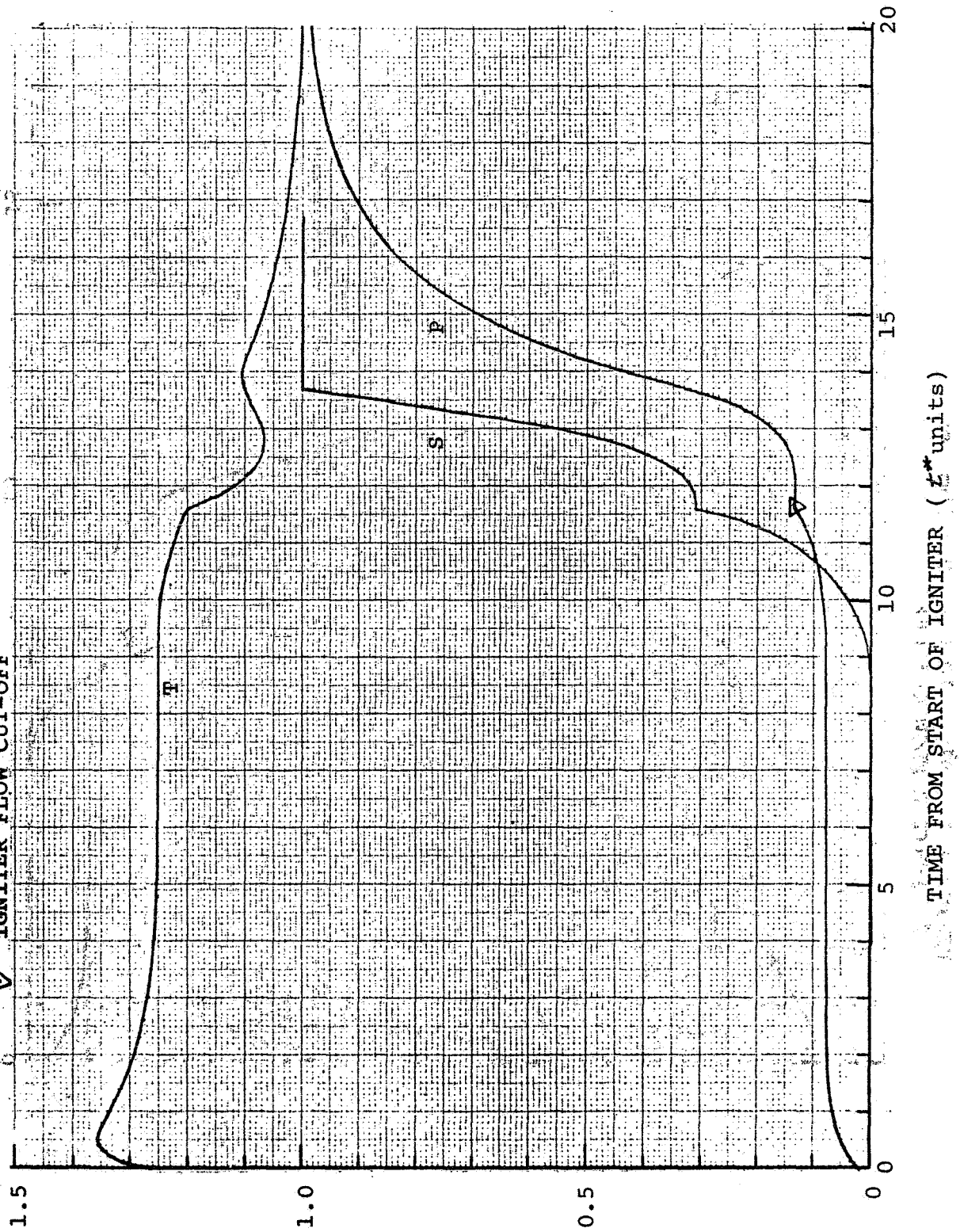


FIGURE 21

SERIES A - FIXED ROCKET GEOMETRY
 VARIOUS IGNITER FLOW RATES
 FIRING A-3 $\dot{m}_{ig} = 10.0 \times 10^{-3}$ lbm/sec
 ∇ IGNITER FLOW CUT-OFF

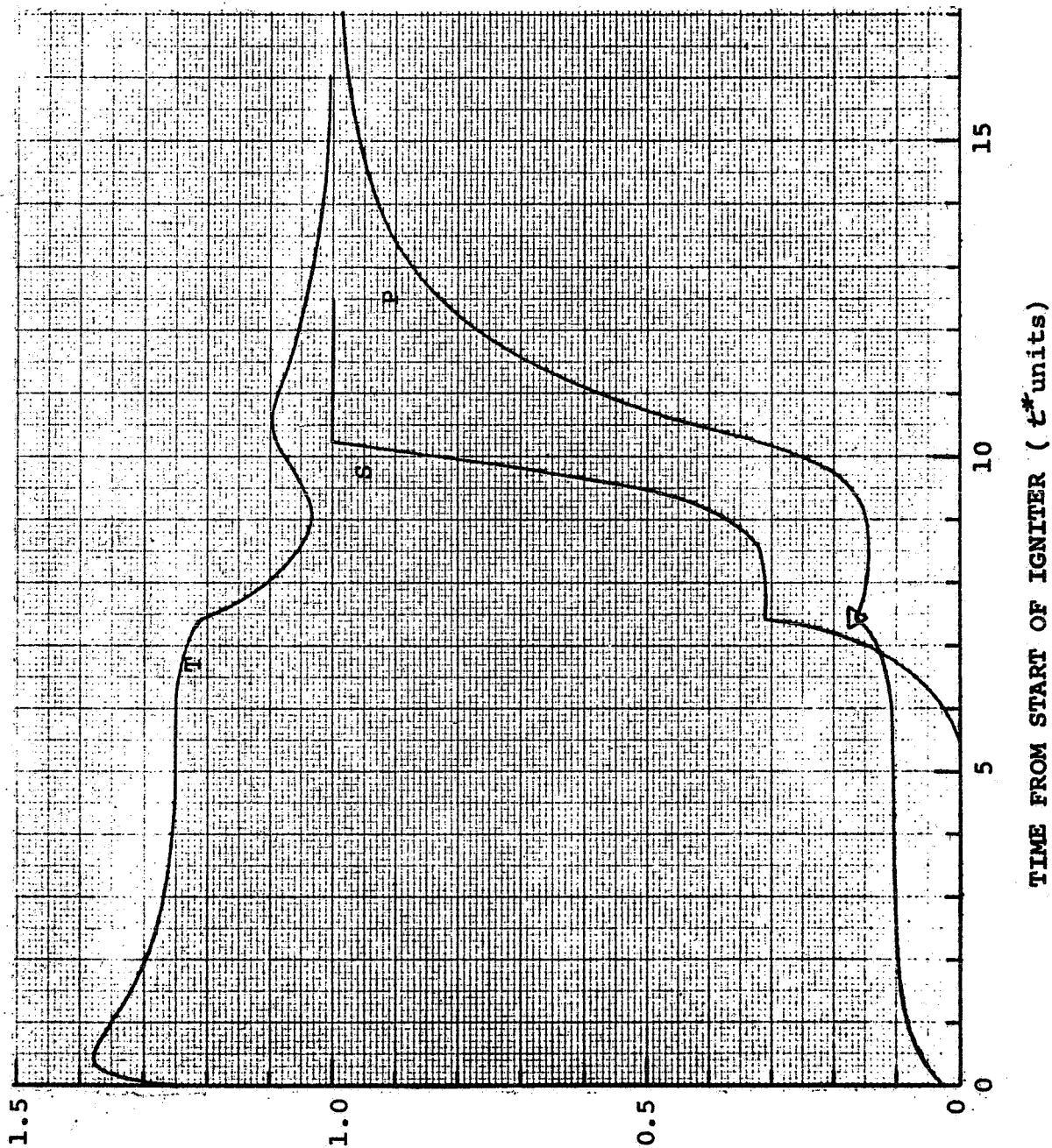
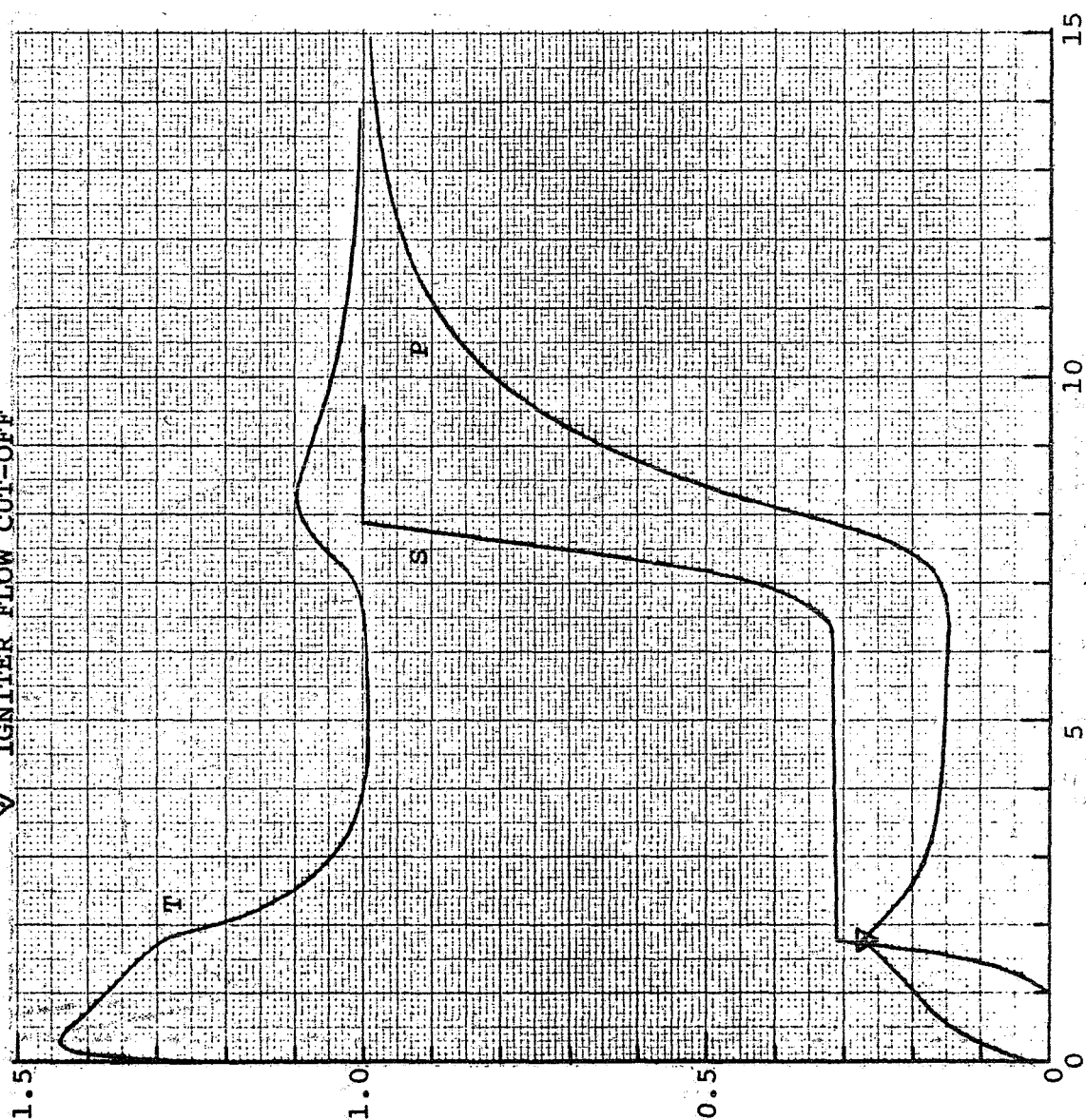


FIGURE 22

SERIES A - FIXED ROCKET GEOMETRY
VARIOUS IGNITER FLOW RATES

FIRING A-4 $\dot{m}_{ign} = 26.5 \times 10^{-3}$ lbm/sec

∇ IGNITER FLOW CUT-OFF



TIME FROM START OF IGNITER (t^* units)

FIGURE 23

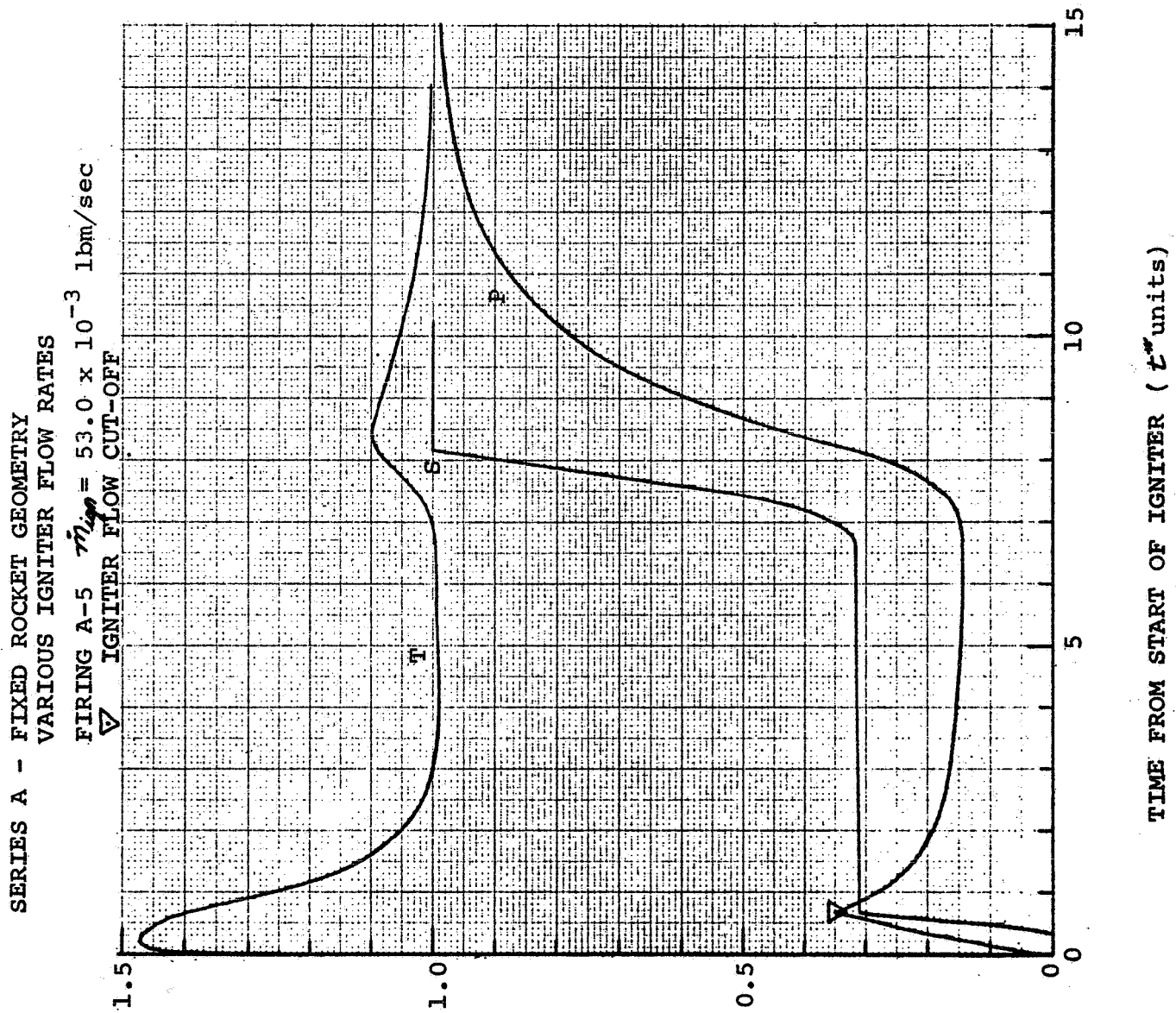


FIGURE 24

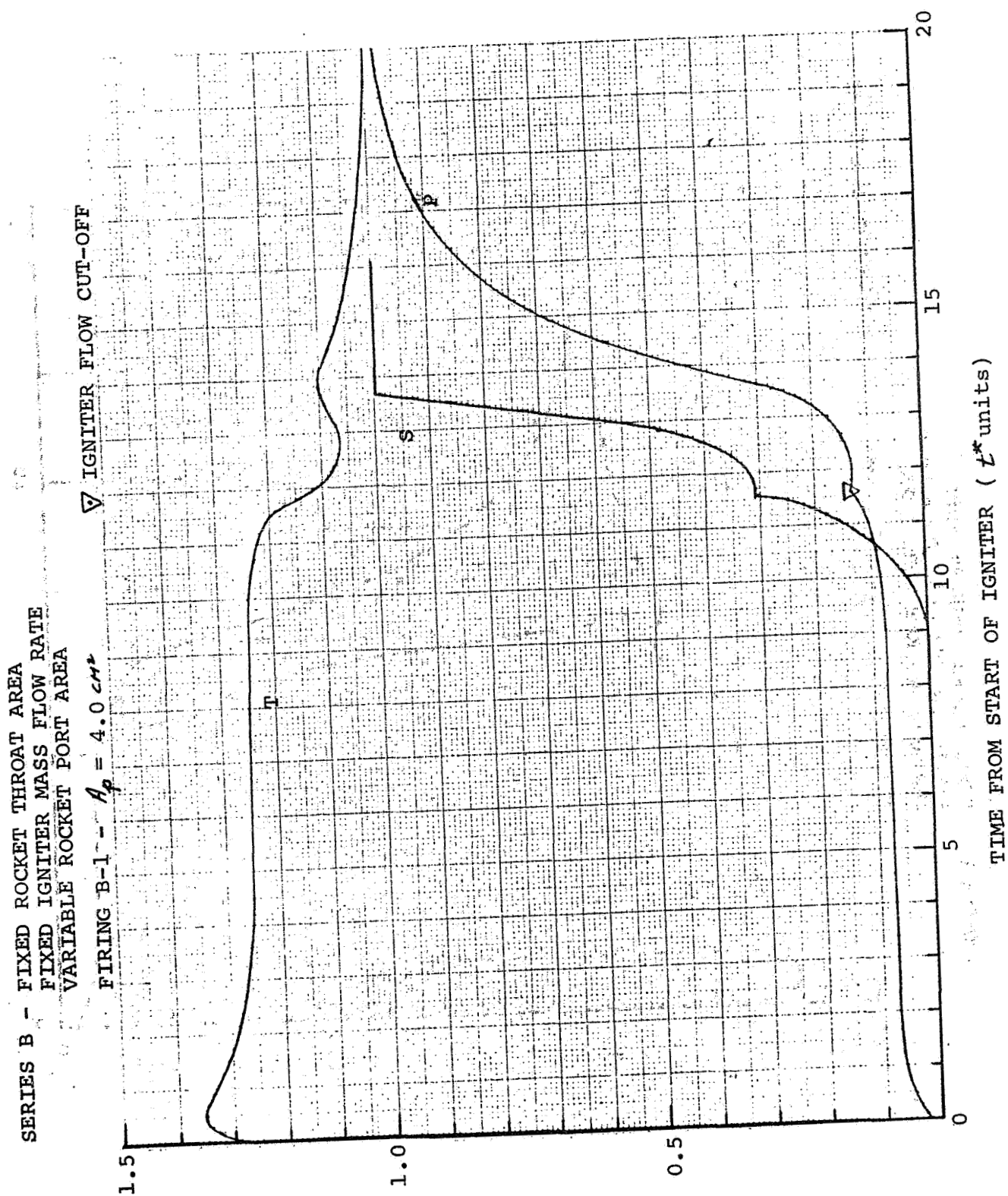


FIGURE 25

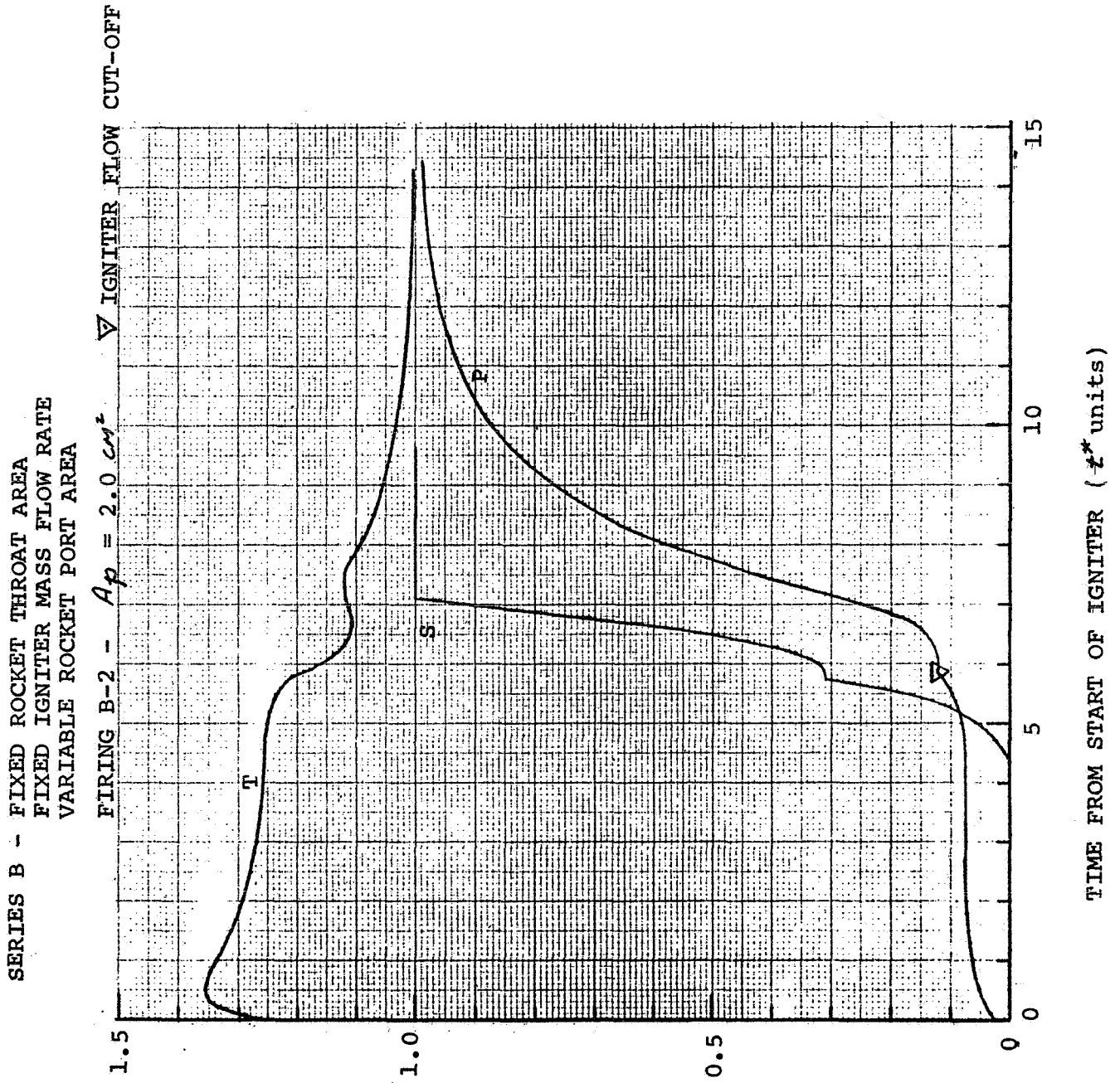


FIGURE 26

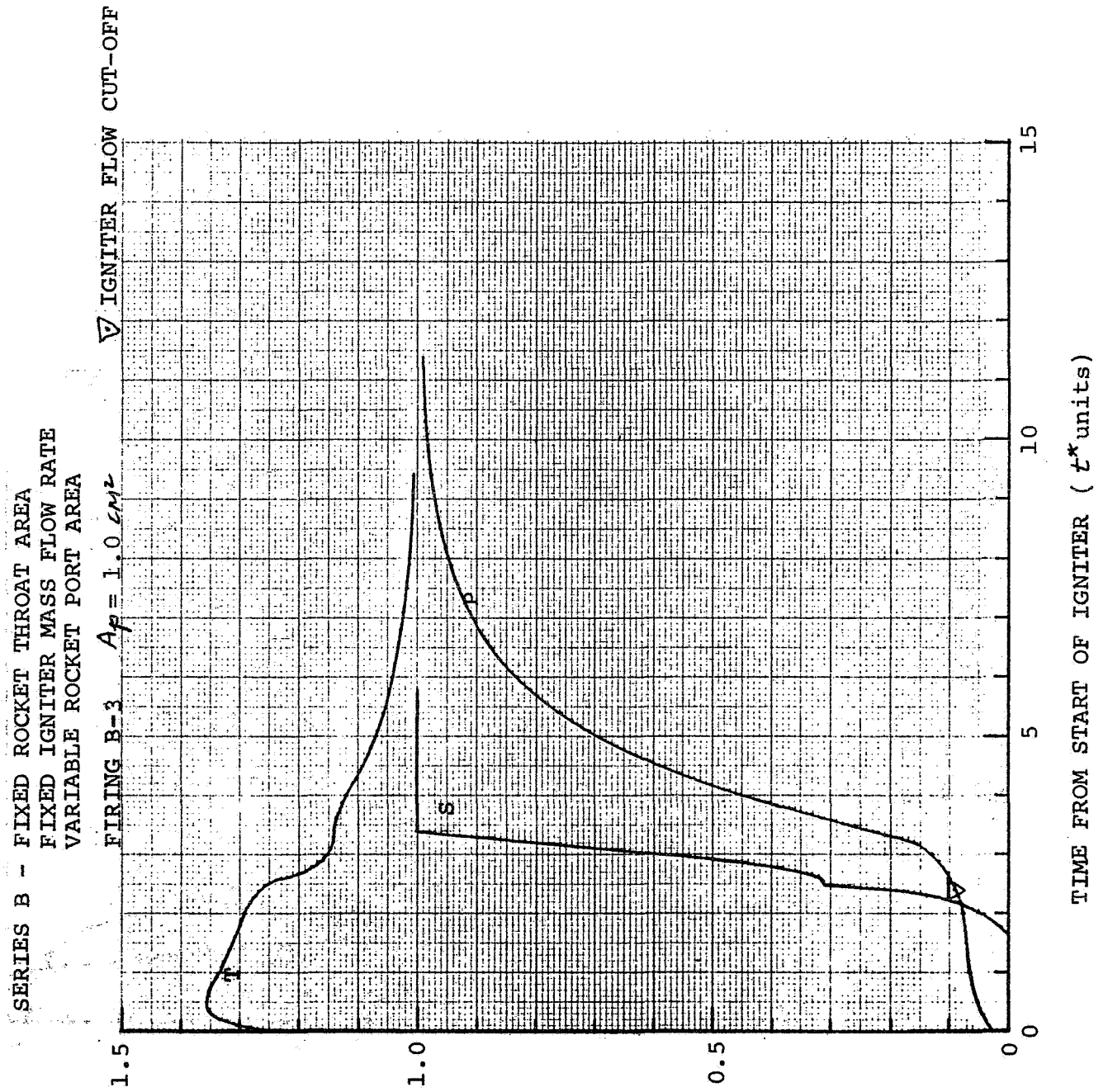


FIGURE 27

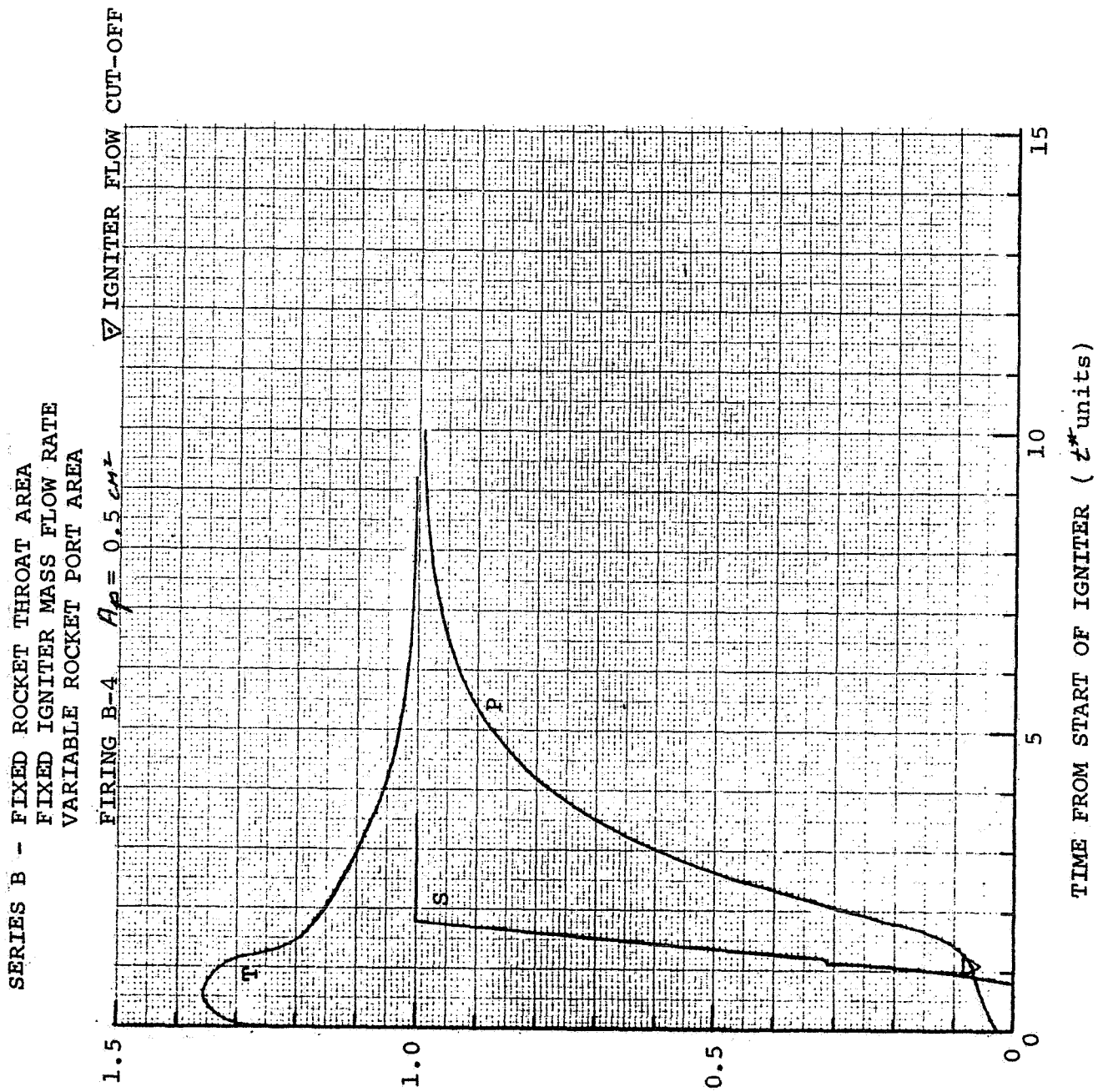


FIGURE 28

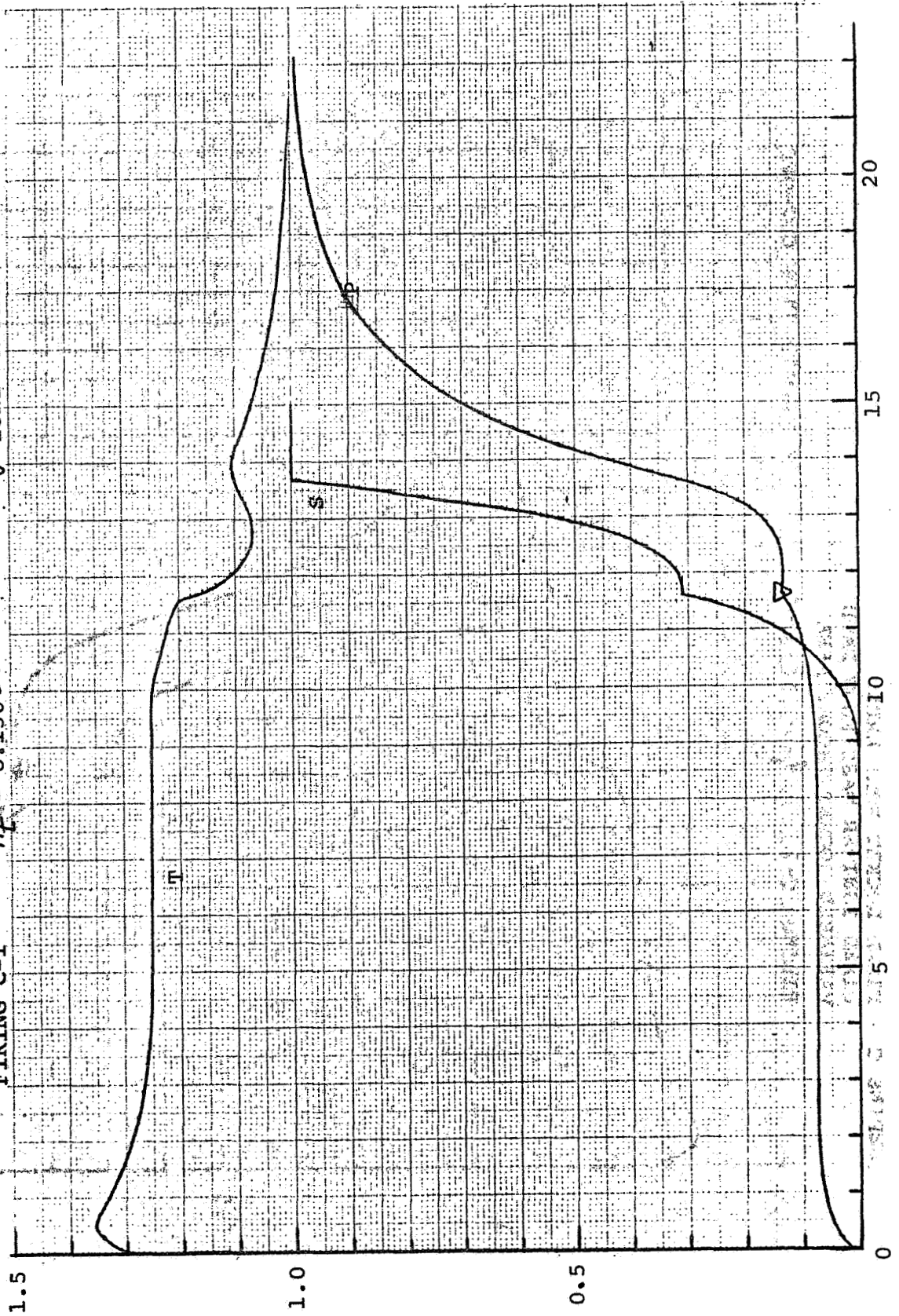
LINE FROM START OF IGNITER (Z* = 0)

SERIES C - FIXED ROCKET PORT AREA

FIXED IGNITER MASS FLOW-RATE
VARIABLE ROCKET THROAT AREA

FIRING C-1 $A_T = 0.150 \text{ cm}^2$

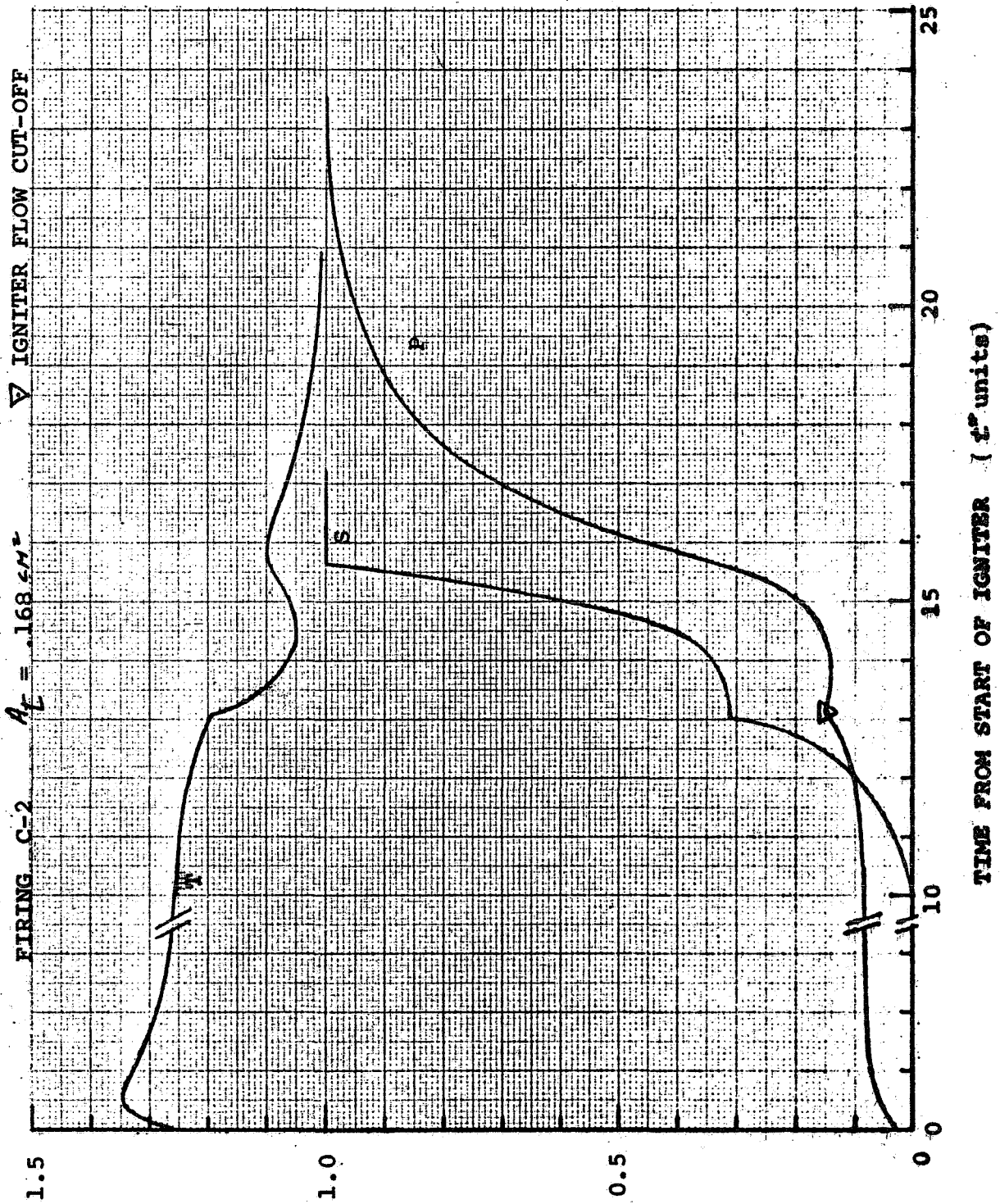
▽ IGNITER FLOW CUT-OFF



TIME FROM START OF IGNITER (Z^* units)

FIGURE 29

SERIES C - FIXED ROCKET PORT AREA
 FIXED IGNITER MASS FLOW RATE
 VARIABLE ROCKET THROAT AREA



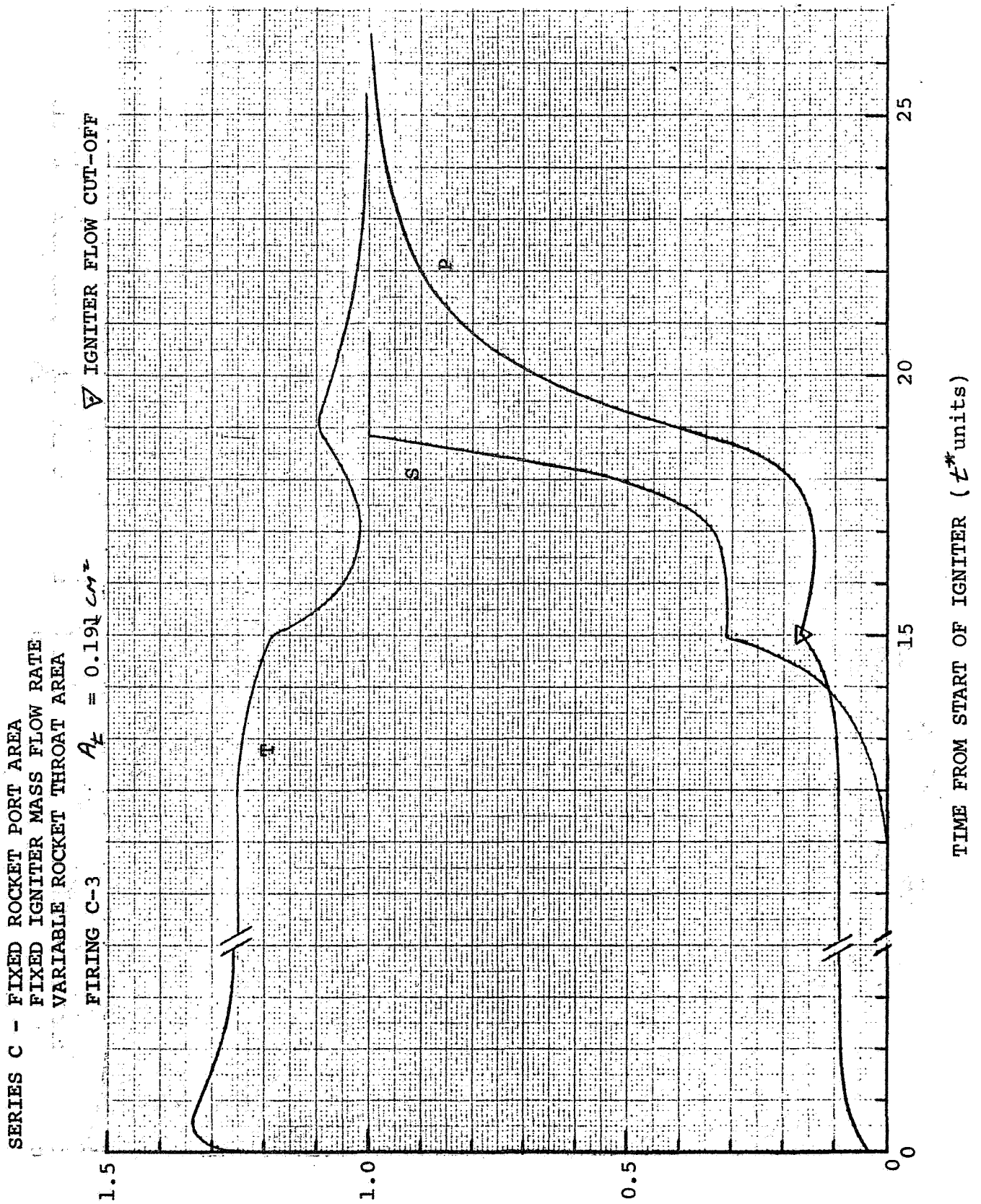


FIGURE 31

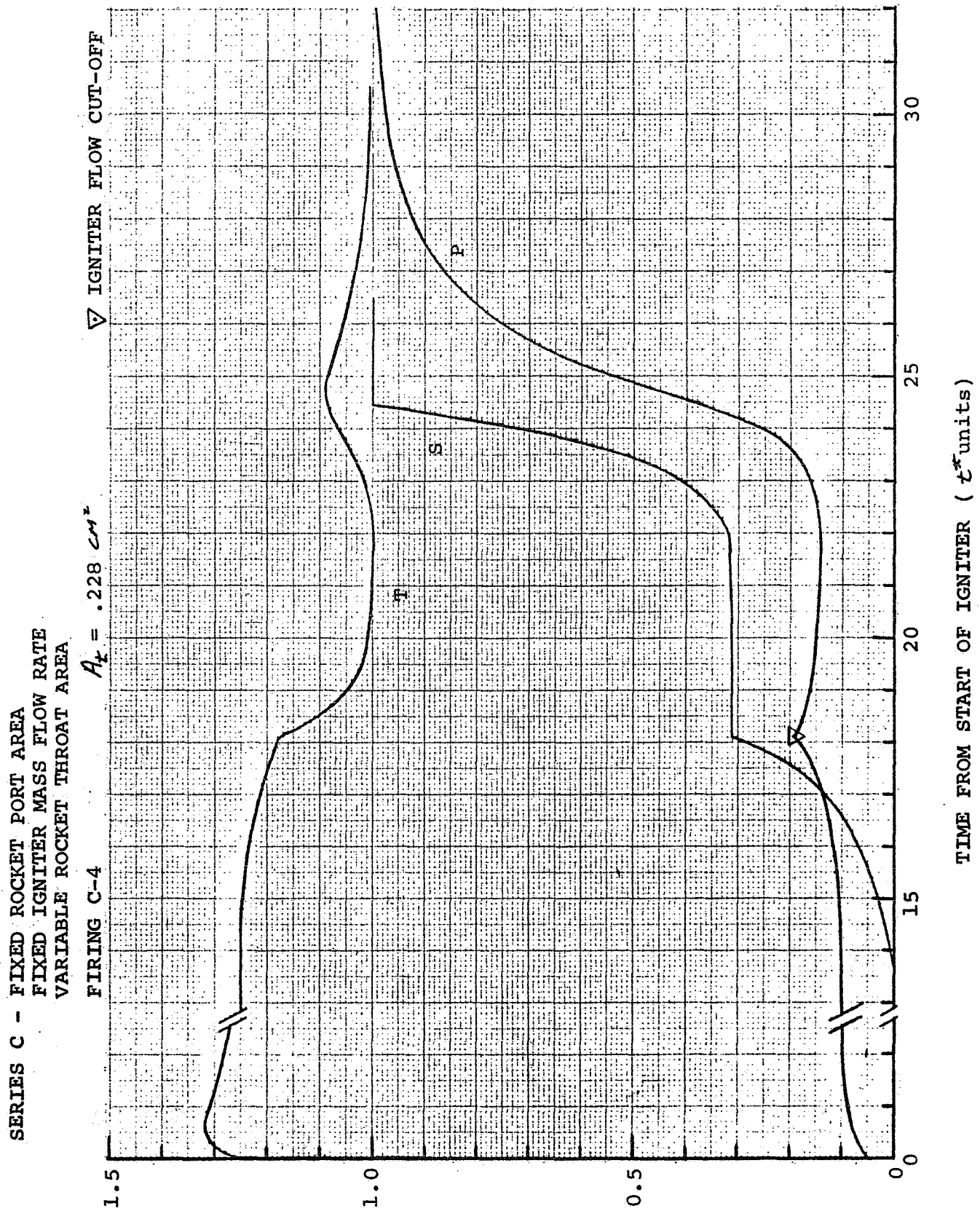
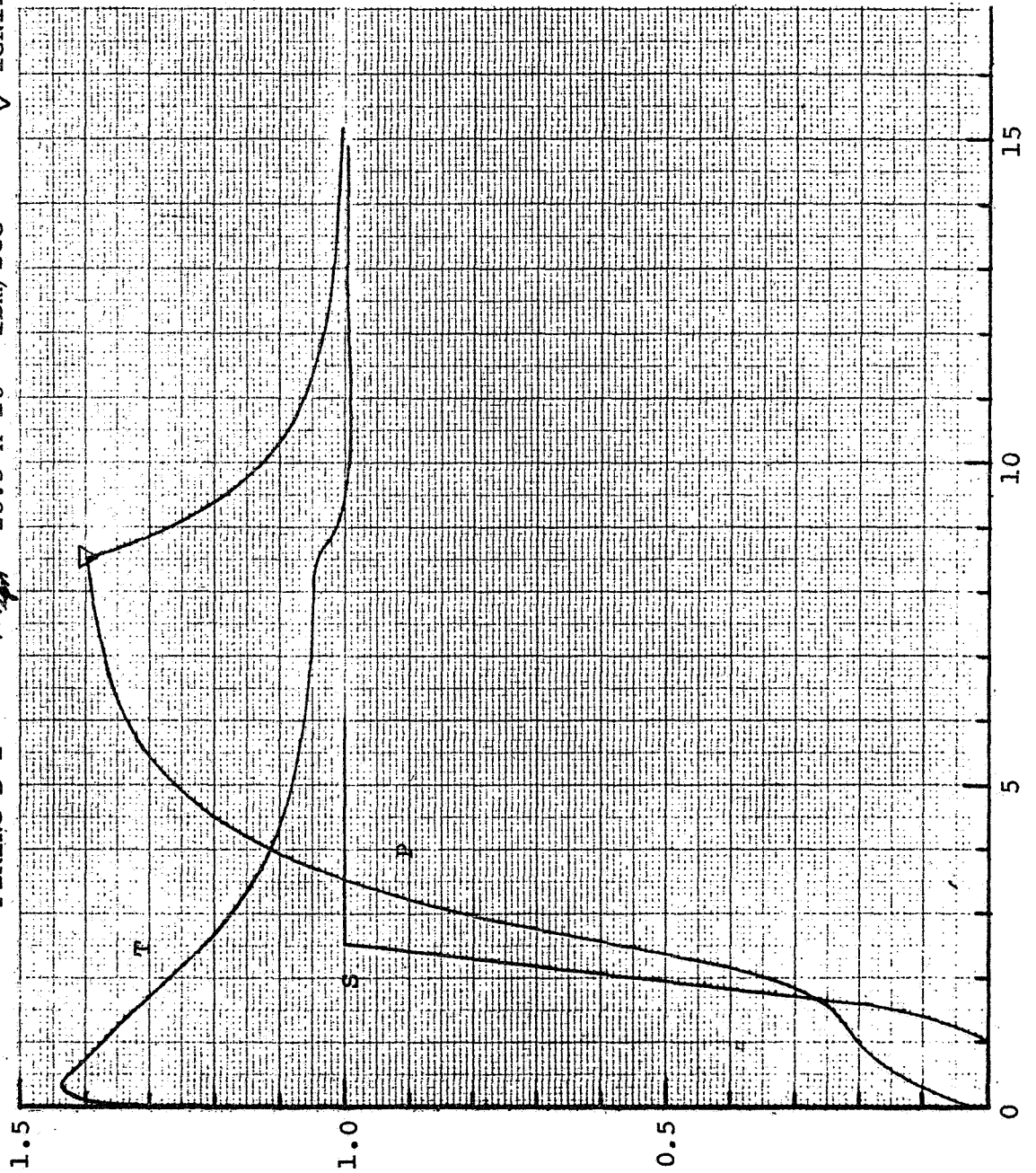


FIGURE 32

SERIES D - FIXED ROCKET GEOMETRY
 VARIOUS IGNITER FLOW RATES
 EXTENDED IGNITER DURATION

FIRING D-1 $\dot{m}_{ig} = 26.5 \times 10^{-3}$ lbm/sec ∇ IGNITER FLOW CUT-OFF



TIME FROM START OF IGNITER (t^* units)

FIGURE 33

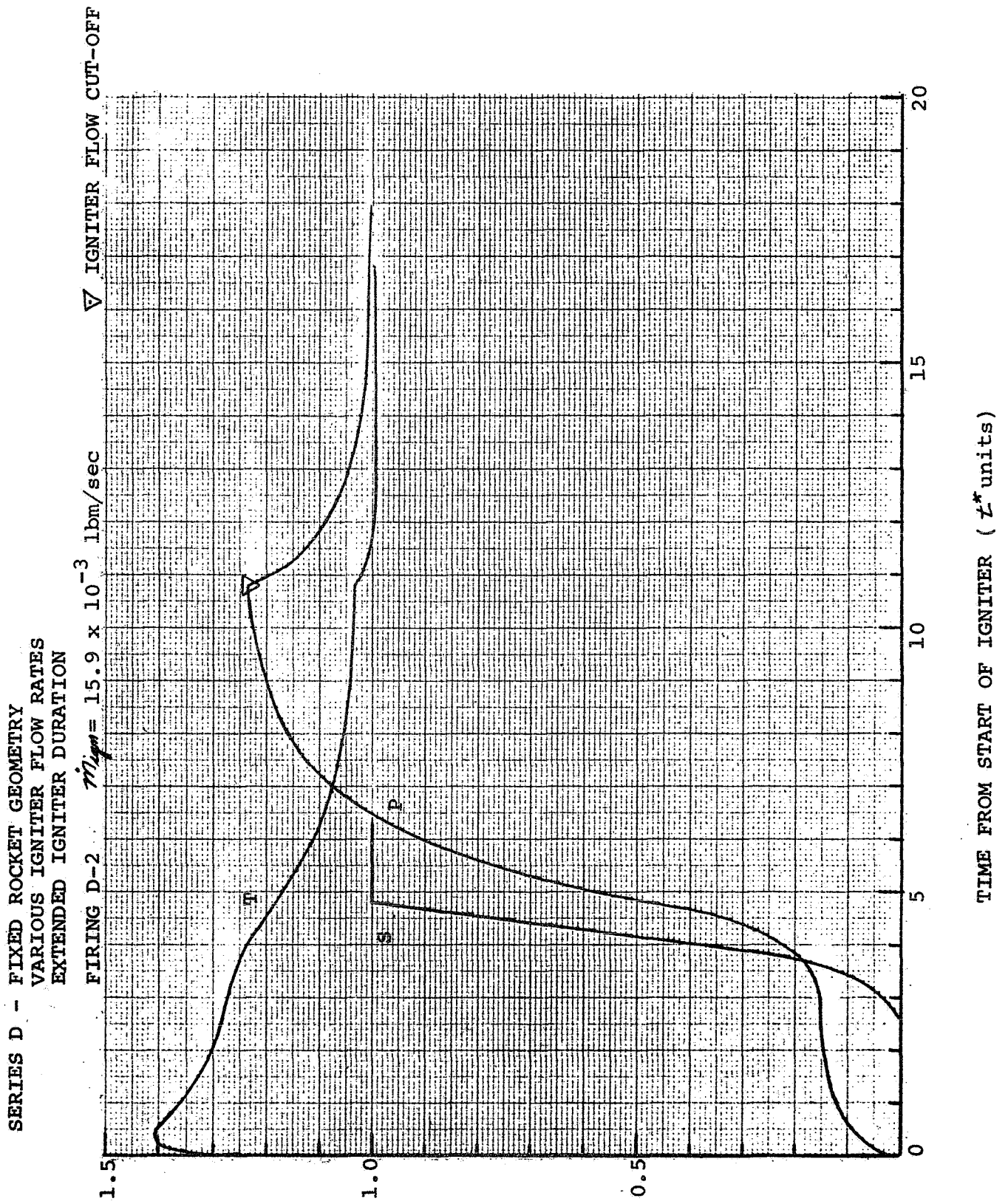


FIGURE 34

SERIES D - FIXED ROCKET GEOMETRY
 VARIOUS IGNITER FLOW RATES
 EXTENDED IGNITER DURATION

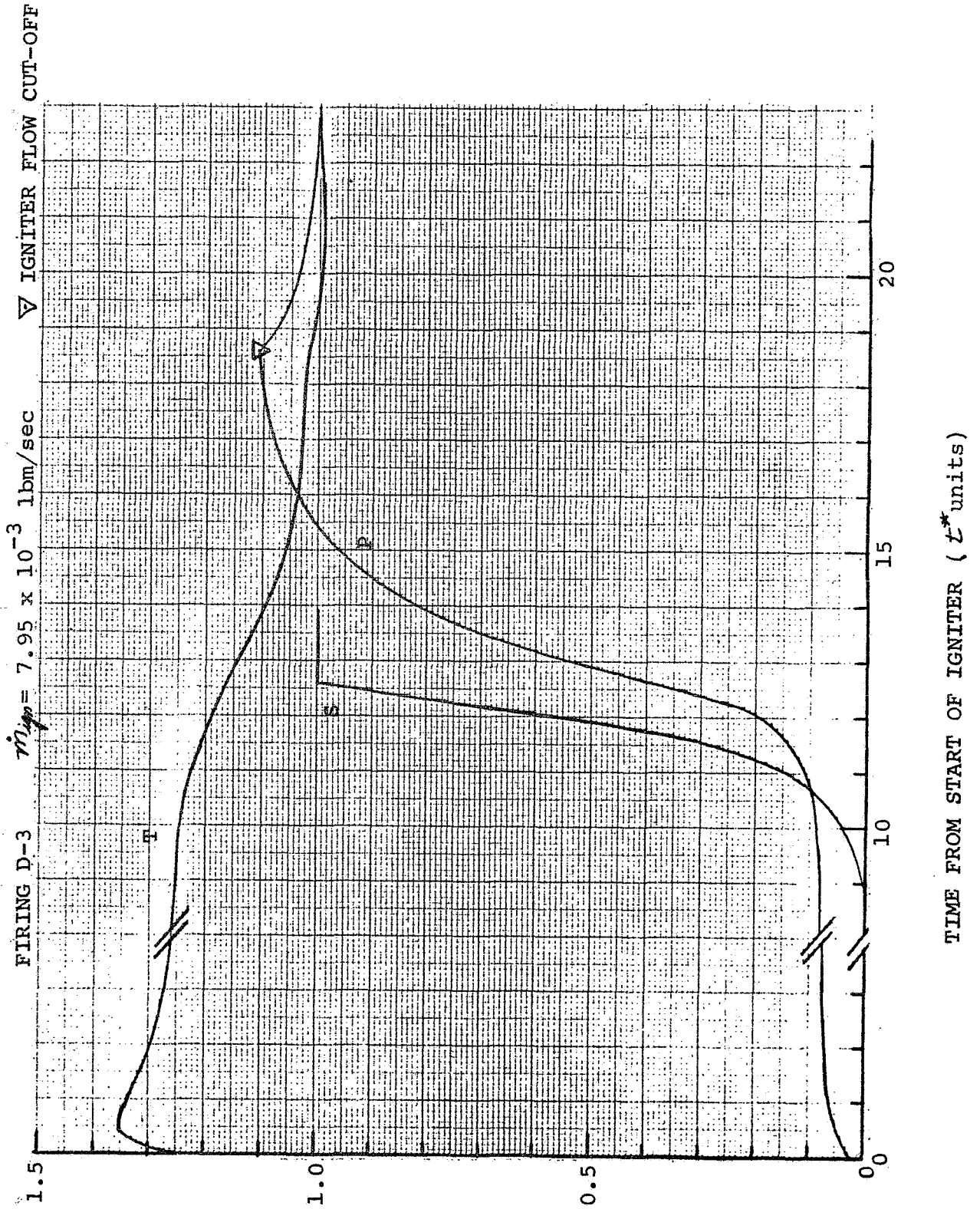


FIGURE 35

SERIES E - FIXED ROCKET GEOMETRY
 FIXED TOTAL IGNITER MASS
 VARIOUS IGNITER FLOW RATES

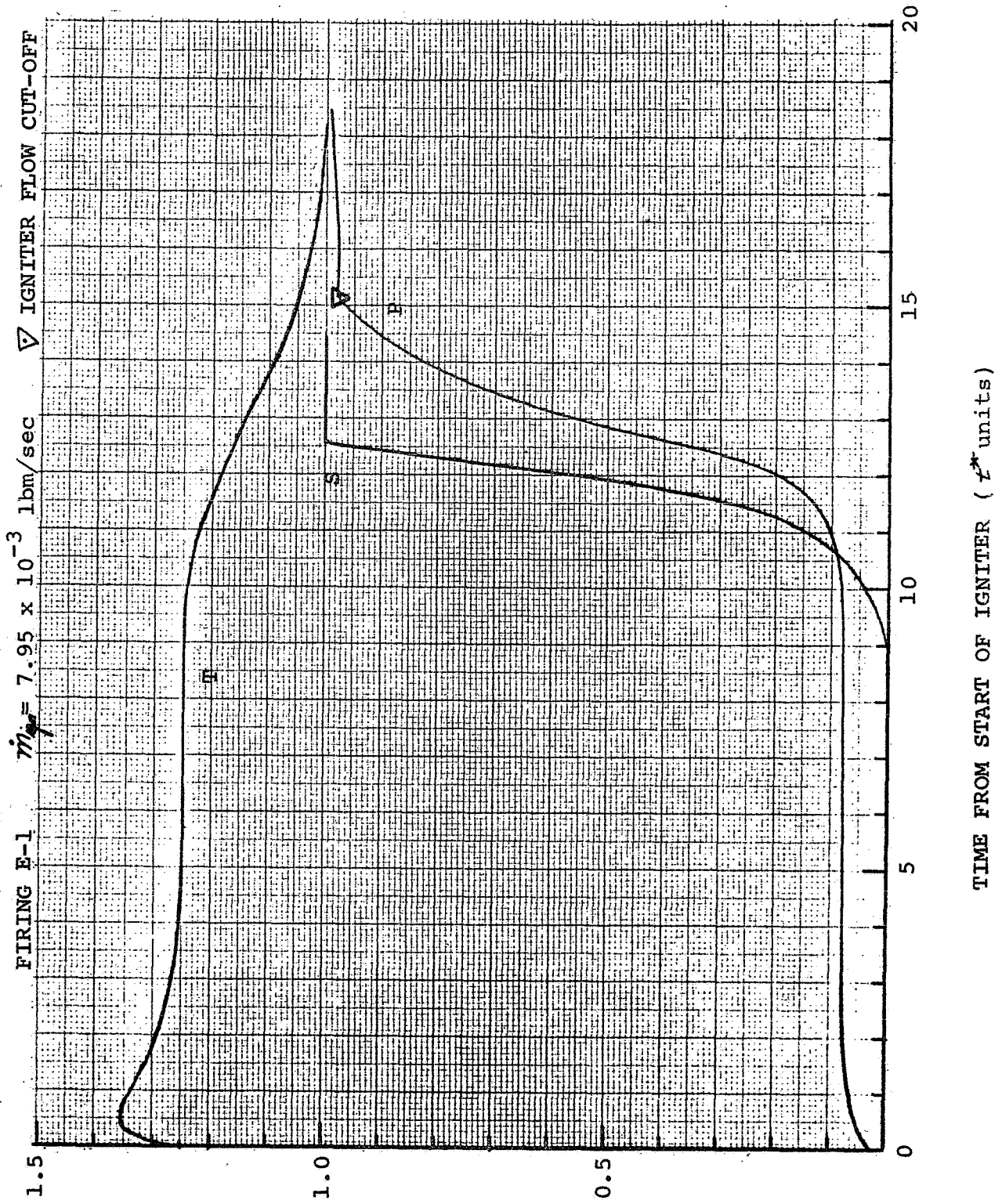


FIGURE 36

SERIES E - FIXED ROCKET GEOMETRY
 FIXED TOTAL IGNITER MASS
 VARIOUS IGNITER FLOW RATES

FIRING E-2 $\dot{m}_{ign} = 6.62 \times 10^{-3}$ lbm/sec

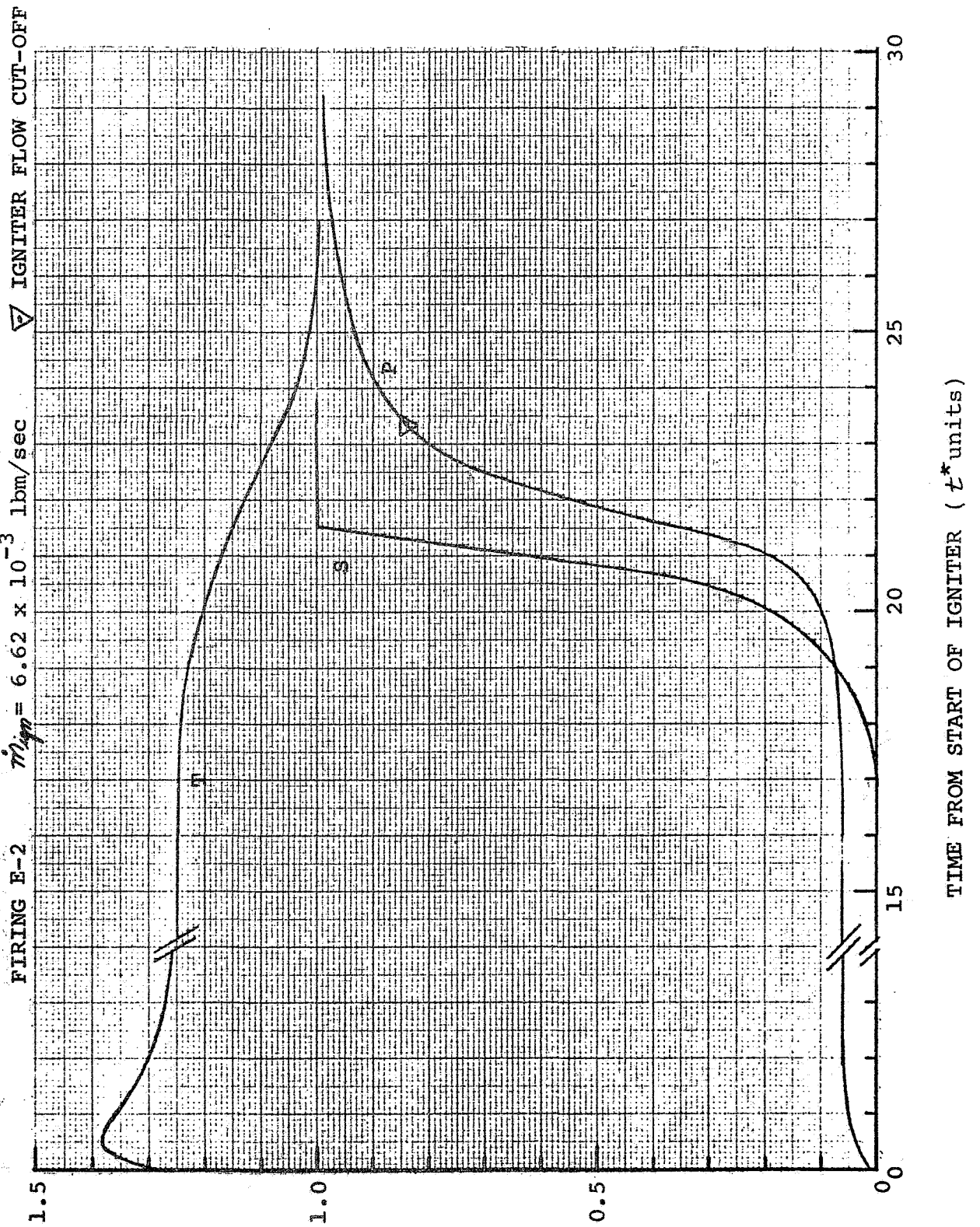


FIGURE 37

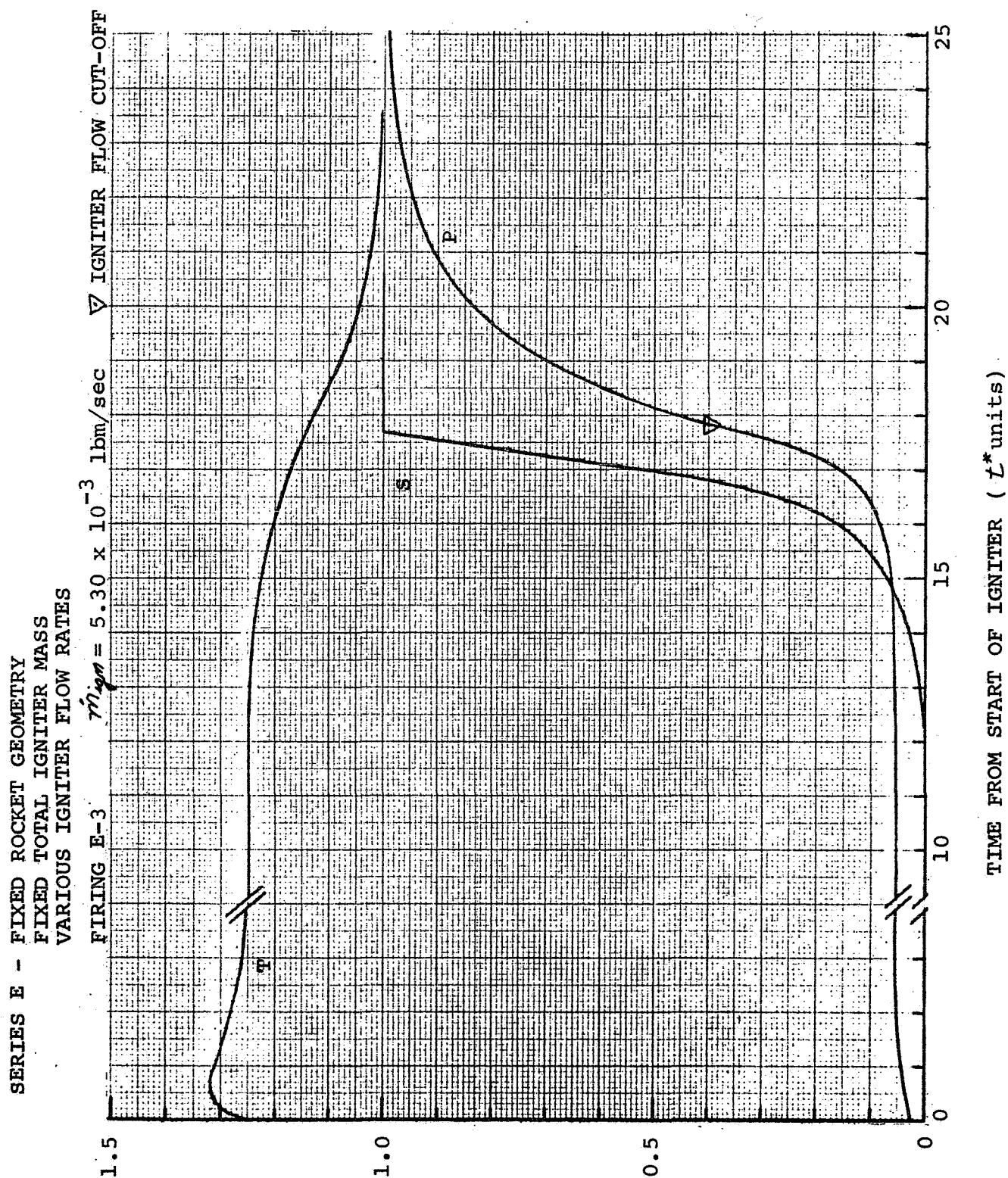


FIGURE 38

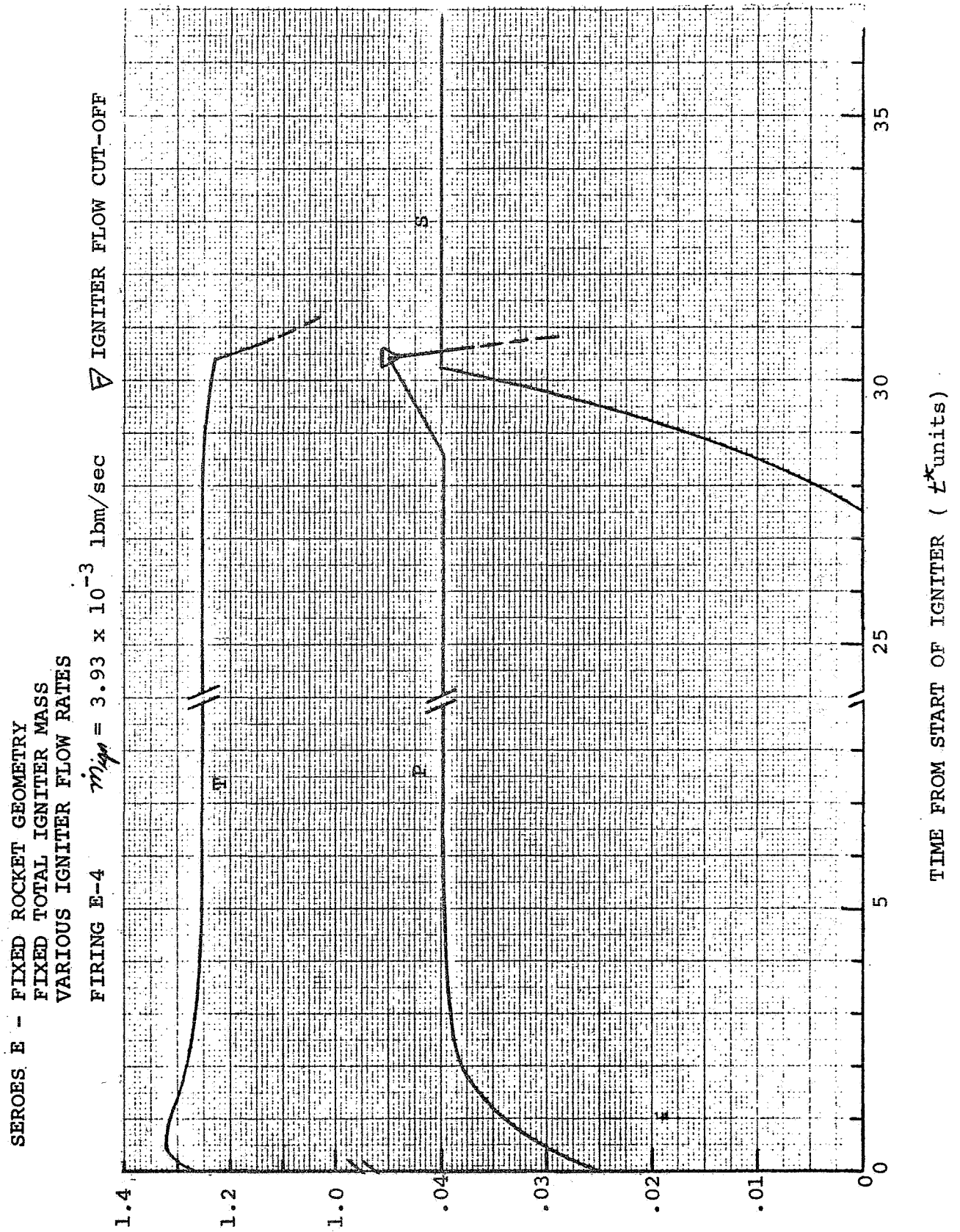


FIGURE 39

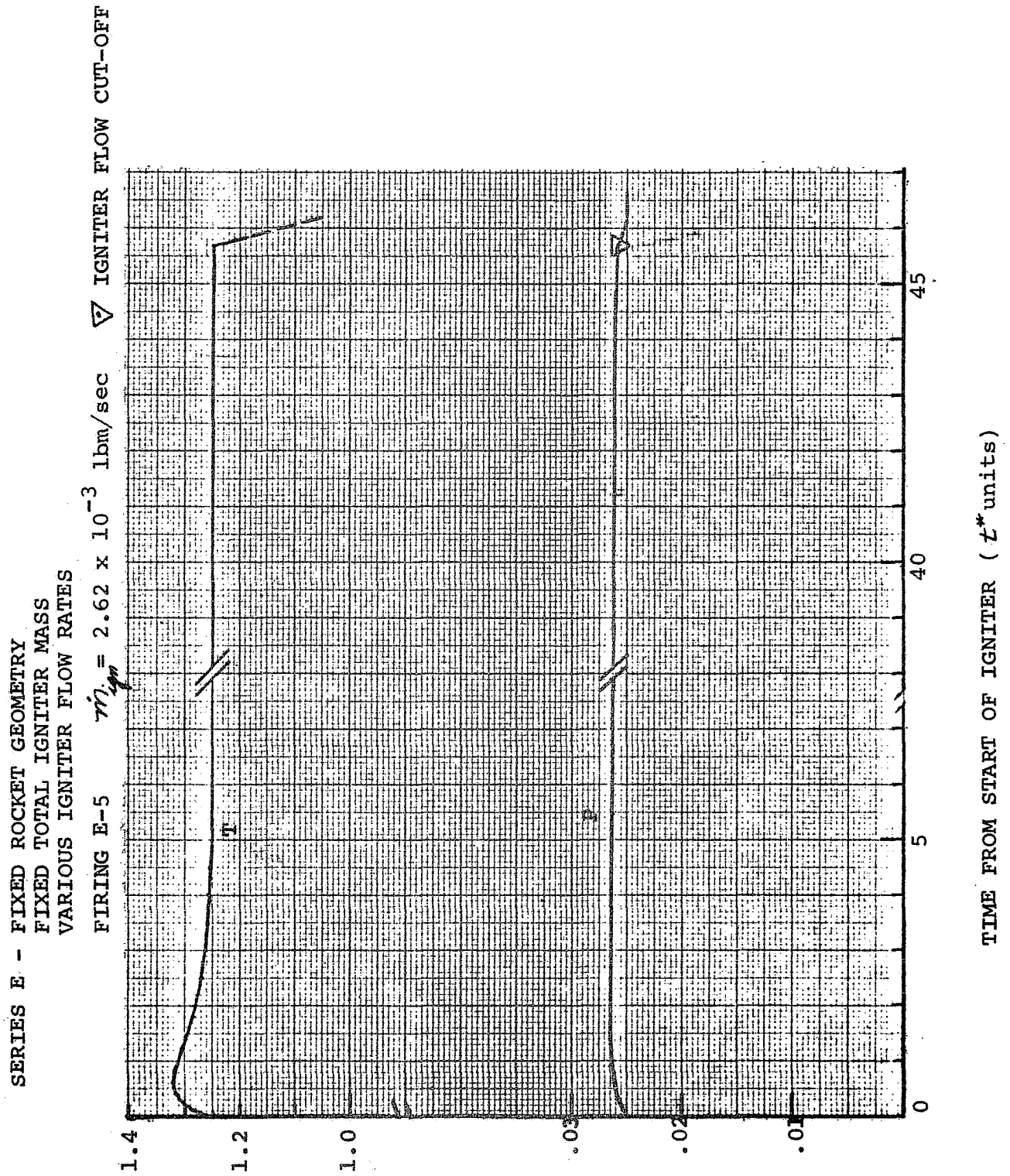


FIGURE 40

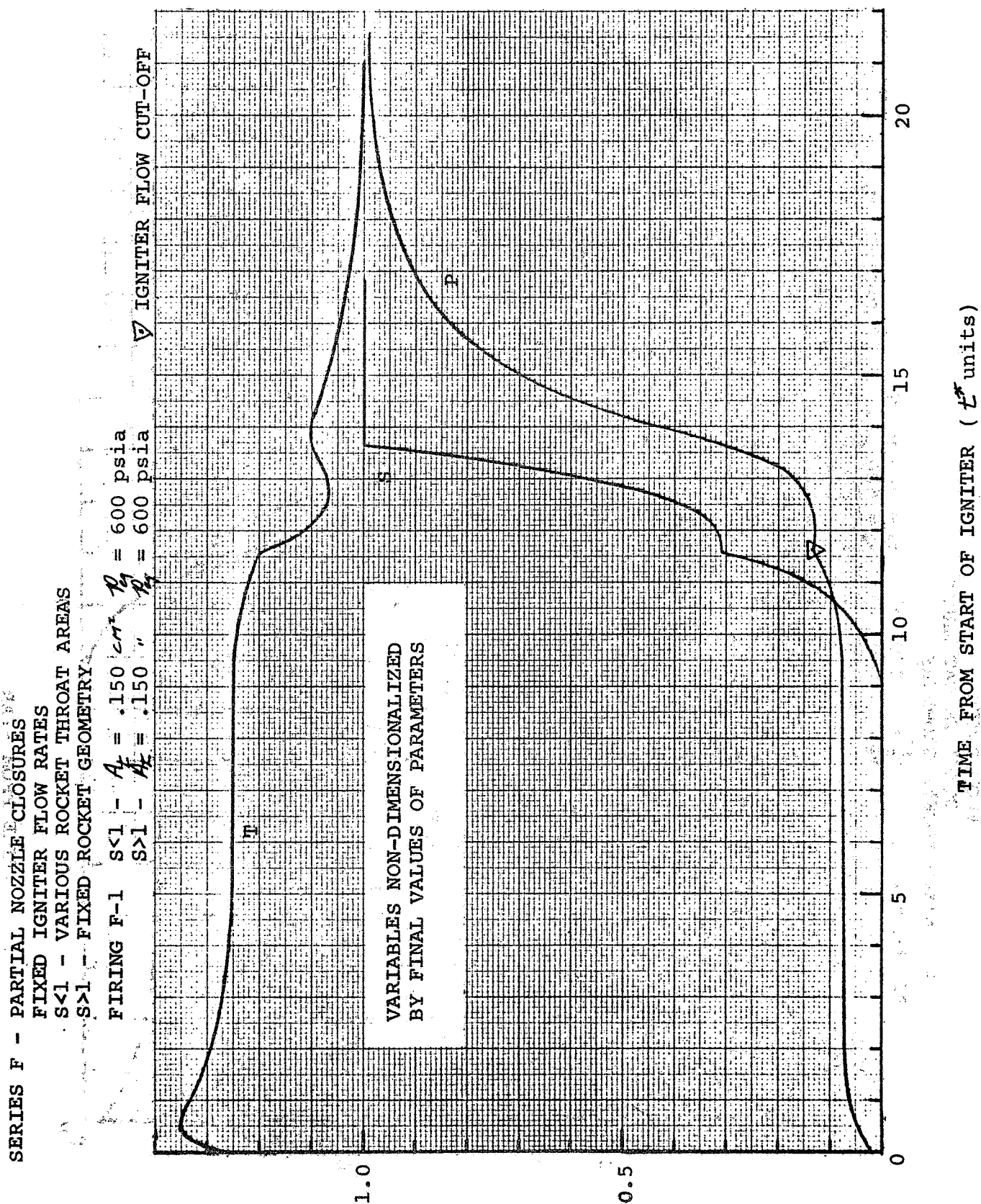
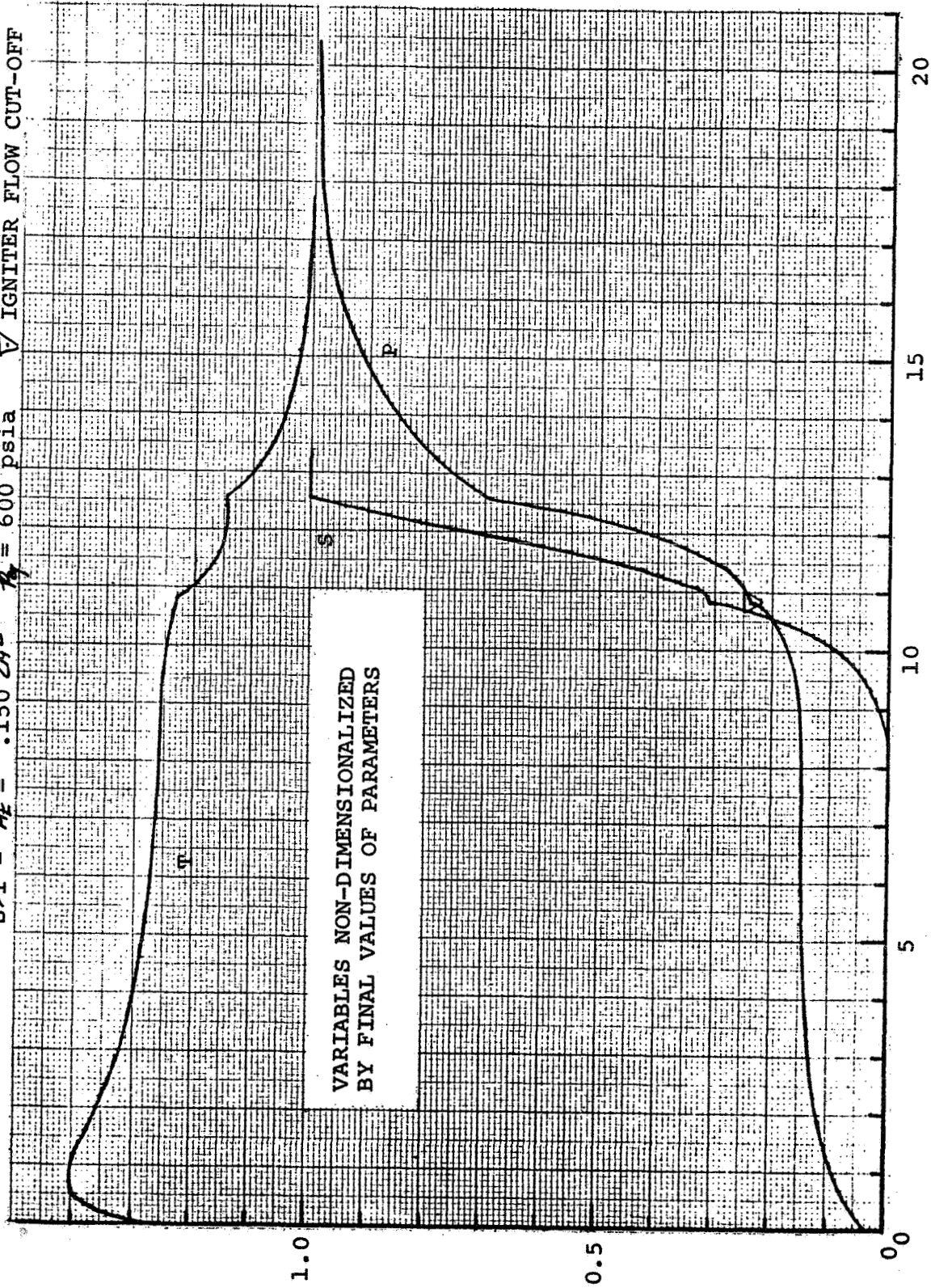


FIGURE 41

SERIES F - PARTIAL NOZZLE CLOSURES
 FIXED IGNITER FLOW RATES
 $S < 1$ - VARIOUS ROCKET THROAT AREAS
 $S > 1$ - FIXED ROCKET GEOMETRY

FIRING F-2 $S < 1 - A_T = .078 \text{ cm}^2$ $P_0 = 800 \text{ psia}$
 $S > 1 - A_T = .150 \text{ cm}^2$ $P_0 = 600 \text{ psia}$

▽ IGNITER FLOW CUT-OFF



TIME FROM START OF IGNITER (t^* units)

FIGURE 42

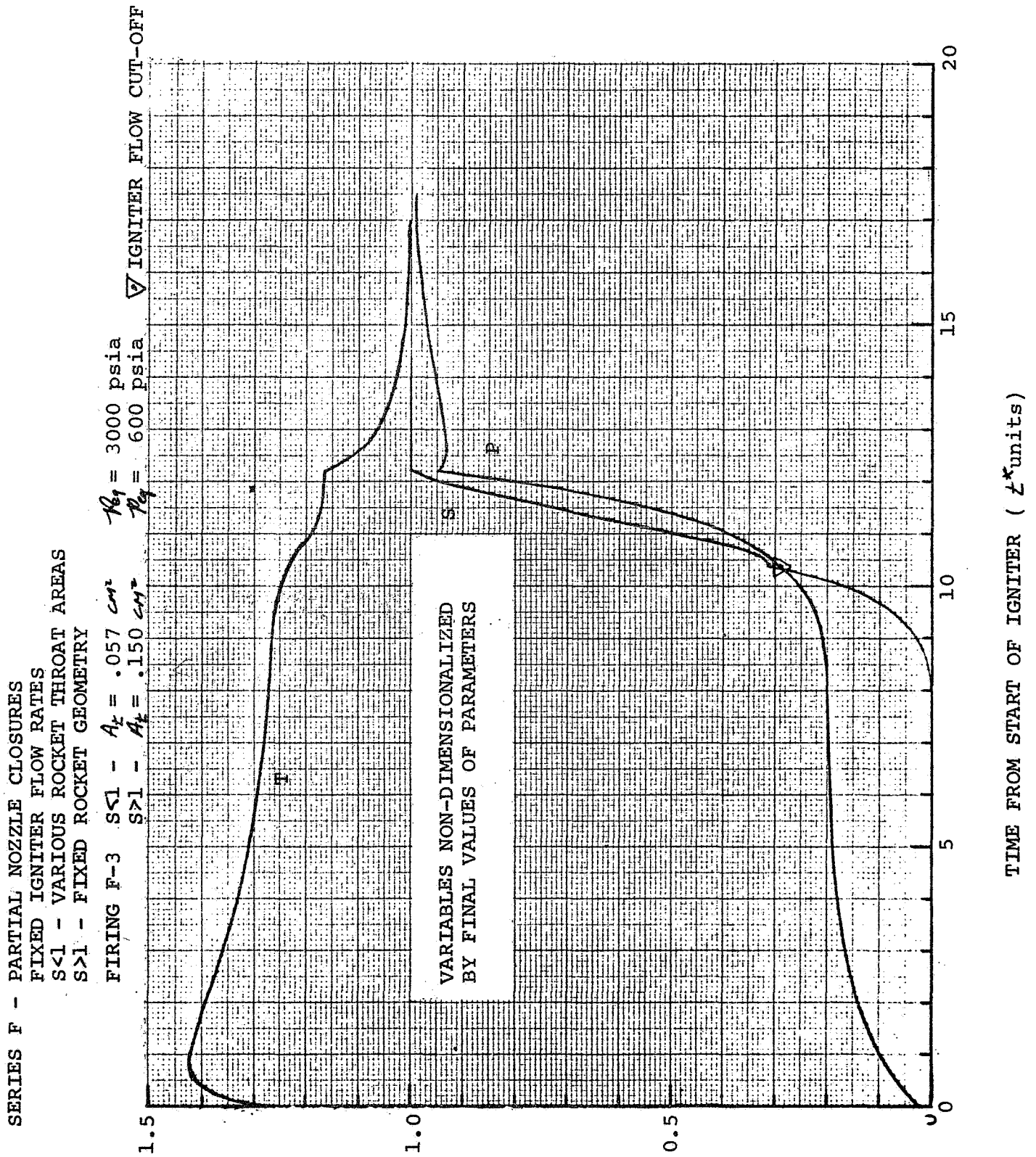


FIGURE 43

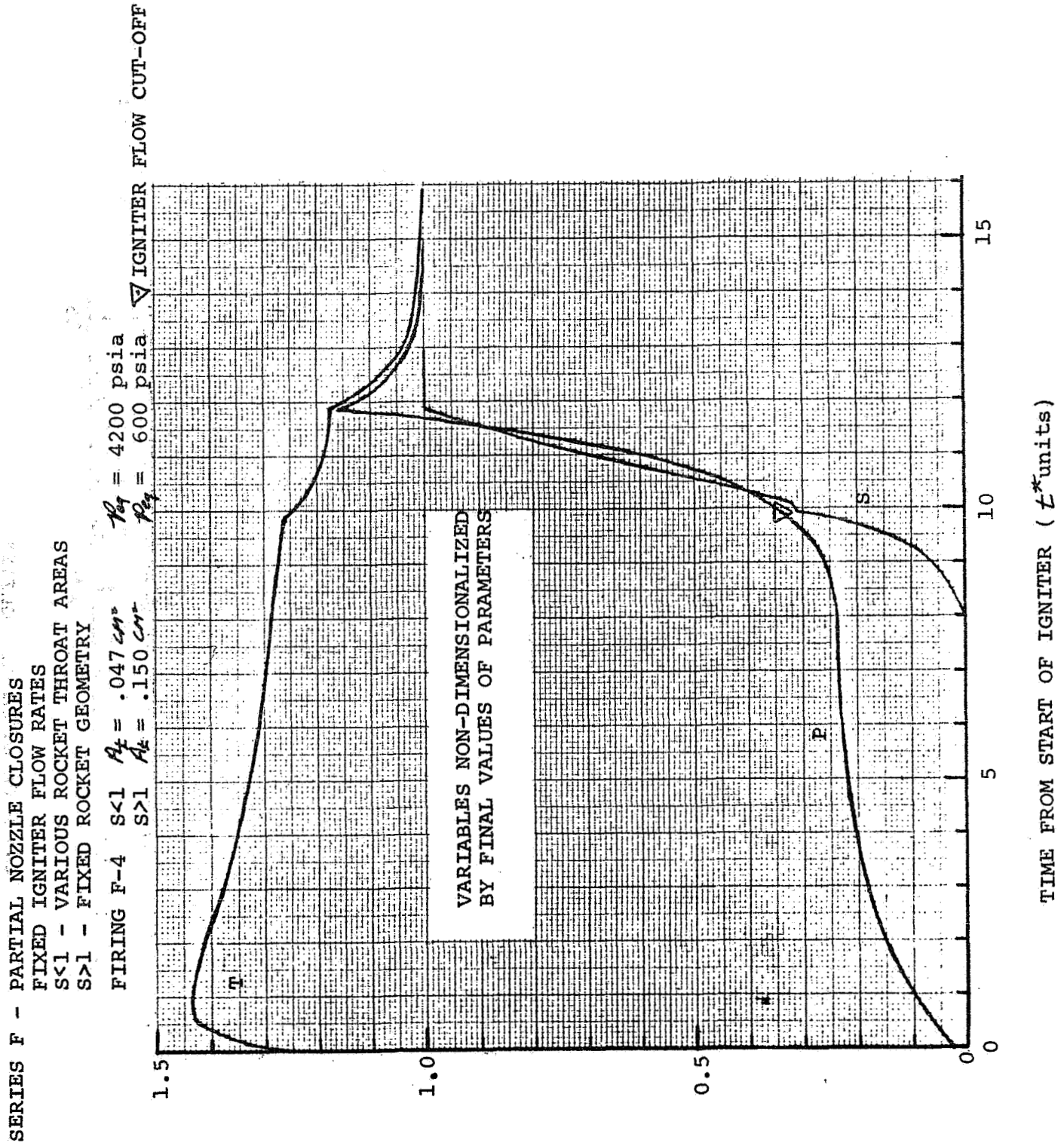


FIGURE 44

APPENDIX IDYNAMIC BURNING RATE

In order to determine how the burning rate varies during a pressure transient, a thermal analysis of a burning propellant is performed. Due to the very low thermal conductivity of solid propellants, the grain may be considered a semi-infinite slab. For time $t < 0$ the solid which is at a uniform initial temperature is ignited, and it is allowed to attain steady state burning at a chamber pressure P_c . The surface temperature is fixed at a value T_s . At $t = 0$ there is a known temperature distribution in the solid, and the chamber pressure is varied continuously with time. The steady state burning rate of the grain is given by the power law $r_{ss} = k p_c^n$.

For analyses involving a moving boundary it is usually convenient to employ a coordinate system which moves with this boundary. Hence for all times $x = 0$ will be the propellant surface. The heat conduction equation in this coordinate system becomes

$$\frac{\partial T}{\partial t} - r_b(t) \frac{\partial T}{\partial x} - \alpha_p \frac{\partial^2 T}{\partial x^2} = 0 \quad \text{AI-1}$$

For this analysis the following notation is used:

subscript "ss" denotes steady state conditions at any pressure level

subscript "b" denotes instantaneous conditions

subscript "eq" denotes equilibrium conditions at the final, equilibrium pressure

For the propellant burning in the steady state prior to the deliberate pressure variation, Equation AI-1 reduces to

$$\alpha_p \frac{d^2 T}{dx^2} + r_{ss} \frac{dT}{dx} = 0, \quad t < 0$$

The boundary conditions necessary for a solution are

$$\begin{aligned} \chi = 0 & , T = T_s \\ \chi \rightarrow \infty & , T \rightarrow T_o \end{aligned}$$

The solution is readily obtained

$$T(\chi) = T_o + (T_s - T_o) e^{-\frac{r_{ss}}{\alpha_p} \chi} \quad \text{AI-2}$$

where the steady state burning is constant and given by

$$r_{ss} = k p_o^n$$

At $t=0$ the pressure is varied, and the initial temperature distribution is given by Equation AI-2. The heat conduction expressed in the form of Equation AI-1 is used. The initial and boundary conditions are:

$$\begin{aligned} t = 0 & , T = T_i(\chi) \\ \chi = 0 & , T = T_s \\ \chi \rightarrow \infty & , T \rightarrow T_o \end{aligned}$$

Since the burning rate is also an unknown, it is necessary to specify a fourth boundary condition -- the heat balance at the surface of the propellant is used. The heat flux from the flame zone is balanced by the heat absorbed or evolved by pyrolysis, Q , and the heat conducted into the interior of the solid.

$$\chi = 0 , \quad -\lambda_p \frac{\partial T}{\partial \chi} + \rho_p Q r_b(t) = q_b(t)$$

where Q is a positive quantity for an endothermic pyrolysis and negative for an exothermic pyrolysis.

(Note: The proper formulation of the conditions at the solid surface is somewhat debatable. A preferable model might be one that allows the surface temperature to vary during the burning rate transient and couples the instantaneous burning rate to the surface temperature through a standard pyrolysis law. The model given here is simpler.)

Since the reactions in the flame zone are expected to occur much faster than the thermal conduction in the solid, it is assumed that the gas phase processes adjust instantaneously to the pressure variations. Using Summerfield's approach in the development of the granular diffusion theory of solid propellant combustion²¹, an effective flame thickness, L , is defined. The heat flux from the flame at any instant can be expressed;

$$q_b = \frac{\lambda_g (T_c - T_s)}{L}$$

This flame thickness can be expressed as a linear function of the instantaneous gas velocity at the surface and the time of reaction,

$$L \approx u t^* = r_b \left(\frac{\rho_p}{\rho_g} \right) t^*$$

The instantaneous heat flux from the flame becomes

$$q_b = \frac{\lambda_g \rho_g}{\rho_p} \frac{(T_c - T_s)}{r_b t^*}$$

Now the assumption of the instantaneous response of the gas phase to pressure changes permits the evaluation of t^* at the steady state condition. From equation AI-2 and the heat balance at the surface

$$\begin{aligned} q_{ss} &= -\frac{\lambda_p}{\alpha_p} r_{ss} (T_s - T_o) + \rho_p Q r_{ss} \\ &= q_b \\ &= \frac{\lambda_g \rho_g}{\rho_p} \frac{(T_c - T_s)}{r_b t^*} \end{aligned}$$

Solving for t^* and using it in the instantaneous flux equation yields

$$q_b = \rho_p [Q + c_p (T_s - T_o)] \frac{r_{ss}^2}{r_b}$$

Finally, the flame temperature, gas properties, and heat of pyrolysis are assumed constant. The surface temperature is also assumed constant, but the resulting analysis will show that extinguishment due to rapid depressurization cannot be predicted. For the extinguishment analysis the surface temperature should be allowed to vary. For the purposes of this work a variable surface temperature is an unnecessary complication.

Recalling the assumed burning rate law for steady state burning, the last boundary condition becomes

$$-\lambda_g \frac{\partial T}{\partial x} + \rho_p Q \gamma_b(t) = \rho_p k^{\frac{1}{2}} [Q + c_p (T_s - T_o)] \frac{p_c^{2\eta}}{\gamma_b}$$

Equation (AI-1) together with the boundary and initial conditions are sufficient to solve for the instantaneous burning rate as a function of time. At this stage of the analysis it is convenient to express all variables in dimensionless form. The following quantities are defined:

$$\Theta \equiv \frac{T - T_o}{T_s - T_o}$$

$$\xi \equiv \frac{x}{\alpha_p / r_{eq}}$$

$$\tau \equiv \frac{t}{\alpha_p / r_{eq}^2}$$

$$r \equiv \frac{r_b}{r_{eq}}$$

$$p \equiv \frac{p_c}{p_{eq}}$$

$$Q' \equiv \frac{Q}{c_p (T_s - T_o)}$$

The reference distance and time are physically meaningful. Examining Equation AI-2 the quantity α_p/v_{eq} is seen to be proportional to the depth of the thermal wave in the propellant at equilibrium, and α_p/v_{eq}^2 is called the reaction time within the solid. Under this transformation the system of equations becomes,

$$\frac{\partial \theta}{\partial \tau} - r \frac{\partial \theta}{\partial \xi} - \frac{\partial^2 \theta}{\partial \xi^2} = 0$$

AI-3

$$\tau = 0, \quad \theta = \theta_I(\xi)$$

$$\xi \rightarrow \infty, \quad \theta \rightarrow 0$$

$$\xi = 0, \quad \theta = 1$$

$$\frac{\partial \theta}{\partial \xi} = Q' r - (Q' + 1) \frac{p^{27}}{r}$$

The pressure $p(\tau)$ is assumed to be a continuous, monotonically increasing or decreasing function of time. Hence there is a one-to-one correspondence between p and τ so that

$$\tau = \tau(p)$$

Defining

$$p' \equiv \frac{1}{\epsilon} \frac{dp}{d\tau}$$

$$\epsilon \equiv \left(\frac{dp}{d\tau} \right)_{MAX}$$

Under this transformation Equations AI-3 becomes

$$\epsilon p'(p) \frac{\partial \theta}{\partial p} - r(p) \frac{\partial \theta}{\partial \xi} - \frac{\partial^2 \theta}{\partial \xi^2} = 0$$

AI-4

$$p = p_I, \quad \theta = \theta_I(\xi')$$

$$\xi' \rightarrow \infty, \quad \theta \rightarrow 0$$

$$\xi' = 0, \quad \theta = 1$$

$$\frac{\partial \theta}{\partial \xi} = Q' r(p) - (Q' + 1) \frac{p^{27}}{r(p)}$$

Due to the poor thermal conductivity of propellants the characteristic thermal distance $\alpha p / v_{eq}$ and the characteristic time $\alpha p / v_{eq}^2$ are very small quantities. Even though (dp/dt) may be very large, the rate of rise of pressure on the characteristic time scale is usually very small. Hence this problem may be analyzed using ϵ as a small perturbation expansion parameter.

Quasi-Steady Solution

In the limit as $\epsilon \rightarrow 0$, Equation AI-4 reduces to

$$r(p) \frac{\partial \theta}{\partial \xi} + \frac{\partial^2 \theta}{\partial \xi^2} = 0$$

Now in order to obtain a solution compatible with the initial condition, the initial temperature distribution must be the steady state distribution at $p = p_I$. This distribution is given by Equation AI-2. If some other temperature distribution is specified, a burning rate transient due to the initial temperature distribution arises. This problem has not been solved in any generality. The solution under the assumed condition is

$$\theta = e^{-p^n \xi}$$

$$r = p^n$$

ϵ Small But Not Negligible

Using the above results a solution for the first order in ϵ can be obtained. Assuming the solution in the form

$$\theta(\xi, p) = e^{-p^n \xi} + \epsilon \phi(\xi, p)$$

$$r(p) = p^n + \epsilon r_1(p)$$

where ϕ and r_1 are correction functions. Using these in Equation AI-4 the heat conduction equation, to order ϵ , becomes

$$\frac{\partial^2 \phi}{\partial \xi^2} + p^n \frac{\partial \phi}{\partial \xi} + (n \xi p' p^{-(1-n)} - r_1 p^n) e^{-p^n \xi} \quad \text{AI-5}$$

$$\begin{aligned} p &= p_I, & \phi &= 0 \\ \xi &\rightarrow \infty, & \phi &= 0 \\ \xi &= 0, & \phi &= 0, \quad \frac{\partial \phi}{\partial \xi} = (2Q' + 1) r_1(p) \end{aligned}$$

The differential equation is linear, second order, and inhomogeneous with solution

$$\phi = \left[\left(\frac{n p'}{p' + n} - r_1 \right) \xi + \frac{n}{2} \frac{p'}{p} \xi^2 \right] e^{-p^n \xi}$$

Using the heat balance at the surface $r_1(p)$ is determined;

$$r_1(p) = \frac{1}{Q' + 1} \frac{n}{2} \frac{p'}{p^{1+n}}$$

Transforming back to the (ξ, τ) space yield the burning rate to order ϵ ;

$$r = p^n + \frac{1}{Q' + 1} \frac{n}{2} \frac{1}{p^{1+n}} \frac{dp}{d\tau} \quad \text{AI-6}$$

Finally transforming back to dimensional quantities, the burning rate is given by the expression

$$r_b = r_{ss} \left[1 + \left(\frac{c_p (T_s - T_o)}{Q + c_p (T_s - T_o)} \frac{n}{2} \frac{\alpha p}{p_c r_{ss}^2} \right) \frac{dp_c}{dt} \right] \quad \text{AI-7}$$

Footnote: Recent references which present a more sophisticated approach to this problem are:

¹Summerfield, M., Krier, H., T'ien, J. Shaw-t., and Sirignano, W. A., "Non-steady Burning Phenomena of Solid Propellants: Theory and Experiment", Princeton University AMS Report No. 793, AFOSR Scientific Report No. 67 1535, July, 1967.

²Krier, H., T'ien, J. S., Sirignano, W. A., and Summerfield, M., "Non-steady Burning Phenomena of Solid Propellants: Theory and Experiment", ICRPG/AIAA Second Propulsion Conference, Anaheim, California, June 6-8, 1967.

APPENDIX IINUMERICAL COMPUTATIONS

The system of equations governing the chamber filling process is derived and discussed in the main text of this report. These dimensional and dimensionless equations used for the numerical calculations are repeated here for convenience and completeness.

Continuity and energy for the chamber free-volume control volume are

$$\frac{dp}{d\tau} = \gamma \left[5p^n - pT^{1/2} + p_{cign} T_{cign}^{1/2} \frac{A_{xign} f(\tau)}{A_t} \right] \quad \text{AII-1}$$

$$\frac{dT}{d\tau} = \frac{T}{p} \left[(\gamma - T) 5p^n - (\gamma - 1) p T^{1/2} + p_{cign} T_{cign}^{1/2} \frac{A_{xign} (\gamma T_{cign} - T) f(\tau)}{A_t} \right] \quad \text{AII-2}$$

The form of the function $f(\tau)$ chosen for the numerical computations is a square wave.

$$f(\tau) = \begin{cases} 1 & 0 \leq \tau \leq \tau_{crit} \\ 0 & \tau > \tau_{crit} \end{cases}$$

The igniter cut-off time, τ_{crit} , was chosen differently for the various series. For series A, B, C, and F, rather than choose an arbitrary time for τ_{crit} , it seemed best to relate it in some way to the transient. For these cases it was decided to cut the igniter off after a prescribed percentage of the propellant surface had ignited. This critical area was taken to be thirty per cent of the final area. Series D was run to show pressure overshoots due to overduration igniters, so the igniter was cut off at some time after equilibrium pressure was reached. This time was chosen to be six t^* units after the end of flame spreading. Finally, Series E was run to show the effect of decreasing igniter flow rate while holding the mass of the igniter constant. The igniter mass was chosen as that mass which would enable the igniter of Firing A-2 to fire until the motor attained ninety-eight per cent of its equilibrium pressure. This was a mass of 2.14×10^{-3} lbs. Thus, for

Series E,

$$\tau_{crit} = \frac{m_{ign}}{\dot{m}_{ign}}$$

where $m_{ign} = 2.14 \times 10^{-3}$ lbs. and \dot{m}_{ign} was varied.

In order to generate the function $S(\tau)$, the heat transferred to the unignited portions of the propellant surface is considered. Convection is assumed to be the dominant mode of heat transfer, and it is adequately described by the following empirical correction:

$$Nu_x = 0.09 Re_x^{0.8}$$

AII-3

The heat conduction equation for the surface temperature of the propellant which is assumed to have a semi-infinite thickness is converted into an integral equation.

$$T_s - T_o = \left(\frac{A}{\pi}\right)^{1/2} \frac{B}{(a/l + \xi)^{0.2}} \int_0^{\tau} (T - T_s) \left[\frac{p}{T^{1/2}} + (1 - \xi) \frac{d}{d\tau} \left(\frac{p}{T} \right) \right]^{0.8} \frac{d\tau'}{(\tau - \tau')^{1/2}}$$

The computation of the left hand side of this equation was done in several stages.

$$Re_x = \left(\frac{p_{eq} A_{z,l}}{c^* A_p \mu_g} \right) \left(\frac{a}{l} + \xi \right) \left[\frac{p}{T^{1/2}} + (1 - \xi) \frac{d}{d\tau} \left(\frac{p}{T} \right) \right] \quad (a)$$

$$h = 0.09 \frac{\lambda_g}{l \left(\frac{a}{l} + \xi \right)} Re_x^{0.8} \quad (b)$$

AII-4

$$q(t) = h(T - T_s) \quad (c)$$

$$T_s - T_o = \frac{\alpha_p^{1/2}}{\pi^{1/2} \lambda_p} \int_0^t \frac{q(t')}{(t - t')^{1/2}} dt' \quad (d)$$

This analysis assumes that T , the temperature of the gases in the combustion chamber, is spacially uniform but is a function of time. This can be considered as a first order approximation. If any reasonable heat transfer correlation is integrated down the length of the propellant grain and resulting total heat subtracted from the gases it quickly becomes apparent that substantial changes in the gas

temperature should occur. This has been verified experimentally.

The surface temperature, T_s , is a function of both time and distance from the forward end of the propellant grain as described below.

It has been found that the measured heat transfer data can be correlated with a $(T - T_s)$ which is constant, independent of both x and t . This constant temperature difference is used in Equation C given above. This does not infer any new assumptions. It is justified on the basis of simplifying the empirical heat transfer correlation.

The ignition criterion is simply the attainment of a critical temperature at the surface of the propellant.

$$T_s = T_{crit}$$

AII-5

Finally, the initial conditions on the combustion chamber properties and burning area are

$$T(0) = T_{c,ign}$$

$$p(0) = \text{ambient pressure}$$

$$S(0) = 0$$

Computational Procedure

With the selected initial conditions, and the p and T time derivatives as functions of p , T , and τ , the p and T vs. τ curves are determined. The numerical scheme used in this report to determine these curves is a predictor-corrector method. Given the previous two points, the predictor formula predicts the next point, then the corrector formula uses this predicted value to correct itself. The corrector formula can be applied as many times as necessary to its own previous value until successive values differ by some specified small amount. The formulas are taken from Reference 22, and are as follows:

The Predictor:

$$p_{M+1}^0 = p_{M-1} + 2\Delta\tau \frac{dp}{d\tau}(p_M, \tau_M)$$

AII-6

The Corrector:
$$P_{M+1}^i = P_M + \frac{\Delta \tau}{2} \left[\frac{dP}{d\tau}(P_M, T_M) + \frac{dP}{d\tau}(P_{M+1}^{(i-1)}, T_{M+1}^{(i-1)}) \right] \quad \text{AII-7}$$

where the superscript i represents the i th time through the corrector formula, and the subscript M represents the number of time-steps taken up to that point. The geometric representation of these two formulas is shown in Figures AII-1 and AII-2. Simultaneous with the above equations, there exist similar equations for T . Since the equations require two points previous to that desired, the second point on the curve must be calculated using a simpler scheme - a Runge-Kutta scheme was used in this report.

The corrector formula is applied until

$$|T_{M+1}^i - T_{M+1}^{i-1}|, |P_{M+1}^i - P_{M+1}^{i-1}| < \epsilon \quad \text{AII-8}$$

where ϵ is specified as input data to the computer program. In the cases presented here, ϵ had the value of 10^{-7} . It was found, for the $\Delta \tau$'s used in this report - from .001 to .05, that Equation AII-8 was always satisfied in less than ten iterations, and generally in 2 or less.

In order to calculate $s(\tau)$ the propellant slab is broken up into a finite number of pieces (in the computations for this report the slab was divided into 100 pieces so $\Delta \xi = 0.01$). Initially, the $\xi = 0.01$ point is considered, later during flame spreading the point $\Delta \xi$ in front of the flame is considered. At the particular ξ position Equations AII-4a, b, c are used to calculate $q(t)$ for each time interval up to the present time. Now using Equation AII-4d the surface temperature of the particular portion of the surface is calculated at the given time.

The integral in Equation AII-4d was evaluated using a straightforward summation process shown in Figure AII-3. In the calculation of $Q(M)$, T_s was taken as the surface temperature of the propellant one $\Delta \tau$ earlier than the point being looked at. The difference between these temperatures was generally less than a degree. The surface temperature is then compared to the ignition criterion, Equation AII-5.

If $T_s < T_{ic}$, the time is advanced by one step, and the heat transfer calculations are performed for the same element up to this new time. This advance in time will continue until this element of surface is such that $T_s \geq T_{ic}$. At the end of each time interval the burning area and the chamber properties are reported. If the element of surface is unsuccessful in reaching T_{ic} , then the $s(\tau)$ to be reported is the same as the $s(\tau)$ that was reported in the previous line.

If $T_s \geq T_{ic}$, then the burning has advanced to this position, and this value along with the time and chamber properties are reported. Time is now held fixed, and the element of surface under consideration is advanced by Δs . The heat transfer to this new element of surface is calculated, and its surface temperature is compared to the criterion. The advance of the surface but not of time is continued until $T_s < T_{ic}$. When this does occur, then the remarks of the previous paragraph are applicable.

After flame spreading is complete, the calculation is very simple. It is as outlined in the first paragraph except $s(\tau) = 1$.

For convenience, the program was divided into a main program and three subroutines. The main program contained all input-output, and made most of the important decisions. Subroutine mxtpt contained the mechanism for integrating the differential equations; subroutine floig calculated the igniter effects; and subroutine warum calculated the surface temperature of the propellant at the required point and time.

The calculations were programmed in Fortran II and run on Princeton's IBM 1620, 7044 and 7094 digital computers. Following are a flow chart of the program (Figure AII-4), a glossary of computer expressions, and a copy of the 7044 version of the program.

GEOMETRICAL REPRESENTATION OF
SECOND ORDER PREDICTOR
(FROM REFERENCE 24)

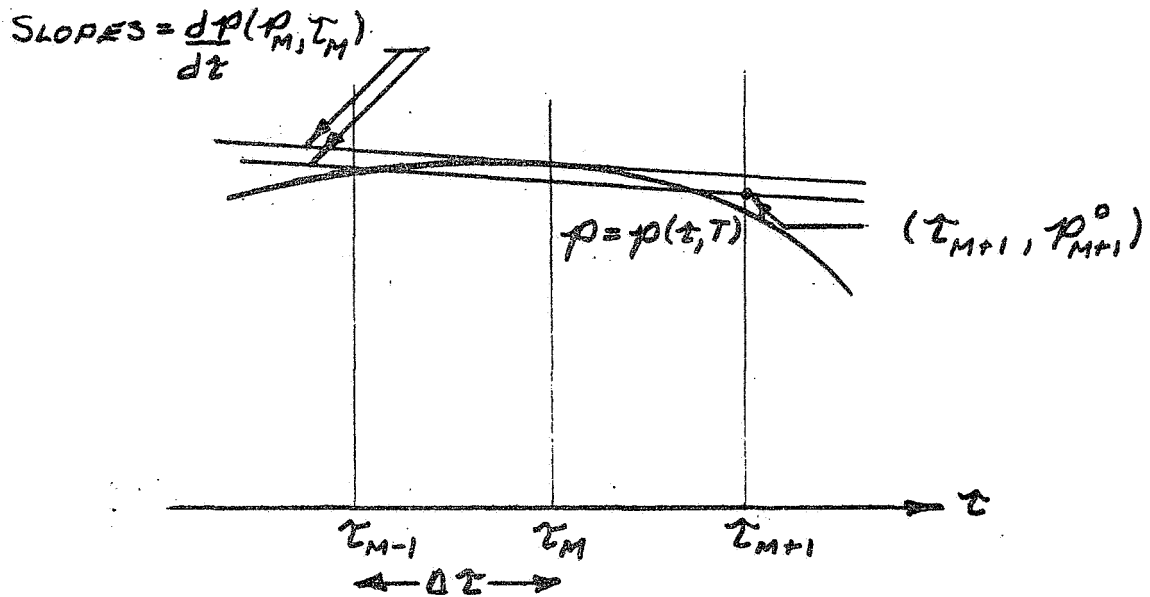


FIGURE B-1
GEOMETRICAL REPRESENTATION OF
SECOND ORDER CORRECTOR
(FROM REFERENCE 24)

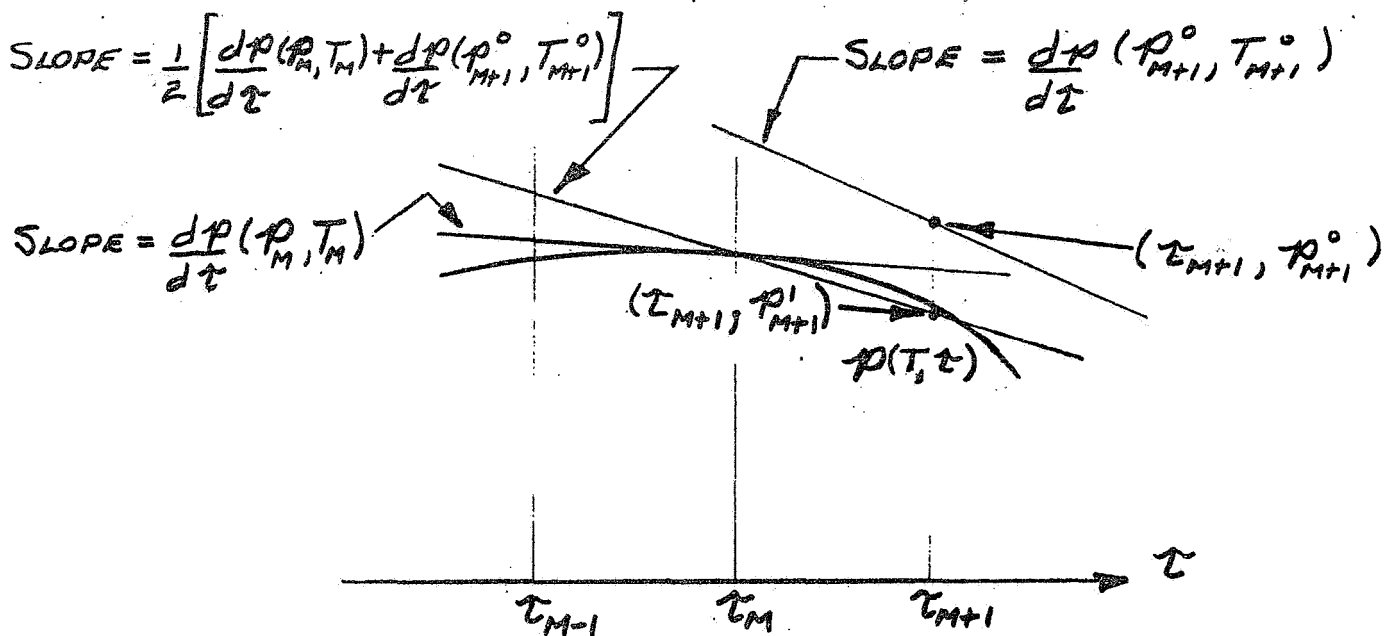


FIGURE B-2

GEOMETRICAL REPRESENTATION OF HEAT TRANSFER
INTEGRATION SCHEME

$$\int_0^t \frac{Q(t')}{(t-t')^{1/2}} dt' = \frac{Q(0)}{t^{1/2}} + \sum_{n=1}^{N-1} \frac{1}{2} \left[\frac{Q(n-1)}{(t-t'+\Delta t)^{1/2}} + \frac{Q(n)}{(t-t')^{1/2}} \right] \Delta t'$$

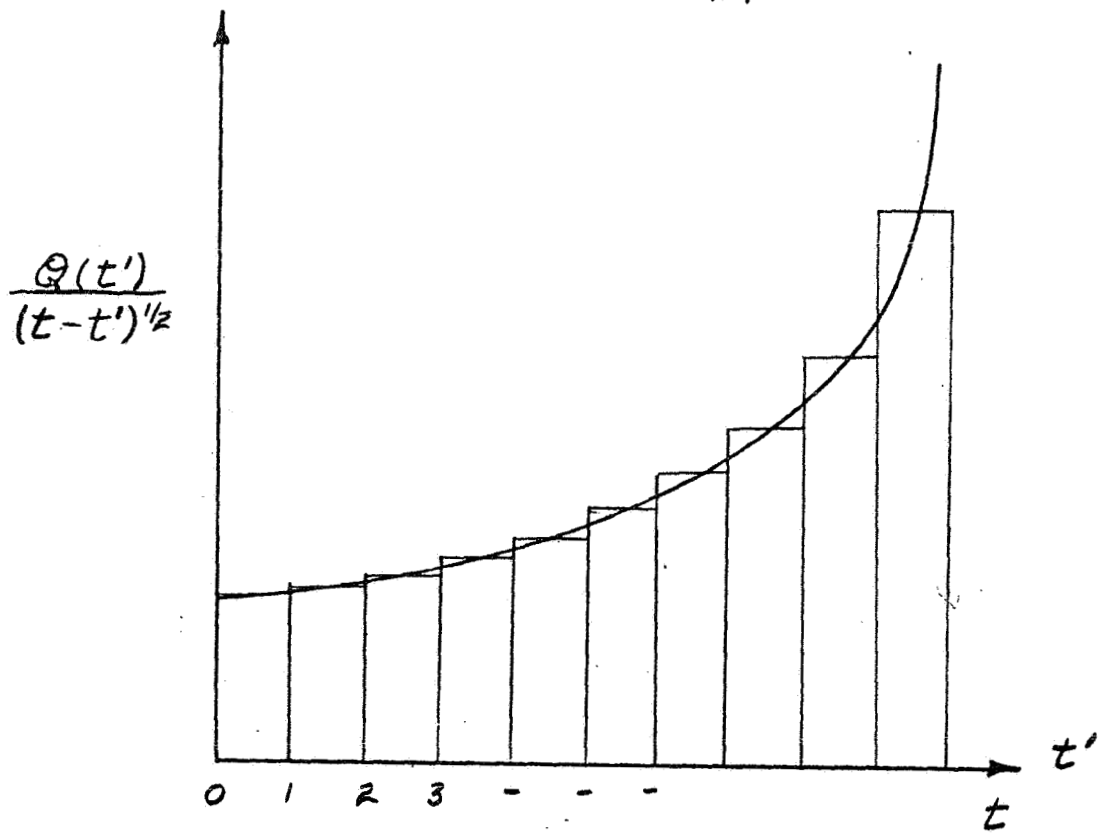


FIGURE B-3

COMPUTER PROGRAM FLOW CHART

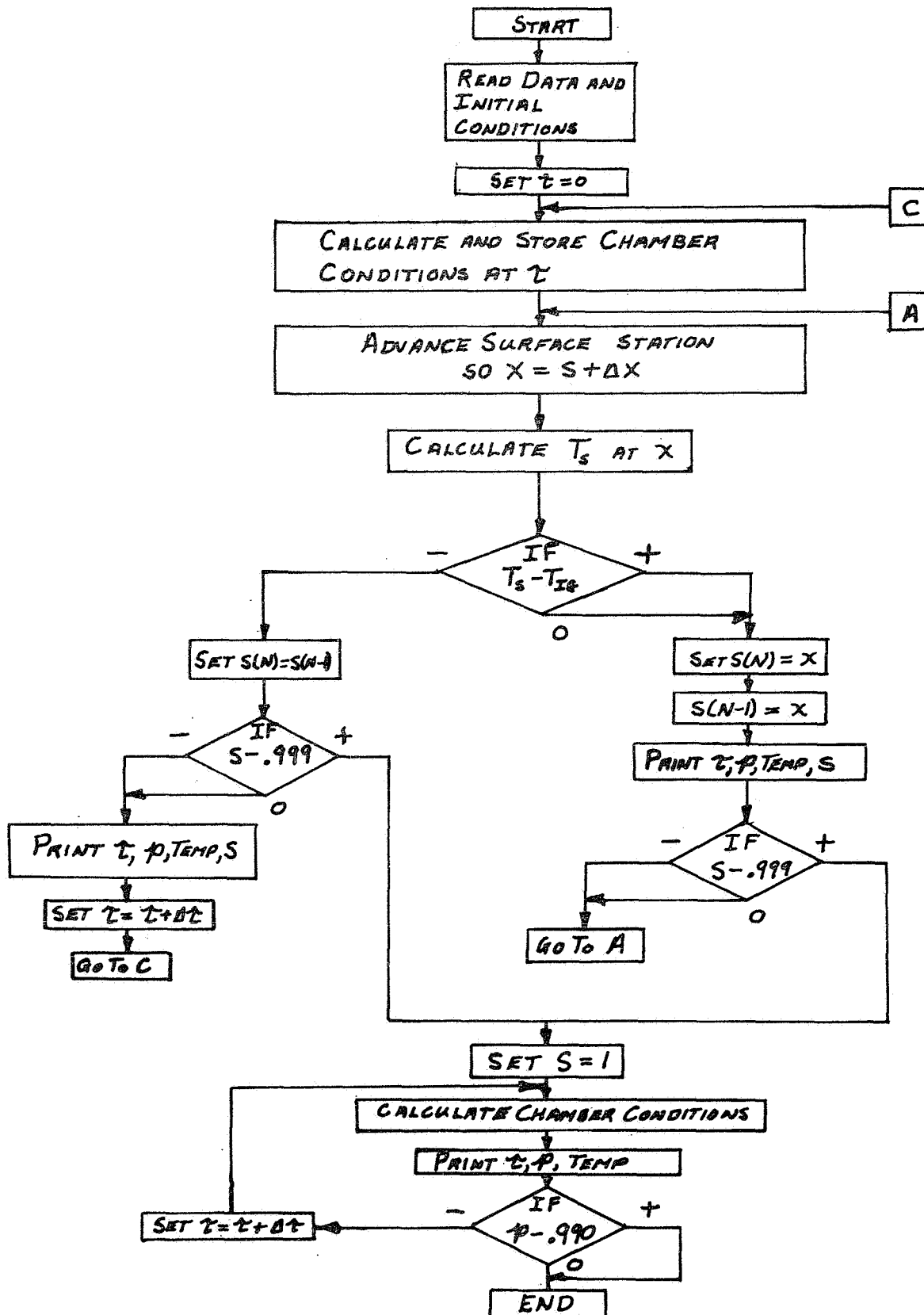


FIGURE B-4

GLOSSARY OF COMPUTER EXPRESSIONS

ACROS	A_p
AL	a/l
ALD	a
ALPHP	α_p
AN	n
AT	A_t
ATIG	A_{ign}
CRIT	area criterion to shut off igniter
CSTAR	C^*
DELT	Δt
DELX	$\Delta \xi$
DT	d_t
DTIG	$d_{t_{ign}}$
GAMMA	γ
GAMSQ	Γ^2
GIM	m_{ign}
P	p
PCIG	$p_{c_{ign}}$
PEQ	p_{eq}
PINIT	$p(0)$
PY	p when $S = 1$
Q (M)	$q(t)$
RENUK	$\left. \begin{array}{l} \\ \end{array} \right\} \begin{array}{l} \text{The heat transfer correlation becomes:} \\ \text{NUX} = \text{RENUK} \quad \text{REX} \quad \text{RENUX} \end{array}$
RENUK	
REX	Re_x

REXQ	$(Re_x)_{0.9} = \frac{P_{0.9} l A_x}{c^* \mu_g A_p}$
S	S
SINIT	S(0)
TAU	τ
TCIG	$T_{c\,ign}$
TDIFE	$T - T_s$
TEMP	T
TEMPY	T when S = 1
TFLME	Adiabatic flame temperature of the propellant
THERM	$\frac{\alpha_p^{1/2}}{\pi^{1/2} \lambda_p}$
TIG	T_{ig}
TINIT	T_0
TMCRT	No. of t^* units after P = 1.0 to cut igniter off (used for Series D)
TREF	t^*
TS	T_s
TSO	T_0
VOL.	V_c
X	ξ
XL	l
XLAMG	λ_g
XLAMP	λ_p
XMUG	μ_g

```

C   LAWRENCE LINDEN  IGNITION TRANSIENT PREDICTION  AFTER G. DI LAURO
C   PROGRAM NUMBER 462138, NAME=PPSPIG, FOR PRESSURE PREDICTION OF
C   SOLID PROPELLANT IGNITION
      DIMENSION S(1500),P(1500),TEMP(1500),RHELP(1500)
      COMMON RENUK,XLAMG,TDIFE,X,XL,AL,REX,RENUX,NLESS,Q,DELT,TREF,N,AT,
1TSO,THERM,TS,TAU,CRIT,PCIG,TCIG,TEMP,GAMMA,PMIG,TMIG,TEMPY,ATIG,
2PEQ,CSTAR,GIM,S,SY,CRIT2,NOS,DELX,REXEQ,P,RHELP,DPDT,DTDT,AN,ITN,
3LALL,TOLER,PY,ETPRES,PCRIT,TMCRIT,TFLME,PLAL,TLAL,PLALM1,TLALM1
100 FORMAT(8F10.6)
201 FORMAT(71H1LAWRENCE H. LINDEN  IGNITION TRANSIENT PREDICTION  AF
1TER G. DI LAURO)
202 FORMAT(5H PEQ=,E13.6,8H  CSTAR=,E13.6)
203 FORMAT(4H XL=,E13.6,6H  ALD=,E13.6,6H  VOL=,E13.6,5H  DT=,E13.6,8H
1  ACROS=,E13.6,7H  DTIG=,E13.6)
204 FORMAT(4H AN=,E13.6,8H  ALPHP=,E13.6,8H  XLAMP=,E13.6)
205 FORMAT(7H XLAMG=,E13.6,7H  XMUG=,E13.6,8H  GAMMA=,E13.6)
206 FORMAT(5H NUX=,F7.4,6H*REX**,F7.4)
207 FORMAT(5H TSO=,E13.6,6H  TIG=,E13.6,8H  TFLME=,E13.6)
208 FORMAT(6H PCIG=,E13.6,7H  TCIG=,E13.6,7H  CRIT=,E13.6,8H  PCRIT=,
1  E13.6,9H  TMCRIT=,E13.6)
209 FORMAT(/5X,3HTAU,11X,1HP,12X,1HS,10X,4HTEMP,9X,3HGIM,10X,4HDPDT,
1  9X,4HDTDT,10X,2HTS,10X,3HITN,7X,6HETPRES)
210 FORMAT(8E13.6,4X,I2,3X,E13.6)
211 FORMAT(7E13.6,17X,I2,3X,E13.6)
212 FORMAT(6H TREF=,E13.6,9H  XLSTAR=,E13.6)
215 FORMAT(7H XDELT=,E13.6,8H  DELT4=,E13.6)
216 FORMAT(7H TOLER=,E13.6/)
C   PEQ, CSTAR, XLSTAR, DTIG, DT, ALD, AND GIM ARE IN ENGLISH UNITS
C   ALL OTHER PARAMETERS ARE IN C.G.S. UNITS
C   INPUT
1  READ(5,100) PEQ,CSTAR
   READ(5,100) XL,ALD,VOL,DT,ACROS,DTIG
   READ(5,100) AN,ALPHP,XLAMP
   READ(5,100) XLAMG,XMUG,GAMMA
   READ(5,100) RENUK,RENUX
   READ(5,100) TSO,TIG,TFLME
   READ(5,100) DELX,DELT1,DELT2,DELT3,DELT4
   READ(5,100) PCIG,TCIG,CRIT,PCRIT,TMCRIT
   READ(5,100) PINIT,TINIT,SINIT
   READ(5,100) TOLER
C   CALCULATION OF PROGRAM CONSTANTS
   THERM = SQRT(ALPHP/3.1416)/XLAMP
   GAMSQ = GAMMA*(2./(GAMMA+1.))*((GAMMA+1.)/(GAMMA-1.))
   AT = 3.1416*(DT*1.27)**2
   XLSTAR = VOL/AT/12./2.54
   ATIG = 3.1416*(DTIG*1.27)**2
   TREF = VOL/(AT*CSTAR*GAMSQ*30.5)
   REXEQ = PEQ*XL*AT/(CSTAR*XMUG*ACROS*6.45)*14600.
   AL = ALD/XL*2.54
C   INITIAL OUTPUT
   WRITE(6,201)
   WRITE(6,202) PEQ,CSTAR
   WRITE(6,203) XL,ALD,VOL,DT,ACROS,DTIG
   WRITE(6,204) AN,ALPHP,XLAMP
   WRITE(6,205) XLAMG,XMUG,GAMMA
   WRITE(6,206) RENUK,RENUX
   WRITE(6,207) TSO,TIG,TFLME

```

```

WRITE(6,208) PCIG,TCIG,CRIT,PCRIT,TMCRIT
WRITE(6,212) TREF,XLSTAR
WRITE(6,215) DELX,DELT4
WRITE(6,216) TOLER
WRITE(6,209)
C INITIAL CONDITIONS
P(1)=PINIT
TEMP(1)=TINIT
S(1)=SINIT
TS = TSO
ITN = 0
DELT = DELT4
DO 10 N=1,2400
C N ADVANCING CORRESPONDS TO ADVANCING TIME
LALL = N
NLESS = N - 1
IF(NLESS)11,11,46
C N=1
11 TAU=0.
CRIT2 = TAU + TMCRIT
CALL NXTPNT
WRITE(6,210) TAU,P(N),S(N),TEMP(N),GIM,DPDT,DTDT,TSO
GO TO 10
C N GREATER THAN 1
46 TAU = TAU + DELT
CRIT2 = TAU + TMCRIT
CALL NXTPNT
C SELECTION OF THE ELEMENT OF SURFACE TO WHICH HEAT IS TRANSFERRED
NOS = (S(N-1)+1.E-7)/DELX
NOS = NOS + 1
GO TO 5
15 NOS = (S(N)+1.E-7)/DELX
NOS = NOS + 1
5 CALL WARUM
C TEST FOR IGNITION
IF(TS-TIG)23,24,24
C IF THE ELEMENT HAS NOT YET IGNITED -- CALCULATE THE PRESENT
C CHAMBER CONDITIONS, ADVANCE TIME BY A DELT (BY GOING TO 10
C --ADVANCING THE DO LOOP INDEX, N, BY ONE), AND THEN EXAMINE THE
C ELEMENT AGAIN
23 S(N)=S(N-1)
CALL FLOIG(S(N),TEMP(N),P(N))
WRITE(6,210) TAU,P(N),S(N),TEMP(N),GIM,DPDT,DTDT,TS,ITN,ETPRES
C TEST FOR END OF FLAME SPREADING
IF(S(N)-.999)20,28,28
20 GO TO 10

```

```

C      IF THE ELEMENT HAS IGNITED -- PRINT THE PREVIOUS CHAMBER
C      CONDITIONS WITH THE NEW AREA, AND THEN LOOK AT THE NEXT ELEMENT
C      (BY GOING TO 15). DO NOT ADVANCE TIME.
24  S(N) = X
    S(N-1) = X
    CALL FLOIG(S(N),TEMP(N),P(N))
    WRITE(6,210) TAU,P(N),S(N),TEMP(N),GIM,DPDT,DTDT,TS,ITN,ETPRES
C      TEST FOR END OF FLAME SPREADING.
    IF(S(N)-.999)29,28,28
29  GO TO 15
10  CONTINUE
C      S=1
28  SY=1.
C      DOUBLING OF STEP SIZE --
    DELT = 2.*DELT
C      PREPARE DATA FOR CHAMBER FILLING
    PLAL = P(LALL)
    TLAL = TEMP(LALL)
    PLALM1 = P(LALL - 2)
    TLALM1 = TEMP(LALL - 2)
    S(LALL) = 1.
    S(LALL-1) = 1.
31  KOUNT=0
C      CHAMBER FILLING CALCULATIONS
32  TAU = TAU + DELT
    CALL NXPNT
    WRITE(6,211)TAU,PY,SY,TEMPY,GIM,DPDT,DTDT,ITN,ETPRES
    KOUNT=KOUNT + 1
    IF(KOUNT - 5000)35,35,34
C      TEST FOR END OF IGNITION TRANSIENT (I.E. ATTAINMENT OF
C      EQUILIBRIUM PRESSURE)
35  IF(PY-.990)32,34,34
34  GO TO 1
    END

```

```

SUBROUTINE NXPNT
C SUBROUTINE INTEGRATES THE DIFFERENTIAL EQUATIONS USING A
C PREDICTOR-CORRECTOR METHOD
  DIMENSION S(1500),P(1500),TEMP(1500),RHELP(1500)
  COMMON RENUK,XLAMG,TDIFE,X,XL,AL,REX,RENUX,NLESS,Q,DELT,TREF,N,AT,
  1TSO,THERM,TS,TAU,CRIT,PCIG,TCIG,TEMP,GAMMA,PMIG,TMIG,TEMPY,ATIG,
  2PEQ,CSTAR,GIM,S,SY,CRIT2,NOS,DELX,REXEQ,P,RHELP,DPDT,DTDT,AN,ITN,
  3LALL,TOLER,PY,ETPRES,PCRIT,TMCRT,TFLME,PLAL,TLAL,PLALM1,TLALM1
  4 IF(N-1)5,5,10
C   S LESS THAN 1
C   INITIAL CONDITIONS -- N=1
  5 ETPRES = 0.
  ETTEMP = 0.
  PN = P(1)**AN
  THA = SQRT(TEMP(N))
  CALL FLOIG(S(1),TEMP(1),P(1))
  DPDT = GAMMA*(S(1)*PN-P(1)*THA+PMIG)
  DTDT=TEMP(1)*((GAMMA-TEMP(1))*S(1)*PN/P(1)-(GAMMA-1.)*THA
  1 +TMIG/P(1))
  RHELP(1) = (DPDT-P(1)*DTDT/TEMP(1))/TEMP(1)
  RETURN
  10 IF(N-2)15,15,20
C   N=2 THE SECOND POINT IS CALCULATED USING A MODIFIED RUNGE-KUTTA
C   SCHEME
  15 PNEW = P(1) + DELT*DPDT
  TNEW = TEMP(1) + DELT*DTDT
  PN = PNEW**AN
  THA = SQRT(TNEW)
  CALL FLOIG(S(1),TNEW,PNEW)
  DPNEW = GAMMA*(S(1)*PN - PNEW*THA + PMIG)
  DTNEW = TNEW*((GAMMA-TNEW)*S(1)*PN/PNEW-(GAMMA-1.)*THA
  1 +TMIG/PNEW)
  P(2) = P(1) +DELT/2.*(DPDT + DPNEW)
  TEMP(2) = TEMP(1) + DELT/2.*(DTDT + DTNEW)
  DPDT = DPNEW
  DTDT = DTNEW
  RHELP(2) = (DPDT-P(2)*DTDT/TEMP(2))/TEMP(2)
  RETURN
C   N GREATER THAN TWO
C   TEST FOR END OF FLAME SPREADING
  20 IF(S(N-1) - .999)21,80,80
  21 ITN = 0
  DPDTL = DPDT
  DTDTL = DTDT
C   THE PREDICTOR----
  POLD = P(N-2) + 2.*DELT*DPDTL
  TOLD = TEMP(N-2) + 2.*DELT*DTDTL
  PPRED = POLD
  TPRED = TOLD
  55 PN = POLD**AN
  THA = SQRT(TOLD)
  CALL FLOIG(S(N-1),TOLD,PPRED)
  DPDT = GAMMA*(S(N-1)*PN-POLD*THA+PMIG)
  DTDT=TOLD*((GAMMA-TOLD)*S(N-1)*PN/POLD-(GAMMA-1.)*THA + TMIG/POLD)
C   THE CORRECTOR ---
  P(N) = P(N-1) + DELT/2.*(DPDTL + DPDT)
  TEMP(N) = TEMP(N-1) + DELT/2.*(DTDTL + DTDT)
C   TEST FOR CONVERGENCE OF INTEGRATION

```



```

      IF (ABS((P(N) - POLD)/P(N)) - TOLER) 62,60,60
62  IF (ABS((TEMP(N) - TOLD)/TEMP(N)) - TOLER) 65,60,60
60  IF (ITN-10) 61,65,65
61  POLD = P(N)
      TOLD = TEMP(N)
      ITN = ITN+1
      GO TO 55
C    ETPRES AND ETTEMP ARE THE TRUNCATION ERRORS ACCUMULATED DURING
C    THE INTEGRATION ITERATIONS, ON THE PRESSURE AND TEMP, RESPECTIVELY
65  P(N) = P(N) + ETPRES
      TEMP(N) = TEMP(N) + ETTEMP
      ETPRES = 0.2*(PPRED-P(N))
      ETTEMP = 0.2*(TPRED-TEMP(N))
      RHELP(N-1) = (DPDT-P(N-1)*DTDT/TEMP(N-1))/TEMP(N-1)
      RETURN
C    S EQUALS ONE -- CHAMBER FILLING INTERVAL
C    INTEGRATING SCHEME SAME AS BEFORE
C    PNM1, PNM2 ARE THE TWO PREVIOUS POINTS. POLD STARTS AS THE
C    PREDICTED PRESSURE, THEN IS ITERATED WITH PY IN THE CORRECTOR
C    FORMULA.
80  PNM1 = PLAL
      TNM1 = TLAL
      PNM2 = PLALM1
      TNM2 = TLALM1
      PN = PNM1**AN
      THA = SQRT(TNM1)
      CALL FLOIG(1.,TNM1,PNM1)
      DPDTL = GAMMA*(PN-PNM1*THA + PMIG)
      DTDTL = TNM1*((GAMMA-TNM1)*PN/PNM1-(GAMMA-1.)*THA+TMIG/PNM1)
      ITN = 0
      POLD = PNM2+2.*DELT*DPDTL
      TOLD = TNM2 + 2.*DELT*DTDTL
      PPRED = POLD
      TPRED = TOLD
85  PN = POLD**AN
      THA = SQRT(TOLD)
      CALL FLOIG(SY,TOLD,PPRED)
      DPDT = GAMMA*(PN-POLD*THA + PMIG)
      DTDT = TOLD*((GAMMA-TOLD)*PN/POLD-(GAMMA-1.)*THA + TMIG/POLD)
      PY = PNM1 + DELT/2.*(DPDTL + DPDT)
      TEMPY = TNM1 + DELT/2.*(DTDTL + DTDT)
      IF (ABS((PY - POLD)/PY) - TOLER) 92,90,90
92  IF (ABS((TEMPY - TOLD)/TEMPY) - TOLER) 95,90,90
90  IF (ITN-10) 91,95,95
91  POLD = PY
      TOLD = TEMPY
      ITN = ITN + 1
      GO TO 85
95  PY = PY + ETPRES
      TEMPY = TEMPY + ETTEMP
      ETPRES = 0.2*(PPRED - PY)
      ETTEMP = 0.2*(TPRED - TEMPY)
C    STORAGE OF LAST TWO POINTS FOR NEXT TIME AROUND
      PLAL = PY
      TLAL = TEMPY
      PLALM1 = PNM1
      TLALM1 = TNM1
      RETURN
      END

```

```

SUBROUTINE WARUM
C  SUBROUTINE CALCULATES THE TEMPERATURE AT A GIVEN STATION BY
C  INTEGRATING THROUGH TIME THE HEAT TRANSFERRED TO IT
C  THE INTEGRATION IS DONE BY SUMMING AREAS. THE AREAS ARE EVALUATED
C  AT THE MIDDLE OF THE INTERVAL SO THAT ERRORS TEND TO CANCEL.
  DIMENSION S(1500),P(1500),TEMP(1500),RHELP(1500)
  COMMON RENUK,XLAMG,TDIFE,X,XL,AL,REX,RENUX,NLESS,Q,DELT,TREF,N,AT,
1TSO,THERM,TS,TAU,CRIT,PCIG,TCIG,TEMP,GAMMA,PMIG,TMIG,TEMPY,ATIG,
2PEQ,CSTAR,GIM,S,SY,CRIT2,NOS,DELX,REXEQ,P,RHELP,DPDT,DTDT,AN,ITN,
3LALL,TOLER,PY,ETPRES,PCRIT,TMCRT,TFLME,PLAL,TLAL,PLALM1,TLALM1
  XK = NOS
  X = XK * DELX
  SUM = 0.
  SAU = 0.
  TDIFE = TEMP(1)*TFLME - TSO - 273.15
  REX = REXEQ*(AL+X)*(P(1)/SQRT(TEMP(1))+(1.-X)*RHELP(1))
  Q1 = RENUK*XLAMG*TDIFE/((AL+X)*XL)*REX**RENUX
  QM = Q1
  IF(NLESS-2)35,10,10
35 CONTINUE
  SUM = Q1*DELT*SQRT(TREF/(TAU-SAU))
  GO TO 25
10 CONTINUE
  DO 20 M=2,NLESS
C  HERE ADVANCING M CORRESPONDS TO ADVANCING TIME.
  QMN1 = QM
C  SAU IS THE DUMMY INTEGRATION VARIABLE
  SAU = SAU + DELT
  DIFF = TAU - SAU
  TDIFE = TEMP(M)*TFLME - THERM*SUM - 273.15
  REX = REXEQ*(AL+X)*(P(M)/SQRT(TEMP(M))+(1.-X)*RHELP(M))
  QM = RENUK*XLAMG*TDIFE/((AL+X)*XL)*REX**RENUX
  TINT = (QM*SQRT(TREF/DIFF) + QMN1*SQRT(TREF/(DIFF+DELT)))/2.
  SUM = SUM + DELT*TINT
20 CONTINUE
  TINT = ((QM - QMN1)/2. + QM)*SQRT(2.*TREF/DELT)
  SUM = SUM + DELT*TINT
25 TS = TSO + THERM*SUM
  RETURN
  END

```

```

      SUBROUTINE FLOIG(SX,TEMPX,PX)
C     SUBROUTINE SUPPLIES THE IGNITER EFFECTS
      DIMENSION S(1500),P(1500),TEMP(1500),RHELP(1500)
      COMMON RENUK,XLAMG,TDIFE,X,XL,AL,REX,RENUX,NLESS,Q,DELT,TREF,N,AT,
      1TSO,THERM,TS,TAU,CRIT,PCIG,TCIG,TEMP,GAMMA,PMIG,TMIG,TEMPY,ATIG,
      2PEQ,CSTAR,GIM,S,SY,CRIT2,NOS,DELX,REXEQ,P,RHELP,DPDT,DTDT,AN,ITN,
      3LALL,TOLER,PY,ETPRES,PCRIT,TMCRIT,TFLME,PLAL,TLAL,PLALM1,TLALM1
C     TEST FOR IGNITER CUT-OFF CRITERIA
      IF(SX-CRIT)60,60,62
60    IF(TAU-CRIT2)61,61,62
61    IF(PX-PCRIT)615,615,617
615   CONTINUE
C     IGNITER TERMS IN DPDT AND DTDT --
616   PMIG = PCIG*SQRT(TCIG)*ATIG/AT
      TMIG = PCIG*(GAMMA*TCIG-TEMPX)/SQRT(TCIG)*ATIG/AT
      GIM = PMIG*PEQ*AT/(CSTAR*TCIG)*32.17/6.45
      GO TO 63
C     IF IGNITER CUT-OFF CRITERION HAS BEEN REACHED ---
617   PCRIT = 0.
62    PMIG = 0.
      TMIG = 0.
      GIM = 0.
63    RETURN
      END

```

NATIONAL AERONAUTICS AND SPACE ADMINISTRATION (RPS) CONTRACTS

BASIC DISTRIBUTION LIST II

National Aeronautics & Space Admin.
Washington, D. C. 20546

Attn: SV/V. L. Lohnson
RV-1/C. Wood
RV/M. B. Ames
RC/J. L. Sloop
RP/A. O. Tischler
RTA/R. V. Hensley
RTP/J. J. Phillips
MGS/E. Hall
MTA/M. C. Waugh

Ballistic Research Laboratory
Aberdeen Proving Ground, Maryland

Attn: Tech. Library

Director
Advanced Research Projects
Agency
The Pentagon, Room 3D154
Washington, D. C. 20301

Attn: Tech. Information Off.

National Aeronautics & Space Admin.
George C. Marshall Space Flight Center
Redstone Arsenal
Huntsville, Alabama 35812

Attn: R-PVE-PPS/R. N. Eilerman

Department of the Air Force
Headquarters, USAF, DCS/D
Washington, D. C. 20545

Attn: AFDRT-AS

National Aeronautics & Space Admin.
Manned Spacecraft Center
Houston, Texas 77058

Attn: J. G. Thibodaux

Air Force Systems Command
Space Systems Division
Air Force Unit Post Office
Los Angeles, Calif. 90045

Attn: Col. H. Robbins

Jet Propulsion Laboratory
California Institute of Technology
4800 Oak Grove Drive
Pasadena, California 91103

Attn: Winston Gin

Commander
Air Force Systems Command
HQ 6593 Test Group (Development)
Edwards Air Force Base, Calif.
93523

Attn: Mr. Don Hart (2)

Commander
Army Ballistic Missile Agency
Redstone Arsenal
Huntsville, Alabama

Attn: ORDAB-HSI

Research and Technology Div. (RPT)
Bolling Air Force Base
Washington, D. C.

Attn: Dr. Leon Green, Jr.

BASIC DISTRIBUTION LIST II (Continued)

Commander Air Force Ballistic
Missile Division
HQ Air Research and Development
Command
P.O. Box 262
San Bernardino, California

Attn: WDSOT

Department of the Army
Office, Chief of Ordnance
Washington, D. C. 20545

Attn: ORDTB

Commander
Army Rocket & Guided Missile
Agency
U.S. Army Ordnance Missile Command
Redstone Arsenal
Huntsville, Alabama

Attn: (1) ORDXR-OTL
(2) Mr. Frank James

Bureau of Naval Weapons
Department of the Navy
Washington, D. C. 20545

Attn: (1) Code RMMP-2
(2) Dr. O. H. Johnson
(3) Mr. Richard F. Gott

Commander
U.S. Naval Ordnance Test Station
China Lake, California 93557

Attn: (1) Mr. Edward W. Price
(2) Tech. Library

Naval Ordnance Laboratory
White Oak
Silver Spring, Maryland

Attn: (1) Mr. Carl Boyars
(2) Tech. Library

Naval Propellant Plant
Indian Head, Maryland

Attn: Tech. Library

Picatinny Arsenal
Dover, New Jersey

Attn: Tech. Library

Institute for Defense Analyses
1666 Connecticut Avenue, N. W.
Washington, D. C.

Attn: Tech. Library

NATIONAL AERONAUTICS AND SPACE ADMINISTRATION (RPS) CONT. TSADDENDUM A

Aerojet-General Corporation
P.O. Box 296
Azusa, California
Attn: Librarian

Amcel Propulsion Company
Subsidiary of Celanese
Corporation of America
1026 17th Street, N. W.
Washington, D. C.

Hercules Powder Company
Allegany Ballistics Laboratory
P.O. Box 210
Cumberland, Maryland
Attn: Librarian

Lockheed Propulsion Company
P.O. Box 111
Redlands, California
Attn: Helen Ashman --
Librarian

Rohm and Haas
Redstone Arsenal Research Div.
Huntsville, Alabama
Attn: Librarian

Space Technology Laboratories, Inc.
5730 Arbor Vitae Street
Los Angeles, California 90045
Attn: Mr. Robert C. Anderson

Thiokol Chemical Corporation
Elkton Division
Elkton, Maryland
Attn: Librarian

Aerojet-General Corporation
P.O. Box 1168
Sacramento, California 95836
Attn: R. G. Weitz, Head,
Tech. Info. Center

Aerospace Corporation
2400 East El Segundo Boulevard
El Segundo, California
Attn: Librarian

Hercules Powder Company
Bacchus Works
Magna, Utah
Attn: Librarian

Rocketdyne
6633 Canoga Avenue
Canoga Park, California
Attn: Library, Dept. 500-306

Thiokol Chemical Corporation
Utah Division
Brigham City, Utah
Attn: Librarian

United Technology Center
P.O. Box 358
Sunnyvale, California
Attn: Librarian

Marquardt Corporation
16555 Saticoy Street
Van Nuys, California
Attn: Librarian

Rocketdyne
Solid Propulsion Operations
P.O. Box 548
McGreggor, Texas
Attn: Librarian

Rocket Power/TALCO
A Division of Gabriel
Falcon Field
Mesa, Arizona
Attn: Librarian

Atlantic Research Corp.
Shirley Highway at Edsall Road
Alexandria, Virginia
Attn: Librarian

Thiokol Chemical Corporation
Redstone Division
Huntsville, Alabama
Attn: Technical Director

Rocket Research
233 Holden Street
Seattle, Washington
Attn: Librarian

Stanford Research Institute
Menlo Park, California